Stony Brook University

The chromatin remodeler Chd5 regulates neural cell fate through the histone demethylase Utx

A Dissertation Presented

by

Dong-Woo Hwang

to

The Graduate School

in Partial Fulfillment of the

Requirements

for the Degree of

Doctor of Philosophy

in

Genetics

Stony Brook University

August 2015

Stony Brook University
The Graduate School

Dong-Woo Hwang

We, the dissertation committee for the above candidate for the
Doctor of Philosophy degree, hereby recommend
acceptance of this dissertation.

Alea A. Mills, Professor
Watson School of Biological Sciences
Cold Spring Harbor Laboratory
Research Advisor

Bruce Futcher, Professor
Department of Molecular Genetics and Microbiology
Stony Brook University
Chairperson of Defense

Bruce Stillman, Professor
Watson School of Biological Sciences
Cold Spring Harbor Laboratory
Committee Member

Christopher Vakoc, Assistant Professor
Watson School of Biological Sciences
Cold Spring Harbor Laboratory
Committee Member

Hongwu Zheng, Assistant Professor
Watson School of Biological Sciences
Cold Spring Harbor Laboratory
Committee Member

This dissertation is accepted by the Graduate School

Charles Taber
Dean of the Graduate School

Abstract of the Dissertation

The chromatin remodeler Chd5 regulates neural cell fate

through the histone demethylase Utx

by

Dong-Woo Hwang

Doctor of Philosophy

in

Genetics

Stony Brook University

2015

Neural stem/progenitor cells (NSCs) in the mammalian brain are multipotent progenitor cells that give rise to the major neural lineages such as neurons, oligodendrocytes and astrocytes. Execution of precise spatiotemporal cell fate decisions of NSCs is regulated by cell type-specific gene expression programs. The role of chromatin remodeling proteins in cell fate decisions is not well understood. Here I present evidence that Chromodomain helicase DNA binding protein 5 (Chd5) facilitates tri-methylation of lysine 27 of histone H3 to modulate the repressive mark H3K27me3, through which neural-specific gene expression programs are specified. Chd5-deficient NSCs have aberrant enrichment of the $CD24^{Low}$ neuronal progenitor population, accompanied by altered cellular properties and augmented expression of NSC markers. Upon differentiation, Chd5-deficient cells generate more astrocytes at the expense of neurons. Chd5 deficiency leads to global gene expression changes and the marked reduction of H3K27me3. Importantly, ectopic expression of Chd5 enhances H3K27me3 and induces neurogenesis, effectively rescuing the cell fate defects of Chd5-deficient NSCs. Lastly, Chd5 functionally interacts with the H3K27me3-specific histone demethylase Utx. These findings underscore the importance of Chd5-mediated regulation of H3K27me3 during differentiation of NSCs and define a novel Chd5-Utx axis that is a crucial determinant of cell fate decisions in the developing mammalian brain.

Table of Contents

ABSTRACT..... **iii**

TABLE OF CONTENTS..... **iv**

LIST OF FIGURES AND TABLES..... **vi**

LIST OF ABBREVIATIONS..... **viii**

ACKNOWLEDGMENTS..... **xii**

Chapter 1. Introduction..... **1**

Chromatin Dynamics during Stem Cell Differentiation..... 1

The Role of Chromatin Regulators in Cellular Differentiation and Cancer..... 8

CHD5 and CHD Family Chromatin Remodelers in Neural Differentiation and Cancers..... 14

Summary..... 20

Chapter 2. Chd5-mediated Chromatin Dynamics in Neural Cell Fate Decisions..... **24**

Expression of Chd5 in Neural Stem/Progenitor Cells and Induction of *Chd5* during Neural Differentiation..... 24

Role of Chd5 in Homeostasis of Neural Stem/Progenitor Cells..... 27

Altered Cell Fate Decisions in Chd5-deficient Neural Stem/Progenitor Cells..... 30

Impact of Chd5 Loss on Global Gene Expression in Neural Stem/Progenitor Cells..... 32

Changes in Chromatin Structure Due to Chd5 Loss and Functional Link between Chd5 and the Histone H3K27me3-specific histone demethlyase Utx..... 35

Chapter 3. Conclusions, Perspectives, and Future Directions **63**

Chd5 Regulates Neural Cell Fate Decision of Neural Stem/Progenitor Cells 63

Chd5 Maintains Neural Cell-Type-Specific Gene Expression Programs 70

Chd5 Modulates H3K27me3 Modification through Utx 73

Chapter 4. Materials and Methods **81**

Primary Neural Stem/Progenitor Cell Culture 81

In Vitro Neural Differentiation of Neural Stem/Progenitor Cells 83

Phase Contrast Image Analysis 85

Immunofluorescent Staining and Image Analysis 85

Cell Surface Marker Assessment of Neural Stem/Progenitor Cells by Flow Cytometry 87

Proliferation Assessment of Neural Stem/Progenitor Cells by Flow Cytometry 88

RNA-sequencing Analysis of Global Gene Expression 88

Quantitative Real-Time PCR of Gene Expression 89

Chromatin Immunoprecipitation Analysis 90

Western Blot Analysis of Protein Expression 92

References **93**

List of Figures

Figure 1. The CHD family of chromatin remodelers..... 23

Figure 2. Expression of Chd5 in embryonic mouse brain..... 39

Figure 3. Expression of Chd5 in neonatal mouse brain.....40

Figure 4. Cell surface marker profiles of primary NSCs.....41

Figure 5. Transcriptional dynamics of Chd5 during *in vitro* neural differentiation.....42

Figure 6. Increased expression of activated NSC markers in *Chd5*-/- NSCs.....43

Figure 7. Decreased expression of early committed neuronal precursor markers in *Chd5*-/- NSCs..... 44

Figure 8. Increased proliferation of *Chd5*-/- NSCs..... 45

Figure 9. Enlarged neurospheres from *Chd5*-/- NSCs..... 46

Figure 10. Enhanced neurosphere formation capacity of *Chd5*-/- NSCs..... 47

Figure 11. Altered neural cell fates of *Chd5*-/- NSCs at day 4 post *in vitro* neurogenesis..... 48

Figure 12. Altered neural cell fates of *Chd5*-/- NSCs at day 7 post *in vitro* neurogenesis..... 49

Figure 13. Rescued neural cell fates of *Chd5*-/- NSCs at day 7 post *in vitro* neurogenesis..... 50

Figure 14. Ectopic expression of Chd5 in Chd5-/-; Chd5 NSCs at day 0 post in vitro neurogenesis..... 51

Figure 15. Hierarchical clustering of gene expression patterns of +/+, *Chd5*+/-, and *Chd5*-/- NSCs..... 52

Figure 16. Gene ontology analysis of differentially expressed genes in *Chd5*+/- NSCs and *Chd5*-/- NSCs..... 53

Figure 17. Decreased expression of neural stem cells markers and increased expression of neural progenitor markers in *Chd5*-/- NSCs..... 54

Figure 18. Deregulated expression of components of signaling pathways in *Chd5*-/- NSCs..... 55

Figure 19. Increased expression of components of RNA polymerase II subunits in *Chd5*-/- NSCs..... 56

Figure 20. Increased expression of chromatin regulators in *Chd5*-/- NSCs..... 57

Figure 21. Reduction of H3K27me3 and H3K27me2 levels in *Chd5*+/- and *Chd5*-/- NSCs..... 58

Figure 22. Reduced H3K27me3 enrichment on various genomic sites in *Chd5*-/- NSCs..... 59

Figure 23. Decreased expression of *Eomes* and increased expression of *Slc1a2* in *Chd5*-/- NSCs..... 60

Figure 24. Increased expression of H3K27me3-specific demethylase Utx in *Chd5-/-* NSCs..... 61

Figure 25. Rescued neural cell fate defects by Utx knockdown in *Chd5-/-* NSCs at day 7 post *in vitro* neurogenesis..... 62

Figure 26. Comparable expression of cell-type-specific markers in *Chd5*+/- and *Chd5*-/- brain..... 79

Figure 27. Expression of Chd5 in primary NSCs and neonatal mouse brain..... 80

List of Tables

Table 1. Sources and conditions of antibodies utilized in immunofluorescent analyses..... 93

Table 2. Sequences of primers utilized in gene expression analyses by RT-qPCR..... 94

Table 3. Sequences of primers utilized in H3K27me3 enrichment analyses by ChIP-qPCR.... 95

Table 4. Sources and conditions of antibodies utilized in western blotting analyses..... 96

List of Abbreviations

Nanog	Nanog homeobox
Fgf-4	Fibroblast growth factor 4
ICM	Inner Cell Mass
NSC	Neural Stem/Progenitor Cell
bHLH	basic Helix-Loop-Helix
Ascl1	Achaete-scute complex homolog 1 (Drosophila)
SVZ	Subventricular Zone
LIF	Leukemia Inhibitory Factor
Bmp	Bone morphogenic protein
Stat3	Signal transducer and activator of transcription 3
Id1	Inhibitor of DNA binding proteins 1
Id3	Inhibitor of DNA binding proteins 3
Erk (Mapk1)	Mitogen-activated protein kinase 1
Wnt	Wingless-type MMTV integration site family
Gsk-3β	Glycogen-synthetase-kinase-3 beta
Igf-I	Insulin-like growth factor 1
Brn2 (Pou3f2)	POU class 3 homeobox 2
Myt1l	Myelin transcription factor 1-like
Oct4 (Pou5F1)	POU class 5 homeobox 1
Sox2	SRY (sex determining region Y)-box 2
Klf4	Kruppel-like factor 4
c-Myc (Myc)	Myelocytomatosis oncogene
MNase	Micrococcal nuclease

DNase I	Deoxyribonuclease I
NFR	Nucleosome Free Regions
TSS	Transcription Start Sites
TAD	Topologically Associating Domains
FISH	Fluorescence In Situ Hybridization
DHS	DNase I Hypersensitive Sites
3C	Chromosome Confirmation Capture
4C	Circularized Chromosome Confirmation Capture
5C	Carbon-Copy Chromosome Confirmation Capture
NPC	Neural Progenitor Cell
LINE	Long Interspersed Elements
SINE	Short Interspersed Elements
Eed	Embryonic ectoderm development
Suz12	Suppressor of zeste 12 homolog
Ezh1	Enhancer of zeste homolog 1
Ezh2	Enhancer of zeste homolog 2
Jarid2	Jumonji, AT rich interactive domain 2
PRC2	Polycomb Repressive Complex 2
Ring1b (Rnf2)	Ring finger protein 2
Bmi1	BMI1 proto-oncogene, polycomb ring finger
Cbx6	Chromobox homolog 6
PRC1	Polycomb Repressive Complex 1
p400/TIP60 (EP400)	E1A binding protein p400
MBD3	Methyl-CpG Binding Domain protein 3
Utx (Kdm6a)	Lysine (K)-specific demethylase 6A

Jmjd3 (Kdm6b)	Lysine (K)-specific demethylase 6B
Uty (Kdm6c)	Lysine (K)-specific demethylase 6C
Snf2 (Smarca4)	SWI/SNF related, matrix associated, actin dependent regulator of chromatin, subfamily a, member 4
INO80	Chromatin-remodeling ATPase INO80
ISW1	Chromatin-remodeling ATPase ISW1
ISW2	Isw2p
SWR1	Chromatin-remodeling protein SWR1
ANP32E	Acidic (leucine-rich) Nuclear Phosphoprotein 32 family, member E
NuRD	Nucleosome Remodeling and Deacetylase
CHD	Chromodomain Helicase DNA binding proteins
HDAC	Histone deacetylases
HAT	Histone acetyltransferases
KMT	Histone lysine methyltransferases
KDM	Histone lysine demethylases
MLL	Myeloid/Lymphoid or Mixed-Lineage Leukemia (trithorax homolog)
MEF	Mouse Embryonic Fibroblasts
HSC	Hematopoietic Stem Cells
HCC	Hematopoietic Cluster Cells
ASD	Autism Spectrum Disorder
CHARGE	Coloboma, Heart defect, Atresia choanae, Retarded growth and development, Genital abnormality, and Ear abnormality
Ebf1	Early B cell factor 1
Pax5	Paired box 5
Pax6	Paired box 6
Sox4	SRY (sex determining region Y)-box 4

Sox11	SRY (sex determining region Y)-box 11
Tbr1	T-box brain gene 1
Tbr2 (Eomes)	Eomesodermin
Slc1a2	Solute carrier family1 (glial high affinity glutamate transporter), member2
Slc1a3	Solute carrier family1 (glial high affinity glutamate transporter), member3
Egfr	Epidermal growth factor receptor
Fgfr	Fibroblasts growth factor receptor
Map2	Microtubule-associated protein 2
Gfap	Glial fibrillary acidic protein
Plxnb2	Plexin B2
Cspg4	Chondroitin sulfate proteoglycan 4
Snap25	Synaptosomal-associated protein, 25kDa
Gjb6	Gap junction protein, beta 6
Nefm	Neurofilament, medium polypeptide

Acknowledgments

This work would not have been possible without the support and guidance of many people. I am especially grateful to my research advisor Alea Mills for giving me an opportunity to conduct my Ph.D thesis in her laboratory. Her passion and uncompromising rigor for science have taught me how to become a scientist. Thanks to her patience and unwavering support, I have been able to endure hard times and have been privileged to reach the final stage of my Ph.D student career.

I am indebted to my thesis committee whose critical guidance and generosity have provided me the opportunities to initiate and complete this work. I appreciate Professor Futcher for being the chair of my thesis committee and his critical inputs. I am thankful for Dr. Stillman for his extremely helpful suggestions. I am especially grateful to Dr. Vakoc who spurred me to find the experimental system to which my work is most relevant. I am extremely grateful to Dr. Zheng for his critical inputs on primary neural stem cell system which has been the basis of my thesis research.

All Mills laboratory members and colleagues around the campus have been the great mentors and friends who made my time here at Cold Spring Harbor Laboratory the most special. My colleagues and friends, with whom I went through the initial periods of graduate school at Stony Brook University, have made my time in New York memorable.

Chapter 1. Introduction

1.1 Chromatin Dynamics during Stem Cell Differentiation

Mammalian development is not merely a growth period during which embryos grow into mature animals but the process whereby the unique identity of each animal is being shaped. Individual uniqueness is the outcome—an emergent property—of diversity embedded at the cellular level. That is to say that the various distinct populations of cells that make up an animal's body collectively contribute to the formation of its identity. This critical process of cellular diversification, or "differentiation," occurs at the early developmental stages in mammals. Cellular differentiation is a transitional process, often composed of multiple successive intermediate stages through which undifferentiated cells such as embryonic stem cells (ES cells), acquire defined cell fates so as to eventually become terminally differentiated lineage-specified cells (Keller, 2005) .

Consequences of misregulated cellular differentiation are often catastrophic. For instance, homozygous disruption the gene encoding the homeobox protein Nanog compromises the differential potentials of ES cells, creating a bias towards the extraembryonic endoderm lineage. Nanog deficiency causes embryonic lethality, providing the ultimate proof that disarrayed differentiation by loss of Nanog halts development (Mitsui et al., 2003). Similarly, deficiency of fibroblast growth factor 4 (Fgf-4) in mouse leads to embryonic lethality shortly after implantation (Feldman et al., 1995). Consistent with its essential role in development, Fgf-4 is required for differentiation of the inner cell mass (ICM) (Rappolee et al., 1994). The neural stem

cell (NSC)-specific basic helix-loop-helix (bHLH) transcription factor Mash1/Ascl1 plays an important role in the developing mouse brain. Deficiency of Mash1 causes a significant reduction of the NSC pool within the subventricular zone (SVZ), leading to depletion of neuronal populations within the basal ganglia and cerebral cortex. Loss of Mash1 in the developing brain eventually causes severe morphological defects in adults (Casarosa et al., 1999; Guillemot et al., 1993). These examples reinforce the concept that aberrant expression of key regulators involved in cellular differentiation can culminate in a failure of normal development. Wisely, evolution has equipped mammals with robust multilayered regulatory mechanisms throughout development to ensure the accurate spatiotemporal execution of differentiation.

Cell-extrinsic signaling pathways have been recognized as a prevailing context-specific regulatory mechanism that choreographs appropriate cellular differentiation. In particular, there has been much progress in understanding of how stem cells prevent precocious differentiation by maintaining self-renewal capacity, thereby safeguarding the pluripotency of ES cells and the multipotency of tissue-specific stem cells (Martello and Smith, 2014; Paridaen and Huttner, 2014). The cytokine leukemia inhibitory factor (LIF) and bone morphogenic protein (Bmp) are well-characterized extracellular molecules involved in maintaining the self-renewal of ES cells. LIF mediates its signals through the interplay with the downstream effector signal transducer and activator of transcription 3 (Stat3), and Bmp suppresses ES cell differentiation by inducing *Id1* and *Id3* genes that encode transcriptional repressor inhibitor of DNA binding proteins 1 and 3 (Id1 and Id3, respectively) (Niwa et al., 1998; Ying et al., 2003). Fibroblast growth factor (Fgf) plays an opposing role, potentiating ES cell differentiation via activation of the kinase Erk (Martello and Smith, 2014). Similarly, Wnt ligand in mouse brain is crucial for maintaining

differentiation potential and for implementing the appropriate cell fate decisions of NSCs. In adult hippocampal stem/progenitor cells, the Wnt/β-catenin signaling pathway promotes neurogenesis through modulation of glycogen-synthetase-kinase-3 beta (Gsk-3β) activity (Faigle and Song, 2013; Kim et al., 2009; Lie et al., 2005). In addition, an *in vitro* study of rat NSCs demonstrates that the prolonged presence of insulin-like growth factor 1 (Igf-1) in the culture medium biases cell fate decision towards the oligodendrocytic lineage (Hsieh et al., 2004). While our understanding of the precise mechanisms of differentiation-associated signaling pathways is still limited, in part due to the interdependent nature of a myriad of signaling pathways, it is clear that stem cell self-renewal and differentiation are under the control of context-dependent extracellular signaling molecules produced by the microenvironment (i.e. the stem cell niche).

Cell-type-specific transcriptional regulation—the central tenet of cell fate decisions—has been recognized as a primary cell-intrinsic regulatory mechanism of cellular differentiation in various stem cell contexts (Jaenisch and Young, 2008; Jojic et al., 2013). Signals from the microenvironment ultimately converge in the nucleus, where they directly or indirectly modulate the activity of downstream transcriptional activators and repressors, which, in turn, regulate the expression of specific sets of genes to execute cell fate decisions (Faigle and Song, 2013). Ablation of neuron-specific transcription factors such as Mash1/Ascl1 and Brn2 provide proof-of-principle that these transcription factors are indispensible for neuronal differentiation. More importantly, ectopic expression of each of these transcription factors is sufficient to promote neuronal lineage specification (Bertrand et al., 2002; Castro et al., 2006). Historically, differentiation has been conceptualized as a unidirectional process, yet recent breakthroughs with induced neuronal cells (iN cells) and induced pluripotent stem cells (iPS cells) provide

compelling evidence that cell fate commitment and differentiation are plastic and can be changed and reverted (Ladewig et al., 2013). When terminally differentiated mouse fibroblasts are transduced with combinations of key transcription factors (e.g. Ascl1, Brn2, and Myt1l for iN cells; Oct4, Sox2, Klf4, and c-Myc for iPS cells) cells transdifferentiate (i.e. convert cell fate) into functionally active neurons, or revert (i.e. are reprogrammed) into undifferentiated ES-cell like induced pluripotent stem cells. These examples provide proof-of-concept that cell-type-specific gene expression programs are necessary and sufficient to drive differentiation into certain lineages and can even reprogram differentiation in a reverse direction (Buganim et al., 2013; Ladewig et al., 2013; Yang et al., 2011).

A unique complexity of eukaryotic transcriptional machinery stems from the structural features of chromatin, molecular assemblies of deoxyribonucleic acid (DNA) and nucleosomes, which occupy a considerable amount of the nucleus. DNA and nucleosomes—composed of two copies of four different canonical histones (i.e. H2A, H2B, H3, H4)—physically interact to form nucleosome cores, with 147 base pairs of DNA being wrapped around each histone octamer (Kornberg and Lorch, 1999; Luger et al., 1997; Rando and Ahmad, 2007). This core serves as a fundamental unit of chromatin, promoting efficient packaging of an otherwise extremely long DNA molecule. And yet, by its nature, chromatin poses immediate challenges: it hinders trans-acting regulators such as transcription factors from gaining access to the underlying DNA. Since transcription factors primarily rely on the physical interaction with cognate DNA sequences present within or adjacent to target genes, the physical hindrance presented by nucleosomes is a major obstacle to be overcome (Bell et al., 2011). At the genomic level, nucleosomes are not uniformly distributed across the genome, but instead tend to be distributed in a stereotypical

manner, suggesting the existence of regulatory mechanisms (Owen-Hughes and Gkikopoulos, 2012). Nucleases such as micrococcal nuclease (MNase) and deoxyribosenuclease I (DNase I), which promote hydrolytic cleavage of the phosphodiester bonds of the DNA backbone, have been used to examine characteristic distribution patterns of nucleosomes across the genome. For instance, there are nucleosome free regions (NFRs) in the vicinity of the transcription start sites (TSS), small regions that lack nucleosome occupancy (Yen et al., 2012). Not being protected by nucleosomes, these genomic elements are more susceptible to the nuclease-mediated cleavage, thus guaranteeing higher DNA accessibility for trans-acting regulators (Rando and Ahmad, 2007; Song et al., 2011; Thurman et al., 2012; Yen et al., 2012). These observations provide evidence that chromatin structure (e.g. DNA accessibility) is an important aspect of eukaryotic transcription. Thus, there are discrete regulatory mechanisms exist to modulate DNAs accessibility to transcription factors and other proteins.

Chromatin is also organized at a higher level. Chromosomes are made up of chromatin and are organized in a spatially distinct manner within the nucleus, which gives rise to the term "chromosome territory." In addition, each chromosome is composed of locally associated functional units dubbed topologically associating domains (TADs) (Bickmore, 2013; Dekker et al., 2013; Gorkin et al., 2014; Ong and Corces, 2014). Chromosome territories were initially discovered by fluorescence *in situ* hybridization (FISH)-based chromosome painting approaches. Studies have shown that chromosomes are located in distinct positions within the nucleus during interphase. This positional organization pattern is not permanently set. It is subject to change during mitosis, which consequently generates different chromosome territories in mother vs. daughter cells. Yet, several studies have revealed a consistent physical clustering between

chromosome territories, characterized by similar transcriptional activities (either active or inactive). In fact, clustered regions of different chromosomes share a similar transcriptional status, as measured by DNase I hypersensitive sites (DHS), the presence of transcriptional activation-associated covalent modifications of histone H3 (e.g. H3K4me3), and comparable gene expression levels, thereby suggesting that chromosomal territories confer a regulatory mechanism in which gene expression is influenced by chromosome organization (Bickmore, 2013; Gorkin et al., 2014). Additionally, the recent development of chromosome conformation capture technologies (e.g. 3C, 4C, 5C and Hi-C) has provided a body of evidence for an extensive degree of local chromosome interactions which are predominantly in cis (i.e. intrachromosomal interactions) and less frequently in trans (i.e. interchromosomal interactions). These local chromosomal interactions are referred to as TADs and are recognized as a fundamental organizational unit of the mammalian genome. More than 90% of the genomes of mouse and human are covered by approximately 2,000 TADs. Intriguingly, the functional properties (e.g. transcriptional activity and replication timing) within each TAD appears to be coordinated, thereby suggesting that TADs serve as a functionally-relevant organizational unit and implicating a regulatory role at the chromosomal level (Gorkin et al., 2014; Pope et al., 2014). Taken together, the structural features of chromatin and the organizational properties of chromosomes support the idea that chromatin is at the epicenter of molecular biology and genomic output.

During cellular differentiation, it is not only cellular morphology but also chromatin structure in the nucleus that undergoes a drastic transformation. Open chromatin —that is, a less compact structure—has been identified as a unique property of ES cells. This open chromatin

state becomes more rigid and compact (i.e. chromatin becomes closed) as ES cells differentiate into neural progenitor cells (NPCs) (Aoto et al., 2006; Meshorer et al., 2006). This important observation has raised several questions. What molecular mechanism is responsible for this open-to-closed chromatin transition? How do these structural changes contribute to or affect regulation of cell-type-specific gene expression programs, which underlie the cell fate decisions of ES cells? Subsequent studies have made other key findings. Bernstein et al. found that ES cells harbor bivalent domains in which two antagonistically-related histone modifications, the transcriptional activation mark H3K4me3 and the transcriptional repression mark H3K27me3, are simultaneously present, decorating a sizable portion of genome (Azuara et al., 2006; Bernstein et al., 2006). Most strikingly, despite the considerable presence of the repressive mark H3K27me3, the ES cells genome is still transcribed at an unusually high extent in comparison with the transcriptional output of differentiated cells. Even non-protein coding parts of the genome—that is, microsatellite repeat sequences, long interspersed elements (LINEs), short interspersed elements (SINEs) and retrotransposons—are highly expressed, thereby bolstering the notion that the enhanced DNA accessibility of the ES cell genome, facilitated by an open chromatin structure, leads to globally elevated transcription. Most significantly, this unique transcriptional hyperactivity decreases as the ES cells differentiate into NPCs (Efroni et al., 2008). Indeed, recent genome-wide studies of chromatin structural and organizational changes have consistently illustrated a progressive compaction of ES cell genome during differentiation (Dixon et al., 2015; Zhu et al., 2013). Notably, a significant disparity between the degree of H3K27me3 in ES cells (~8%) and differentiated cells (~40%) has been observed. Most importantly, the extent of H3K27me3-decorated portion of the genome in differentiated cells correlates with a lower transcriptional output (Zhu et al., 2013). Furthermore, studies of *Eed*-/-

and *Suz12*-/- ES cells—which are deficient for core components Eed and Suz12 of polycomb repressive complex 2 (PRC2)—illustrate that the global reduction of H3K27me3 not only leads to a disarray in ES cell self-renewal capacity but also aberrant differentiation, thereby highlighting the pivotal role of H3K27me3 and its regulators in ES cell maintenance, differentiation, and chromatin compaction (Boyer et al., 2006; Pasini et al., 2007). Together, these findings illustrate that chromatin undergoes structural and organizational changes during differentiation and that perturbation of this process impairs cellular differentiation via inappropriate execution of cell-type-specific gene expression programs, thereby supporting the notion that chromatin dynamics is a driver of the cellular differentiation process.

1.2 The Role of Chromatin Regulators in Cellular Differentiation and Cancer

To regulate such diverse aspects of chromatin biology, eukaryotic systems implement multiple mechanisms. A wide range of regulators (collectively known as chromatin regulators) exists to carry out context-specific modulation of chromatin structure and organization. Based on their biochemical properties, chromatin regulators can be broadly categorized into three major classes: chromatin remodelers (e.g. Snf2-related ATP-dependent chromatin remodelers), histone modifying enzymes (e.g. histone acetyltransferases/deacetylases, lysine methyltransferases/ demethylases) and histone chaperones (e.g. the histone chaperone ANP32E) (Weber and Henikoff, 2014). Each class of chromatin regulator consists of a long list of family members that confer similar or slightly different biochemical functions. To add an additional layer of complexity, chromatin regulators of one class may work individually as well as in conjunction with members of another class. For example, the transcription repressor complex NuRD

(Nucleosome Remodeling and Deacetylase) in mammals contain at least two histone-interacting proteins: chromatin remodelers (CHD3/4) and histone modifying enzymes (HDAC1/2). Indeed, the interdependent relationship within a particular class as well as between classes appears to be a common theme of chromatin regulators in eukaryotes (Venkatesh and Workman, 2015). Chromatin regulators are multifaceted molecular machines, and the regulatory mechanisms that they exert are multifactorial, interconnected, and highly context-dependent.

Eukaryotic chromatin remodelers are characterized by the presence of Snf2-related helicase-like domain (i.e. Walker box). Snf2 is a catalytic subunit of the SWI/SNF chromatin remodeler complex in *Saccharomyces cerevisiae* and was one of the first characterized helicase proteins. Biochemical approaches unambiguously demonstrate that these Snf2- related helicases are able to convert chemical energy generated from ATP-hydrolysis to mechanical movement. Similar biochemical approaches revealed that several other Snf2-related helicase-like proteins can move or reorganize nucleosome arrays on DNA templates, thus providing evidence that Snf2-related helicases are ATP-dependent chromatin remodelers (Flaus et al., 2006; Narlikar et al., 2013). In eukaryotes, the Snf2-related chromatin remodeler family comprises 24 subfamilies, all of which share various versions of the Snf2-related helicase domain (Flaus et al., 2006).

It has been postulated that chromatin remodelers have direct and indirect roles in transcriptional regulation on the basis of *in vitro* biochemical evidence that these enzymes can mobilize nucleosomes. Furthermore, *in vivo* studies in yeast have uncovered quintessential aspects of chromatin remodelers across the genome—that is, chromatin remodelers are located in

the vicinity of the TSS and within the coding regions of a considerable fraction of protein coding genes (~50%) (Yen et al., 2012). Yet, each chromatin remodeler seems to have a relatively distinct genomic localization pattern. In yeast, Chd1 is localized throughout the coding region of its target genes, whereas Snf2 is primarily enriched at promoters and in the 5' portion of genes. Intriguingly, several chromatin remodelers (e.g. INO80, ISW1, and ISW2) are localized at the first nucleosome—that is, the +1 nucleosome that directly follows the NFR of the TSS (Gkikopoulos et al., 2011; Yen et al., 2012). These characteristic genomic localization patterns of chromatin remodelers relative to genes suggest that chromatin regulators are involved in global transcriptional regulation and that they do so by modulating DNA accessibility (Cairns, 2009; Narlikar et al., 2013). As proof-of-concept, deletion of the genes encoding the chromatin remodeler Chd1 in mouse ES cells and hematopoietic progenitors revealed that Chd1 deficiency hampers global gene expression. In the absence of Chd1, genome-wide transcription was significantly reduced (Guzman-Ayala et al., 2015; Koh et al., 2015). Most importantly, reduced gene expression correlates with inefficient nucleosome reorganization around the TSS, providing evidence for a causal relationship between nucleosome occupancy and gene expression. In a separate study, Skene et al. demonstrate that in the absence of Chd1, RNA polymerase II-directed Chd1-mediated nucleosome eviction is not efficient, thereby confirming the hypothesis that improper nucleosome reorganization around the TSS affects global transcriptional output (Skene et al., 2014). Taken together, these findings support a model in which a chromatin remodeler physically modulates nucleosome organization in the vicinity of genes, directly influencing transcription.

Histones that make up nucleosomes are subject to post-translational modifications. For example, specific residues (e.g. lysine 4 and lysine 27) in amino terminal domain or in the core region of histones are subject to covalent modifications (Suganuma and Workman, 2011; Zentner and Henikoff, 2013). In eukaryotic systems, the diverse groups of enzymes that modify histones can be divided into several subgroups based upon the biochemical nature of the modifications they evoke. For example, proteins that add acetyl groups to lysine residues of histones H3 and H4 are histone acetyltransferases (HATs), and their antagonistic counterparts are histone deacetylases (HDACs) (Lee and Workman, 2007). By a similar naming convention, histone lysine methyltransferases (KMTs) mediate methylation of lysine residues of histone H3 and H4, whereas histone lysine demethylases (KDMs) remove methyl groups from these residues. Several mechanisms as to how histone modifications work have been proposed. Histone modifications may affect nucleosome structure and organization, thereby modulating DNA accessibility so as to facilitate or to hinder the physical binding of trans-acting regulators (e.g. transcription factors). Another possibility is that histone marks present themselves as signals to be recognized by other trans-acting regulators such as chromatin regulators, thereby in effect serving as docking platforms (Kouzarides, 2007; Suganuma and Workman, 2011). As an example for the first case, acetylation of histone tail residues (e.g. H4K5, H4K8, H4K12) or core residues (e.g. H3K64 and H3K122) have been shown to destabilize the DNA-nucleosome interaction, and this destabilization, in turn, enhances DNA accessibility (Dion et al., 2005; Tessarz and Kouzarides, 2014). On the other hand, the presence of specific histone marks (e.g. H3K27me3) facilitates recruitment of trans-acting regulators. With H3K27me3 binding modules such as the Cbx subunits of polycomb repressive complex 1 (PRC1) and the Eed subunit of polycomb repressive complex 2 (PRC2), PRC complexes physically interact with histones with

the transcription repressive mark H3K27me3, thereby regulating transcription of PRC1/2-target genes (Simon and Kingston, 2013). Notably, modulation of DNA accessibility and facilitation of transcription are not mutually exclusive, as destabilization of the DNA-nucleosome interaction can further facilitate recruitment of trans-acting regulators by creating favorable conditions.

Histone exchange is an alternative mechanism that can weaken or enhance the DNA-nucleosome contacts by replacing canonical histones with specific variants (e.g. histone H2A.Z and histone H3.3) that structurally differ from canonical histones (e.g. histone H2A and histone H3) (Venkatesh and Workman, 2015; Weber and Henikoff, 2014). As is the case for histone modifying enzymes, multiple histone chaperones are involved in histone exchange. For instance, human histone H2A.Z is incorporated by the chaperone ANP32E, which is part of the histone exchange complex p400/TIP60, the human SWR1 (Obri et al., 2014). From a structural perspective H2A.Z incorporation contributes to destabilization of histone octamers by altering the interface between H2A.Z-H2B dimers and H3-H4 dimers (Suto et al., 2000). From a transcriptional point of view, incorporation of H2A.Z increases DNA accessibility, thereby reinforcing transcriptional activation (Venkatesh and Workman, 2015). In mouse embryonic fibroblasts (MEFs) the majority of H2A.Z peaks are located at promoters, coinciding with the presence of H3K4me3. It has been shown that in yeast, incorporation of H2A.Z at promoters is modulated by two chromatin remodeling complexes (INO80 and SWR1) that have opposing roles—that is, incorporation and removal of H2A.Z, respectively (Luk et al., 2010; Papamichos-Chronakis et al., 2011; Ranjan et al., 2013). Notably, in this instance, one class of chromatin regulators (chromatin remodelers) work in concert with the other class (histone chaperones) to dynamically regulate H2A.Z incorporation at the genomic level, thereby creating a specific

transcriptional context. This mechanism epitomizes the multi-modular nature of chromatin-based biology in the context of transcriptional regulation.

Consistent with the aforementioned changes in structure and organization of chromatin during ES cell differentiation, chromatin regulators are essential for early development, cell fate decisions and stem cell maintenance. Gene targeted disruption of genes encoding PRC2 core subunits (Ezh2, Eed and Suz12) and PRC1 core component Ring1b in mouse leads to an embryonic lethal phenotype between E7.5-E10.5, accompanied by gastrulation defects (Faust et al., 1995; O'Carroll et al., 2001; Pasini et al., 2004; Voncken et al., 2003). In addition, chromatin regulators are indispensible for cell fate decisions of both ES cells and tissue-specific stem cells (Laugesen and Helin, 2014). Indeed, genetic ablation of the core component of PRC1 (Bmi1) in hematopoietic stem cells (HSCs) leads to promiscuous expression of key B cell-specific transcription factors (i.e. Ebf1 and Pax5), which in turn leads to aberrant lymphoid specification and depletion of the HSC pool (Oguro et al., 2010). Given their integral roles in development and cellular differentiation, it may not come as a surprise that numerous chromatin regulators are found frequently mutated in a variety of diseases such as cancer and autism spectrum disorder (ASD) (Iossifov et al., 2014; Ronemus et al., 2014; Suva et al., 2013). In particular, there is an unusually high mutational load in chromatin regulators across multiple types of cancer. Pan-cancer studies show that many tumors harbor driver mutations in gene encoding a wide range of chromatin regulators such as the chromatin remodeler CHD4 and the chromatin remodeler SMARCA4 (i.e. BRG1). Genes encoding histone modifying enzymes such as the H3K4-specific lysine methyltransferase MLL2/MLL3/MLL4, the H3K27-specific methyltransferases EZH1/EZH2, the H3K27-specific lysine demethylase KDM6A (i.e. UTX) are frequently mutated.

Lastly, genes encoding histones HIST1H1E/HIST1H3B/HIST1H4E are also found frequently mutated (Kandoth et al., 2013; Lawrence et al., 2014). These findings clearly illustrate the integral roles of chromatin regulators and underscore the importance of faithful maintenance of chromatin structure and organizaiton in the context of cellular differentiation, development, and cancer.

Whole-genome sequencing studies have generated long lists of functionally important genes in many types of cancer and provide a clue as to how important cellular and molecular contexts are and how much they can dictate the underlying pathobiology of diseases (Garraway and Lander, 2013; Stratton et al., 2009). It has been long speculated that reversed differentiation (i.e. dedifferentiation) is the basis of certain tumor types (Friedmann-Morvinski and Verma, 2014; Kreso and Dick, 2014; Yates and Campbell, 2012; Ziv et al., 2013). Although this argument still remains to be proven, chromatin regulators seem to be a missing link between differentiation and cancer. Findings of frequent mutations of well-known chromatin regulators in cancer reinforce the notion that these two processes are tightly interrelated, perhaps two sides of the same coin: they share chromatin regulators as a common denominator.

1.3 CHD5 and CHD Family Chromatin Remodelers in Neural Differentiation and Brain Cancer

Since the first characterization of mouse Chd1 in 1993, the CHD family of chromatin remodelers (i.e. chromodomain helicase DNA binding proteins) have been the subject of a broad spectrum of functional and molecular studies. From a disease-related perspective, this group of

chromatin remodelers is known for their close connection to various diseases, such as dermatomyositis, cancer (e.g. glioma and neuroblastoma), complex birth defects (e.g. CHARGE syndrome), and developmental disorders (e.g. autism spectrum disorder). From a mechanistic perspective, well-characterized members such as Chd1 and Chd4 have discrete roles in regulating chromatin structure and organization to modulate transcription. While grouped together based on the structural similarity of their Snf2-related helicase domains, CHD chromatin remodelers are functionally diverse and are involved in many different cellular aspects.

Based on primary structure, the CHD family is classified as a subfamily of Snf2-related chromatin remodeler, consisting of 9 family members, from CHD1 to CHD9 (Flaus et al., 2006; Yap and Zhou, 2011) (Figure 1). The CHD family is further divided into three distinct subgroups: subgroup I (consisting of CHD1 and CHD2), subgroup II (consisting of CHD3, CHD4 and CHD5), and subgroup III (consisting of CHD6, CHD7, CHD8 and CHD9) (Flaus et al., 2006). Prototypical proteins for each subgroup are CHD1, CHD4, and CHD7, respectively. Each of the CHD family members share a Snf2-related helicase domain as well as a pair of tandem chromodomains that can facilitate interaction with either methylated histone tails or DNA. For example, CHD1 interacts with H3K4me3, whereas dMi-2 (the *Drosophila* CHD4) directly interacts with DNA (Bouazoune et al., 2002; Flanagan et al., 2005; Sims et al., 2005). In addition to tandem chromodomains, subgroup II proteins are unique in that they contain a second chromatin-interacting module—tandem PHD fingers (i.e. plant homeodomain zinc fingers)—with which CHD proteins can interact with either modified or unmodified histone tails (Egan et al., 2013; Oliver et al., 2012; Paul et al., 2013)

Mouse Chd1 is the archetype of the CHD family proteins as it was the first member to be characterized, and extensive biochemical studies have been conducted on yeast Chd1 and human CHD1 to elucidate its and molecular properties (Flaus et al., 2006). From a molecular perspective, CHD1 utilizes tandem chromodomains to recognize H3K4me3 across the genome to further facilitate the recruitment of the general splicing machinery, thereby conferring a transcriptional modulatory function (Sims et al., 2007). Yet, recent *in vivo* studies have revealed that *S. cerevisiae* Chd1 directly regulates active transcription; it changes the nucleosome organization around the TSS, thus exerting a direct modulatory role (Guzman-Ayala et al., 2015; Koh et al., 2015; Skene et al., 2014). Additionally, *H. sapiens CHD1* is found frequently mutated in castration-resistant prostate cancer, suggesting a connection between chromatin misregulation and prostate malignancy (Gao et al., 2014; Grasso et al., 2012).

Among members of CHD subgroup II, Chd3 (Mi-2α) and Chd4 (Mi-2β) were initially identified based on their structural similarity to the autoantigens Mi-2α and Mi-2β that are produced in the autoimmune disease dermatomyositis, and hence they were named Mi-2α/β (Aubry et al., 1998). Yet, it was the study of *Drosophila* dMi-2 (i.e. the ortholog of human CHD4) that uncovered its role in the transcriptional repression of homeotic genes (i.e. HOX) (Kehle et al., 1998). Seminal biochemical studies soon followed, identifying CHD3 and CHD4 as components of the multi-protein complex NuRD. This complex is composed of several chromatin/DNA-interacting components such as CHD3/4, histone deacetylase HDAC1/2 and methyl-CpG-binding protein 3 (MBD3) (Xue et al., 1998; Zhang et al., 1998). Via its histone deacetylase activity, NuRD acts as a transcriptional repressor. In addition, *CHD4* has been broadly implicated in multiple types of cancer (Lawrence et al., 2014). From a structural

perspective, subgroup II is unique in that Chd3/4/5 proteins have paired PHD zinc fingers. In particular, CHD5 physically interacts with both modified and unmodified histone tails via their PHDs (Oliver et al., 2012; Paul et al., 2013).

The last member of this subgroup, *CHD5*, was initially identified as a novel tumor suppressor gene located in a discrete region on the short arm of chromosome 1 (i.e. 1p36), which is frequently deleted in glioma as well in many other cancers (Bagchi and Mills, 2008; Bagchi et al., 2007). Our laboratory made this discovery, being the first to implicate a member of the CHD protein family in cancer (Bagchi and Mills, 2008; Bagchi et al., 2007). Multiple somatic mutations not only in *CHD5* but in other CHD family members (e.g. *CHD1* and *CHD4*) in a broad range of cancer types have been found since then (Grasso et al., 2012; Kolla et al., 2014; Lawrence et al., 2014). For the past several years, *CHD5* has been the center of attention for its novel connection with a broad range of cancers. In addition to frequent mutations and genomic alterations, *CHD5* is also subject to extensive DNA methylation at CpG sites within its promoter, providing evidence that *CHD5* is subject to inactivation by several mechanisms (Kolla et al., 2014; Koyama et al., 2012; Mulero-Navarro and Esteller, 2008). Together, these findings have confirmed our initial discovery of the tumor suppressor role of Chd5 (Bagchi et al., 2007; Kolla et al., 2014). Yet, our group and other groups have recently broadened the spectrum of the functional roles of Chd5. We and other groups found that Chd5 has an integral function in regulating chromatin compaction and in maintenance of chromatin integrity during sperm development, as Chd5-deficiency leads to male infertility, defective chromatin compaction, and genomic instability in male mice (Li et al., 2014; Zhuang et al., 2014). Of note, we reported that men with compromised fertility have decreased CHD5 expression (Li et al., 2014). Chd5 also

plays a critical role in neuronal differentiation during early development of mouse brain (Egan et al., 2013). Acute abolishment of Chd5 using *in utero* electroporation during a critical period of embryonic brain development (i.e. E14.5-E18.5) hampers migration of differentiating neocortical neuronal progenitors and expands the neural progenitor pool in the germinal zone (i.e. the ventricular, subventricular, and intermediate zones) (Egan et al., 2013). Notably, Chd5 appears to have distinct functional roles in different tissue types (i.e. sperm and brain), thus suggesting that its function is dependent on tissue-specific or cell-type-specific contexts.

Acute knockdown of Chd5 at E14.5-E18.5 severely compromises migration of neural progenitor cells within mouse embryonic neocortex (Egan et al., 2013). The majority of cells transduced with shRNA against Chd5 (i.e. shChd5) fail to exit the germinal zone. At the molecular level, Chd5 knockdown in ES cell-derived NPCs leads to a failure to induce expression of neuronal genes, thereby confirming a role of Chd5 in transcriptional regulation of neuronal differentiation. From this study, it seems evident that Chd5 is involved in transcriptional regulation of neuronal genes in NPCs, and that perturbation of Chd5 hinders proper neuronal migration in mouse embryonic brain. Yet, this study was limited in that shRNA-mediated knockdown does not completely abolish Chd5 expression (>60% reduction). In addition, neuronal differentiation and corticogenesis still take place. The neocortex structure also appears to be retained (Egan et al., 2013). Thus, more work is warranted to determine whether Chd5 deficiency broadly affects neuronal differentiation or more strictly impairs neuronal migration. To determine the role of Chd5 in chromatin dynamics and gene expression in neuronal differentiation, a well-defined cellular system is necessary.

At the molecular level, Chd5 interacts with unmethylated hisone tails through its tandem PHD zinc fingers, and this interaction is critical for transcription regulation (i.e. both repression and activation) of cancer-related target genes (Paul et al., 2013). Additionally, *in vitro* biochemical approaches show that Chd5 physically interacts with modified histone tails (i.e. H3K27me3), and that the chromodomains are required for this interaction, as the interaction between Chd5 fragments and H3K27me3 peptides are significantly attenuated in the absence of tandem chromodomains (Egan et al., 2013; Paul et al., 2013). Additionally, purified human CHD5 is capable of reorganizing nucleosome arrays on DNA templates, thus verifying its chromatin remodeling function (Quan and Yusufzai, 2014). Taken together, these findings underscore an important role for Chd5 inactivation in pathobiology of multiple types of cancer and shed light on its molecular functions in regulating chromatin and gene expression.

CHD subgroup III has been unambiguously implicated in two diseases. *CHD7* is identified as the most frequently mutated gene in the complex birth defect CHARGE syndrome (i.e. coloboma, heart defect, atresia choanae, retarded growth and development, genital abnormality, and ear abnormality), where multiple organs are malformed at birth (Vissers et al., 2004; Wong et al., 2015). Haploinsufficiency and loss-of-function mutations in *CHD7* during early development has been identified as its cause of CHARGE syndrome. At the molecular level, disrupted neurogenesis has been the most plausible mechanism that underlies the molecular pathology of the disease (Kim and Roberts, 2013; Vissers et al., 2004; Wong et al., 2015). A mouse model study revealed that in NSCs Chd7 is involved in transcriptional regulation of genes encoding key neuron-specific transcription factors—that is, Sox4 and Sox11—by modulation of chromatin organization at promoters of these two genes (Feng et al., 2013). *CHD8*, on the other

hand, has recently been identified as one of the most frequently mutated genes in ASD (i.e. autism spectrum disorder) patients, thus providing a clue for mechanisms for chromatin-related disease mechanisms (Iossifov et al., 2014; O'Roak et al., 2012).

1.4 Summary

Taken together, the examples discussed above highlight the importance of faithfully regulating chromatin structure and organization in the context of transcriptional regulation, cellular differentiation, and cancer. Disarrayed chromatin structure and organization leads to aberrant transcription of cell-type-specific and tissue-specific gene expression programs, which in turn impedes precise spatiotemporal execution of cell fate decisions during cellular differentiation and development. Altered cellular differentiation can underlie certain types of cancer. As a proof-of-principle, pan-cancer genomic studies have identified multiple chromatin regulators that are subject to mutation across many different types of cancer.

Given such a close connection between chromatin and cancer, how misregulation of chromatin regulators sets the stage for the formation and progression of tumors is an essential question. Yet, a clear-cut answer has not been obtained. It is difficult to infer a direct functional consequence of chromatin misregulation because chromatin is deeply integrated into the eukaryotic cellular systems at the most fundamental level; missteps in chromatin regulation may bring multifactorial consequences. Therefore, unless there is prior knowledge about the context-specificity of chromatin regulators, relevant functional studies may not be quite straightforward.

In this regard, previous studies provide useful clues about tissue-specific and cell-type-specific contexts where Chd5 is biologically relevant. We and other groups found that Chd5 is robustly expressed in the adult mouse brain (Vestin and Mills, 2013). Its expression is most prominent in terminally differentiated post mitotic neurons, yet Chd5 is also detected in a considerable fraction of late-stage neural progenitors (see Chapter 2) (Egan et al., 2013). Given its implication in brain cancers such as glioma, it is feasible that Chd5 has a specialized function in the brain (Bagchi et al., 2007). Support for this idea has been obtained in our lab as Chd5-deficient mice have abundant behaviors and altered dendritic arborization (Horev et al., unpublished). In parallel to my work, our group also revealed an integral role of Chd5 in the male germline during the sperm-specific chromatin remodeling process of spermiogenesis (Li et al., 2014). Consistent with the observation of low CHD5 expression in infertile men, Chd5 deficiency causes defective sperm chromatin compaction, DNA damage, loss of genomic integrity, and male infertility in mice (Li et al., 2014). Most importantly, these two findings suggest that its functional role is highly dependent on the tissue and cellular context, as Chd5 confers seemingly distinct functions in two different contexts in which it had been analyzed.

To this end, I focused my thesis research on neural stem/progenitor cells, as my key observation indicated that Chd5 was expressed in a subpopulation of Pax6-positive transit amplifying progenitors (i.e. type C cells) in both embryonic and neonatal mouse brain. Subsequently, I implemented a primary NSCs culture system to examine the cellular properties of Chd5-deficient NSCs. I found that loss of Chd5 fundamentally changed the properties of these cells and their stem cell characteristics, which was accompanied by changes in NSC-specific gene expression programs. While the differentiation capacity of *Chd5*-/- NSCs to give rise to the

major neural lineages (i.e. neurons and astrocytes) remained intact, cell fate was biased towards the astrocytic lineage. At the chromatin level, Chd5 loss led to the marked global reduction in the repressive histone mark H3K27me3. In Chd5-deficient NSCs, promoters of key neuronal precursor markers (i.e. *Eomes*) displayed retained H3K27me3 levels, suggesting Chd5/H3K27me3-mediated transcription repressive mechanisms on a select group of neuronal genes. At the mechanistic level, loss of Chd5 led to an increase in expression of the H3K27me3-specific demethylase Utx, thereby accounting for global reduction of H3K27me3. Together, these findings underscore an important functional role of Chd5 in the context of neural differentiation.

In the following chapters, I will present evidence for altered neural cell fate decisions of *Chd5*-/- NSCs and the underlying responsible molecular mechanisms. I will further provide experimental evidence that Chd5 regulates gene expression programs of lineage-specific genes by modulating structure of chromatin specifically at promoters. I will then present evidence for a functional interplay between Chd5 and the H3K27me3-specific histone demethylase Utx. Together, I will comprehensively show that Chd5 is deeply rooted in brain development, and misregulation of Chd5 loss leads to aberrant neural cell fate decisions.

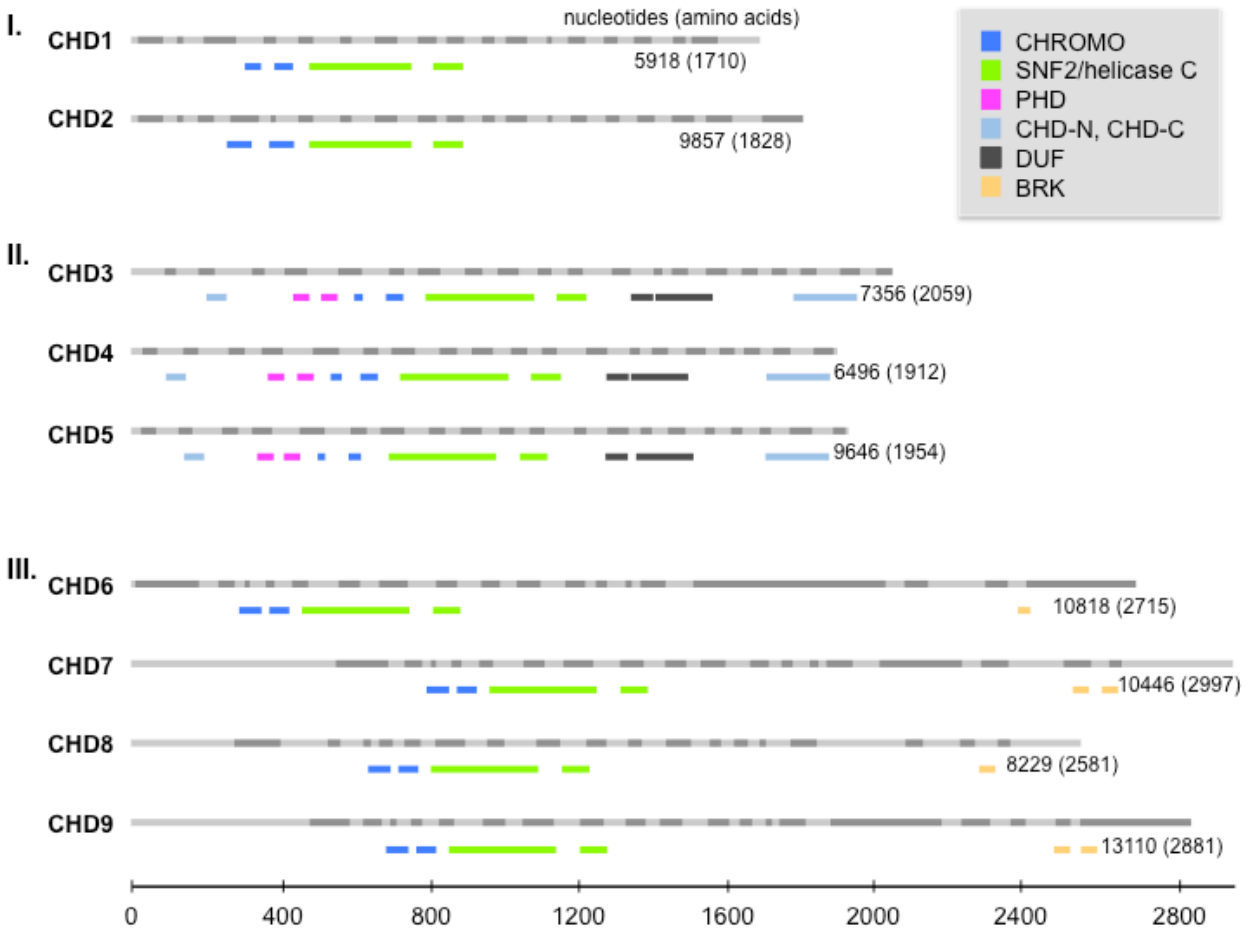

Figure 1: The CHD family of chromatin remodelers

CHD proteins are classified into three sub-families (Roman numerals) based on their functional motifs (see legend). The human CHD family based on Ensembl is drawn to scale, with light and gray bars depicting alternating exons (above) and the functional motifs from PFAM (a database of protein families of multiple sequence alignments generated using hidden Markov models) shown in color (below) for each CHD member. The number of nucleotides and amino acids for the CHD transcript and protein, respectively, are shown.

BRK: Brahma and Kismet domains; CHD: chromodomain helicase DNA binding; CHROMO: Chromodomain; CHD-N, CHD-C: CHD_N and CHD_C are shown in upstream and downstream region, respectively; DUF: Domain of unknown function; PHD: Plant homeodomain; SNF2/Helicase C: SNF2_N and Helicase_C are shown in upstream and downstream region, respectively. Figure from Li et al. (2014)

Chapter 2. Chd5-mediated Chromatin Dynamics in Neural Cell Fate Decisions

2.1 Expression of Chd5 in Neural Stem/Progenitor Cells and Induction of *Chd5* during Neural Differentiation

It has been demonstrated that Chd5 shows tissue-specific expression patterns; transcript or protein are highly abundant in the central nervous system (CNS) and testes, whereas expression is either low or undetectable in other tissues, including heart and lung (Potts et al., 2011). At the cell-type-specific expression level, robust expression of Chd5 has been detected in terminally differentiated neurons and spermatids of the adult mouse (Li et al., 2014; Vestin and Mills, 2013). Based on its predominant expression pattern in post-mitotic neurons, it has been postulated that Chd5 confers a specific function in the neuronal lineage.

Despite the initial focus on its robust expression in neurons, our study as well as that of an independent group consistently demonstrated that Chd5 is expressed in subsets of type C neural transit amplifying progenitors (i.e. Nestin-positive neural progenitors and Sox3-positive late-stage neural progenitors) and in the type A early committed neuronal precursor population (i.e. Dcx-positive neuronal precursor cells) at later stages of gestation (E18.5) (Egan et al., 2013; Vestin and Mills, 2013). Based on its expression pattern in early committed neuronal precursors, terminally differentiated neurons, and the compromised neuronal migration phenotype in embryos that had been transduced with a short hairpin targeting Chd5, it has been suggested that Chd5 played a crucial role in neuronal differentiation (Egan et al., 2013). Yet, it had been unclear until my thesis work whether Chd5 plays a specific role in the uncommitted multipotent NSC

population, and the functional importance of Chd5 during early brain development had yet to be explored.

To examine expression of Chd5 in NSCs, I examined the cell-type-specific expression pattern of Chd5 in mouse embryonic brain (E15.5) and neonatal brain (P1) using immunofluorescent analysis. In particular, I focused on expression of Chd5 within the Pax6-positive NSC population that resides in periventricular regions, spanning ventricular zone-subventricular zone (i.e. VZ-SVZ) of embryonic and neonatal brain so as to probe the mutual relationship between Chd5 and NSCs (Ihrie and Alvarez-Buylla, 2011; Kriegstein and Alvarez-Buylla, 2009; Lim and Alvarez-Buylla, 2014). Representative images of immunofluorescent analysis are shown in Figures 2-3. Chd5 was expressed in a subset of Pax6-positive neural stem/progenitor cells in the periventricular regions of both E15.5 and P1 neonatal brain. While a considerable fraction of cells displayed co-expression pattern, most of the cells that expressed distinctively high level of Pax6 appeared to lack Chd5 expression, either missing or expressing low levels of Chd5. Conversely, the vast majority of Chd5-expressing cells (presumably differentiating neurons) were missing Pax6 expression. A plausible interpretation of this nearly mutually exclusive co-expression pattern is that Chd5 expression is induced as Pax6 expression declines in NSCs. During neural differentiation, Chd5 expression may begin to increase as NSCs exit from multipotent and uncommitted progenitor state. In the same analysis, the absence of Chd5 expression in homozygous brain samples was confirmed, demonstrating that the disrupted *Chd5* allele is functionally null, yet Pax6 expression was still detected (Data not shown). These observations verify that Chd5 is indeed expressed in multipotent Pax6-positive transit amplifying progenitor cells (i.e. NSCs), thereby implicating its role in neural progenitor population.

Based on this finding, I hypothesized that Chd5 confers a specific function in the differentiation of NSCs. In order to test my hypothesis, I first devised primary neural stem/progenitor cell culture system (NSCs) (Deleyrolle and Reynolds, 2009; Marshall et al., 2008; Reynolds and Weiss, 1992). Hereafter I will use the term, "primary NSCs," to refer to primary NSC cultures. Subsequent characterization of cells utilizing flow cytometry analysis showed that as expected, primary NSCs from wild type mice were comprised of heterogeneous cell populations. Less proliferative Cd133-positive neural stem cells made up of the smallest proportion (~22%). Highly proliferative Egfr-positive transit amplifying neural progenitor cells—that is, Nestin-positive and Pax6-positive cells—constituted the largest proportion of primary NSCs (~86%) (Figure 4A). Surprisingly, a considerable proportion of the cells were composed of cells expressing early committed neuronal precursor cell marker Cd24, which represented ~51% of $Cd24^{Low}$ and ~2% of $Cd24^{High}$, respectively. However, the exact identity of the $Cd24^{Low}$ population is still debatable, as Egfr-positive transit amplifying neural progenitor cells also have low expression of Cd24 (Mich et al., 2014). Strikingly, a comparison of cell surface marker expression profiles in wild type (+/+), heterozygous (+/-), and homozygous (-/-) NSCs revealed that +/- NSCs significantly differed from +/+ and -/- NSCs (Figure 4B). Yet, there was also a notable difference in Cd24-positive profiles between +/+ and , *Chd5*-/- NSCs which constituted 53% and 65% of the populations, respectively. This difference in cell surface marker profiles between different genotypes is not only a reflection of distinct differentiation states of those cells but also suggestive of differing cellular properties depending on genotype, both of which directly or indirectly affects neural differentiation.

It has been observed that Chd5 is robustly expressed in terminally differentiated neurons (Egan et al., 2013; Potts et al., 2011; Vestin and Mills, 2013). As I described, Chd5 was also expressed in Pax6-positive NSCs. Based on these observations, the timing of *Chd5* induction was arbitrarily inferred as some time during early brain development. However, the exact time frame and the extent of changes in *Chd5* expression during neural differentiation had yet to be defined. To address this, I compared Chd5 expression in +/+ primary NSCs and +/+ NSC-derived neural cells (i.e. day 4 samples of *in vitro* neurogenesis). Importantly, these primary NSCs were capable of giving rise to major neural lineages (i.e. neurons and astrocytes), as previously described (Figure 11) (Louis et al., 2013). I then measured expression levels of *Chd5* transcript in undifferentiated +/+ NSCs and differentiated +/+ NSC-derived neural cells using RT-qPCR. As expected, *Chd5* expression in +/+ NSCs was low. Normalized expression value relative to the endogenous control *Actb* (ΔCt) was 13-14. Expression of *Chd5*, however, drastically increased by ~25 fold in differentiated +/+ neural cells (at day 4 of differentiation) (Figure 5). In summary, the marked induction of *Chd5* suggests that Chd5 plays a role at early stages of *in vitro* neural differentiation and indicates that Chd5 is under a fine regulatory control during this process.

2.2 Role of Chd5 in Homeostasis of Neural Stem/Progenitor Cells

Recent studies in which neural stem cells isolated from mouse brain identify two distinct cellular populations. Codega et al. reported that NSCs can be divided into two groups based on cell surface marker expression profiles: less proliferative quiescent NSCs (qNSCs) and highly proliferative activated NSCs (aNSCs). Intriguingly, qNSCs (i.e. Egfr-negative population) and

aNSCs (Egfr-positive population) display not only distinct cell surface marker expression profiles, but these cells also have inherently different cellular properties and behaviors with regards to proliferation, neurosphere formation capacity, and *in vivo* differentiation propensity (Codega et al., 2014). Similarly, Mich et al. report that quiescent and activeed populations of NSCs display consistently distinct cell surface marker expression profiles and have different cellular properties (Mich et al., 2014).

In line with these findings, I observed that cell surface marker expression profiles of $Cd24^{Low}$ populations in +/+ and -/- primary NSCs substantially differed, and hence this difference may be indicative of distinct cellular states of two groups. To test this hypothesis, I first examined expression of cell-type-specific markers by western blot analysis. As a result, I found that Nestin and Pax6—markers for highly proliferative aNSCs—were increased in total cell lysates of *Chd5*-/- NSCs. A marked increase in Nestin expression in *Chd5*-/- NSCs was confirmed by immunofluorescent image analysis (Figure 6A-B). In addition, I found that Tbr1 and Tbr2—markers for early committed neuronal precursor cells—were decreased in total cell lysates of *Chd5*-/- NSCs, which was consistent with downregulation of *Tbr1* and *Eomes* (Tbr2) transcripts in *Chd5*-/- NSCs (Figure 7). Together, these findings indicate that Chd5 loss in primary NSCs leads to a skewed enrichment of the Nestin-positive aNSCs population.

Next, I examined proliferation of +/+ and *Chd5*-/- primary NSCs over a period of 6 days. +/+ NSCs (n=2) and *Chd5*-/- NSCs (n=3) were seeded at the same cell density and maintained as neurosphere cultures for 6 days. Changes in cell number were monitored over the period of time

by counting dissociated cells. As expected, cell counts of *Chd5*-/- NSCs were higher than that of wild type counterparts between day 4 and day 6 (Figure 8). I assessed neurosphere formation capacity as a proxy measure of self-renewal capacity in +/+ (n=3) and *Chd5*-/- NSCs (n=3) by measuring diameters of neurspheres. Strikingly, *Chd5*-/- NSCs formed significantly larger neurospheres (Figure 9). Quantification clearly showed that the overall size of *Chd5*-/- NSCs was significantly larger than that of +/+ NSCs (Figure 10A). Most intriguingly, this trend was reversed when mouse *Chd5* cDNA (*Chd5* variant 2, NCBI Reference Sequence ID: NM_029216.2) was ectopically expressed in *Chd5*-/- NSCs (Figure 10B). These findings provide evidence that Chd5 is directly involved in maintaining homeostasis of NSCs. When Chd5 is deficient, proliferation and self-renewal of NSCs were enhanced. Yet, it is unclear whether changes in proliferation and self-renewal are a reflection of changed properties of the whole population or whether these changes affect a specific subpopulation. The latter is certainly plausible as Egfr-positive population is more proliferative than other Cd133-positive and $Cd24^{Low}$/$Cd24^{High}$ populations.

Taken together, changes in cell surface marker expression profiles and altered cellular properties of *Chd5*-/- NSCs corroborate the notion that Chd5 loss leads to aberrant enrichment of a specific population of NSCs—that is, highly proliferative aNSCs. It is likely that increased proliferation and enhanced neurosphere formation capacity are the consequences of enrichment of aNSC population. More importantly, it is plausible that enrichment of aNSCs population in *Chd5*-/- NSCs consequently affects neural differentiation.

2.3 Altered Cell Fate Decisions in Chd5-deficient Neural Stem/Progenitor Cells

As previously discussed, I hypothesized that Chd5 confers a specific function in neural differentiation. Aforementioned changes in cell surface marker expression profiles and changed cellular properties caused by Chd5 loss, suggest that neural differentiation is affected. To directly test this hypothesis, I implemented *in vitro* neural differentiation assays. Briefly, +/+ NSCs and *Chd5*-/- NSCs were enzymatically dissociated and subsequently seeded onto poly-D-lysine/laminin-coated tissue culture chamber slides or plates. These NSC-derived adherent cultures were subject to *in vitro* neural differentiation assays. Subsequently, samples were collected at the initial time point (i.e. day 0) and the final time point (i.e. day 4 or day 7), and samples were analyzed for their morphological features and cell-type-specific marker expression patterns by immunofluorescent image analysis.

As a result, two major neural lineages (i.e. neurons and astrocytes) were generated at day 4 and day 7 of differentiation (Figures 11-12). Cell-type-specific marker expression analysis by immunofluorescent staining identified cells expressing the neuronal marker Map2 and the astrocytic marker Gfap. In particular, these differentiated neurons appeared to be young neurons because they had only (2-3) neuronal projections (i.e. neurites) per cell (Figure 10A). Day 4 +/+ differentiated cultures were mainly comprised of Map2-positive neurons (~56%), with a smaller fraction of Gfap-astrocytes (~23%) (Figure 11A-B). In contrast, *Chd5*-/- differentiated cultures showed a significantly different cellular composition, in which Gfap-positive astrocytes made up of the largest fraction (~50%), with Map2-positive neurons making up a smaller fraction (~34%). Thus, Chd5 deficiency led to a significantly skewed cellular composition (i.e. altered cell fate)

(Figure 11A-B). Consistent with this observation, day 7 *Chd5*-/- differentiated cultures displayed a similar astrocytic propensity as I had observed at day 4 of differentiation. More Gfap-positive astrocytes (~63%) and fewer Map2-positive neurons (~23%) were observed in *Chd5*-/- cells in comparison with the wild type counter parts (Figure 11). Notably, comparison between day 4 and day 7 of differentiation revealed differences depending on the duration of differentiation, as both +/+ and *Chd5*-/- day 7 samples were composed of a lower proportion of Map2-positive neurons and a higher proportion of Gfap-positive astrocytes than the corresponding day 4 samples (Figures 11-12). A plausible explanation for this phenomenon is that as differentiation proceeds, the more proliferative astrocytes thrive, which eventually leads to the increased presence of astrocytes. Therefore, both day 4 and day 7 results are consistent as they clearly showed that loss of Chd5 did not entirely abolish neuronal differentiation, but rather altered cell fates by skewing toward the astrocytic fate.

To validate the causal relationship between Chd5 loss and skewed cell fate decisions, neural differentiation assays were performed using +/+ and *Chd5*-/- NSCs transduced with mouse *Chd5* cDNA (*Chd5* variant 2, NCBI Reference Sequence ID: NM_029216.2). As a result, day 7 control cultures (i.e. +/+; empty vector and *Chd5*-/-; empty vector) had cellular compositions that were consistent with the results of previous experiments using untreated cells, where loss of Chd5 led to a skewed cellular composition toward the astrocytic lineage in *Chd5*-/-; EV neural cells (~13% of Map-positive neurons and ~72% of Gfap-positive astrocytes) (Figure 13A-B). Strikingly, both +/+ and *Chd5*-/- samples expressing exogenous Chd5 (i.e. +/+; Chd5 and *Chd5*-/-; Chd5) displayed a significantly increased propensity toward the neuronal lineage; both groups generated more neurons than corresponding empty vector controls being increased

from ~31% to ~50% in +/+ differentiated neuronal cells, and being increased from ~13% to ~29% in *Chd5*-/- differentiated neuronal cells (Figure 13A-B). Importantly, the cellular composition of *Chd5*-/-; Chd5 cultures were comparable to that of +/+; EV, thereby indicating ectopic expression of Chd5 effectively rescued cell fate defects caused by Chd5 deficiency (Figure 13). The estimated extent of Chd5 overexpression in +/+; Chd5 cells were ~3-fold increase at the mRNA level (Data not shown), and ectopic expression of Chd5 in *Chd5*-/-; Chd5 cells was demonstrated by immunofluorescent analysis (Figure 14). Taken together, these findings indicate that Chd5 is involved in cell fate decisions and that loss of Chd5 leads to increased propensity toward the astrocytic lineage and decreased propensity toward the neuronal lineage. Ectopic expression of Chd5 in *Chd5*-/- NSCs reverted cell fate defects, thereby providing evidence that Chd5 is necessary and sufficient for proper spatiotemporal cell fate decisions of neural lineages.

2.4 Impact of Chd5 Loss on Global Gene Expression in Neural Stem/Progenitor Cells

Previous studies reported that knockout of Chd1 in ES cells and $Cd31^+$ endothelial cells alters global gene expression programs. In ES cells, glial lineage-specific genes are aberrantly upregulated, and hematopoietic cluster cells (HCC)-specific genes are downregulated in $Cd31^+$ endothelial cells (Gaspar-Maia et al., 2009; Koh et al., 2015). Based on these previous findings showing that a family member CHD protein is directly involved in transcriptional regulation of cell-type-specific genes, I hypothesized that loss of Chd5 leads to altered NSC-specific gene expression programs that underlie the cell fate defects of *Chd5*-/- NSCs.

To test my hypothesis, I examined global gene expression patterns of +/+ NSCs (n=2), *Chd5*+/- NSCs (n=5), and *Chd5*-/- NSCs (n=2) by RNA-seq analysis. As a result, a large number of genes (n=1040) were found differentially expressed between +/+, *Chd5*+/-, and *Chd5*-/- NSCs. Most strikingly, the majority of differentially expressed genes (n=981) were upregulated in *Chd5*-/- NSCs and two of the five *Chd5*+/- NSCs, whereas a small number of genes (n=59) were downregulated in these samples, thus suggesting that Chd5 is involved predominantly in transcriptional repression (Figure 15). Hierarchical clustering analysis further revealed a bimodal nature of the *Chd5*+/- NSC samples. That is, expression patterns of three *Chd5*+/- NSCs samples clustered with that of +/+ NSCs, whereas expression patterns of the other two clustered with that of *Chd5*-/- NSCs (Figure 15). Consistent with this finding, we have previously identified bimodal characteristic of *Chd5*+/- animals in other aspects, including quantitative behaviors and neuronal dendritic arborization (Horev et al., unpublished).

Another notable feature was that 68% of genes among differentially expressed genes showed variability across the genotypes (i.e. +/+, *Chd5*+/-, and *Chd5*-/-) mostly due to bimodal expression patterns of *Chd5*+/- samples. Therefore, the list of differentially expressed genes was partitioned into two groups: consistently altered genes and inconsistently altered genes (Figure 16). Subsequent gene ontology analyses revealed that altered genes were highly enriched for various biological processes (Mi et al., 2013). In particular, consistently altered genes were highly enriched for translation (GO:0006412) and cellular protein metabolic process (GO:0044267) (Figure 16A). Inconsistently altered genes were highly enriched for neuron-specific processes such as positive regulation of dendritic spine development (GO:0060999) and regulation of dendritic spine development (GO:0060998) (Figure 16B).

Among consistently altered genes, I identified the quiescent neural stem cell markers *Slc1a3* and *Id1* as being downreguated (~2.4 fold downregulation and ~2.9 fold downregulation, respectively) (Figure 17) (Kumamoto and Hanashima, 2014; Nam and Benezra, 2009). Conversely, the neural progenitor cell marker *Plxnb2* was upregulated (~1.9 fold upregulation), thereby supporting the notion that loss of Chd5 leads to aberrant enrichment of the highly proliferative activated neural progenitor population and causes changes in cellular states, switching to activated neural progenitors (Figure 17) (Mich et al., 2014). Genes encoding either extracellular signaling molecules or their cognate receptors were significantly upregulated in *Chd5*-/- NSCs. Interestingly, *Fgfr1* (~2.3 fold upregulation), *Bmp3* (~62.5 fold upregulation), and *Wnt7b* (~2.1 fold upregulation) are implicated in early telencephalic development (Figure 18) (Hebert and Fishell, 2008; Kumamoto and Hanashima, 2014). In addition, a group of genes (i.e. *Polr2a*, *Polr2c*, *Polr2e*, *Polr2i*, and *Polr2f*) that encode components of RNA polymerase II subunits was collectively upregulated (1.9-4.5 fold upregulation) in *Chd5*-/- NSCs, suggesting that *Chd5*-/- NSCs undergo a general hypertranscriptional state, where demand for RNA polymerase II was increased (Figure 19). Despite a general upregulation trend and increased expression of RNA polymerase II subunit genes, several components of transcriptional repressive chromatin regulator complexes, including genes encoding Cbx6 of PRC1, Jarid2 of PRC2, and Mbd3 of NuRD, were upregulated in *Chd5*-/- NSCs (2.3-3.5 fold upregulation) (Figure 20). This suggests that chromatin regulation, and/or chromatin homeostasis, are also affected by Chd5 deficiency.

Taken together, our results clearly indicate that loss of Chd5 alters global gene expression programs by inducing the vast number of genes, which were otherwise repressed in +/+ NSCs.

Therefore, Chd5 appears to work as a transcriptional repressor in primary NSCs. When analyzed for gene ontology categories, these differentially expressed genes were enriched for protein homeostasis and regulation of neuronal dendritic development. Among consistently altered genes, expression patterns of important cell-type-specific markers supports the hypothesis that loss of Chd5 leads to enrichment of activated neural progenitor cells. In addition, Collective upregulation of multiple subunits of RNA polymerase II indicates that *Chd5*-/- NSCs are in hypertranscriptional state. Lastly, upregulation of components of signaling pathways critical for early telencephalon development and transcriptional repressive chromatin regulator complexes may indicate a disarray in chromatin structure and organization.

2.5 Changes in Chromatin Structure Due to Chd5 Loss and Functional Link between Chd5 and the Histone H3K27me3-specific histone demethlyase Utx

It has been demonstrated that Chd5 physically interacts with the N-terminal tail of histone H3. Yet, it also interacts with covalently modified histone tail such as H3K27me3 (Egan et al., 2013; Paul et al., 2013). As discussed earlier, the transcriptional repression mark H3K27me3 undergoes dynamic changes during ES cells differentiation. In addition, the gene set enrichment analysis (GSEA) identified a subset of differentially expressed genes in *Chd5*+/- NSCs, and *Chd5*-/- NSCs were significantly enriched for the gene sets whose promoters are decorated with bivalent histone marks (i.e. H3K4me3 and H3K27me3) in mouse brain (Data not shown). Importantly, these genes tend to be those that encode factors critical for development (Meissner et al., 2008). Therefore, I hypothesized that Chd5 mediates H3K27me3 dynamics during neural differentiation, and that this is key for modulating cell fate decisions.

To test this hypothesis, I initially examined the overall level of H3K27me3 in +/+, *Chd5*+/-, and *Chd5*-/- NSCs by western blot analysis. Intriguingly, a marked reduction in H3K27me3 levels was observed in *Chd5*+/- and *Chd5*-/- NSCs (Figure 21A). Subsequently, immunofluorescent analysis confirmed a global reduction of H3K27me3 as well as H3K27me2 in *Chd5*-/- NSCs (Figure 21B). Remarkably, ectopic expression of Chd5 cDNA (*Chd5* variant 2, NCBI Reference Sequence ID: NM_029216.2) significantly increased the overall level of H3K27me3 in both +/+ and *Chd5*-/- NSCs, thereby suggesting a direct regulation of H3K27me3 by Chd5 (Figure 21C).

These findings raised an important question regarding the status of H3K27me3 across the genome in *Chd5*-/- NSCs. To answer this question, I performed chromatin immunoprecipitation and analyzed the extent of enrichment for H3K27m33 at specific loci using qPCR (ChIP-qPCR). I assessed the enrichment of H3K27me3 at promoters using primers specific for the loci (i.e. the upstream genomic region within 1kb from the TSS of each gene) and gene bodies using primers specific for the regions (i.e. downstream intragenic region between 2.0 and 6.5 kb from the TSS of each gene) of eight cell-type-specific marker genes in +/+ and *Chd5*-/- NSCs (Figure 22A-B). *Pax6*, *Ascl1*, and *Sox4* are genes that encode important transcription factors for neural progenitor cells and are expressed in primary NSCs (Kriegstein and Alvarez-Buylla, 2009). *Eomes* (i.e. Tbr2) and *Cux1* are critical transcription factors for cortical neuron development and are expected to be expressed to a lesser extent in these cells (Franco and Muller, 2013). *Cspg4* encodes a prominent marker for a subtype of oligodendrocyte progenitors (OPC), yet its expression is also detected in neural progenitors (Aguirre et al., 2007). *Snap25* encodes a marker

for neurons, and *Slc1a2* is a marker for astrocytes (Franco and Muller, 2013); expression of both genes are relatively low in NSCs.

I observed differing enrichment of H3K27me3 over the 16 genomic sites that I analyzed. Consistent with results from western blots and immunofluorescent analyses, overall H3K27me3 enrichment was significantly lower in *Chd5*-/- NSCs (Figure 22C). When H3K27me3 enrichment patterns between +/+ and *Chd5*-/- NSCs were compared, all genes except *Eomes* showed consistent reduction in H3K27me3 enrichment in *Chd5*-/- NSCs. At promoter and gene body of *Eomes*, H3K27me3 enrichment was similar, or slightly higher, and significantly higher, respectively, in *Chd5*-/- NSCs (Figure 22A-B). Importantly, this enrichment pattern was inversely correlated with the expression levels of *Eomes*; it was significantly downregulated in *Chd5*-/- NSCs, thereby suggesting a causal relationship (Figure 23). In contrast, *Slc1a2* displayed lower H3K27me3 both at the promoter and within gene bodies, and its mRNA expression was upregulated in *Chd5*-/- NSCs (Figure 23). These results indicated that there were two distinct mechanisms existing to modulate H3K27me3 at different genomic sites. H3K27me3 enrichment patterns are inversely correlated with expression of *Eomes* and *Slc1a2*, and hence transcription of at least these two genes are directly influenced by the higher and lower enrichment levels of H3K27me3.

It remained unclear how H3K27me3 was reduced in *Chd5*-/- NSCs. In particular, Chd5 is not equipped with either a histone methyl transferase or a histone demethylase module. Therefore, I reasoned that Chd5 functionally or physically interacts with either H3K27me3-

specific histone methyltransferase (i.e. Ezh2) or H3K27me-specific histone lysine demethylases (i.e. Utx or Jmjd3) to modulate H3K27me3 levels in *Chd5*-/- NSCs. RT-qPCR and western blot analyses demonstrated that an increased level of Utx (*Kdm6a*) in *Chd5*-/- NSCs (Figure 24). Importantly, shRNA-mediated knockdown of Utx rescued the cell fate defects of *Chd5*-/- NSCs, thereby providing evidence that Utx is responsible for a global reduction of H3K27me3 and that H3K27me3 levels are regulated by the functional interplay between Chd5 and Utx (Figure 25).

Taken together, these results demonstrate that loss of Chd5 leads to a global reduction of H3K27me3, which can be restored by ectopic expression of Chd5. At the genomic level, Chd5 loss consistently caused significant reduction of H3K27me3 at specific loci. Yet, at the promoter and within the gene body of *Eomes*, H3K27me3 levels are retained and even increased. Importantly, this distinct difference in the H3K27me3 enrichment pattern accounts for the downregulation of *Eomes* expression in *Chd5*-/- NSCs. The global reduction of H3K27me3 can be explained by the enhanced Utx expression in *Chd5*-/- NSCs. When Utx is depleted by shRNA-mediated knockdown, cell fate defects of *Chd5*-/- NSCs are rescued and H3K27me3 levels are re-established.

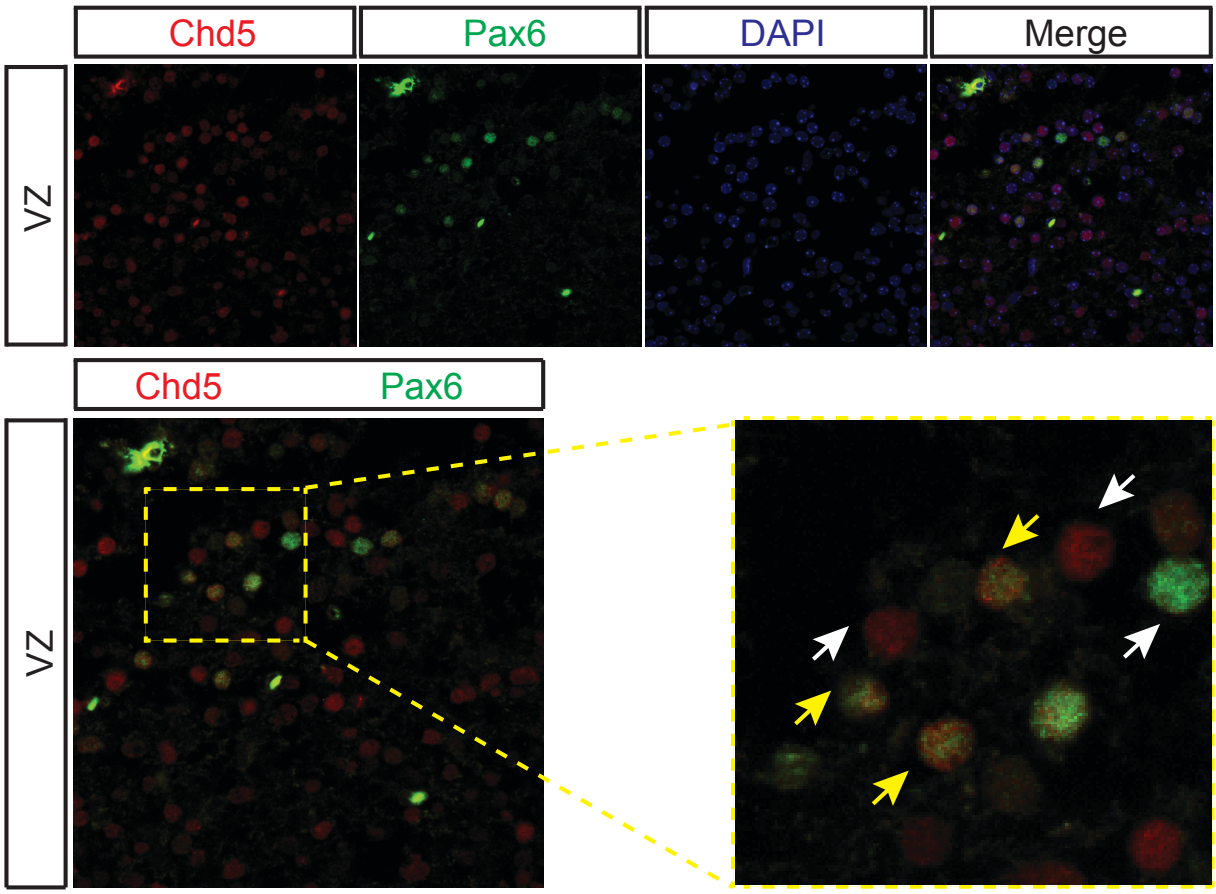

Figure 2: Expression of Chd5 in embryonic mouse brain

Expression of Chd5 was examined by immunofluorescent analyses of embryonic mouse brain sections. Shown are representative images of ventricular zone (VZ) of embryonic day 15.5 (E15.5) wild type mouse brain. Individual channels, Chd5 (red), Pax6 (green), DAPI (blue), and merged (merge), are shown (above).

Chd5 (red) and Pax6 (green) are shown in the merged image (left, below). Enlarged image of area (demarcated by yellow dashed line), where Chd5 (red)/Pax6 (green)-positive cells (yellow arrows) are present, is shown (right, below). Only Chd5-positive or only Pax6-positive are marked by white arrows.

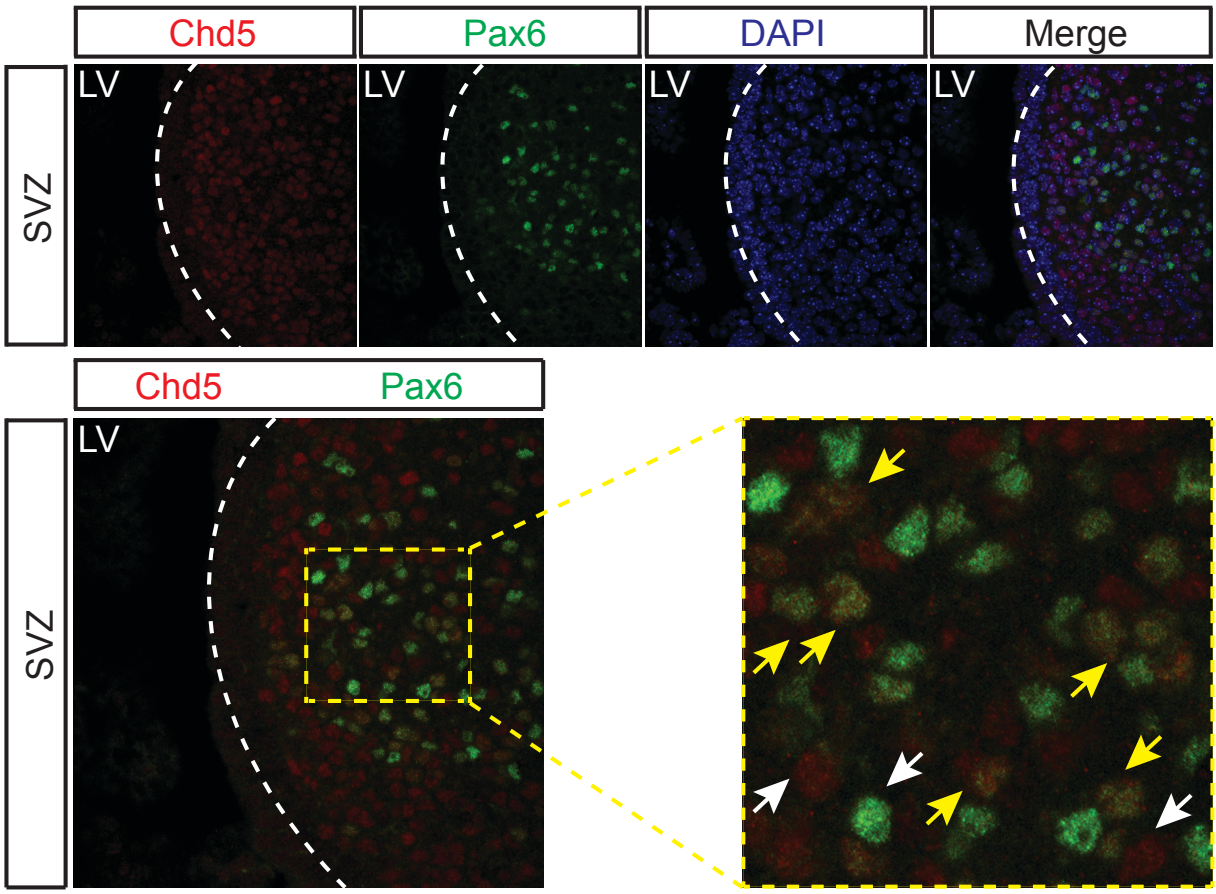

Figure 3: Expression of Chd5 in neonatal mouse brain

Expression of Chd5 was examined by immunofluorescent analyses of neonatal mouse brain sections. Shown are representative images of the subventricular zone (SVZ) of postnatal day 1 (P1) wild type mouse brain. Individual channels, Chd5 (red), Pax6 (green), DAPI (blue), and merged (merge), are shown (above). Dashed line (white) demarcates the border between LV (lateral ventricle) and periventricular area.

Chd5 (red) and Pax6 (green) are shown in the merged image (left, below). Enlarged image of area (demarcated by yellow dashed line), where Chd5 (red)/Pax6 (green)-positive cells (yellow arrows) are present, is shown (right, below). Only Chd5-positive or only Pax6-positive are marked by white arrows. LV: Lateral Ventricle

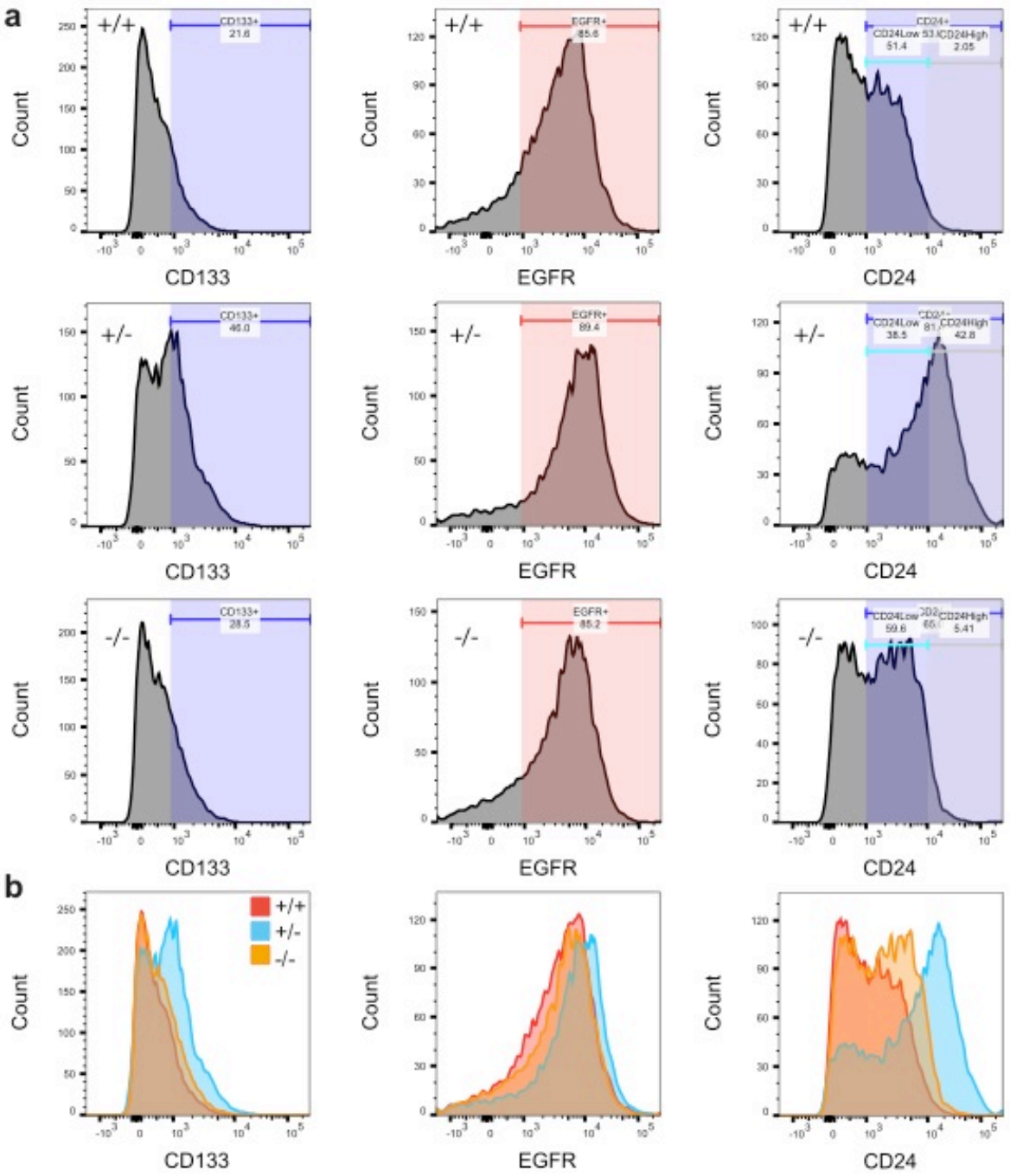

Figure 4: Cell surface marker profiles of primary NSCs
Primary NSCs were analyzed by acute immunostaining and multicolor flow cytometry. (a) Shown are representative profiles of Cd133-, Egfr-, and Cd24-positive populations in +/+, *Chd5*+/-, and *Chd5*-/- NSCs. Gated area (shaded) shows significantly enriched population, compared with unstained controls. Numbers indicate the percentage of the gated population (n=1) (b) Composite profiles (ungated) of +/+ (red), *Chd5*+/- (blue), and *Chd5*-/- NSCs (yellow) for Cd133-, Egfr-, and Cd24-positive populations are shown.

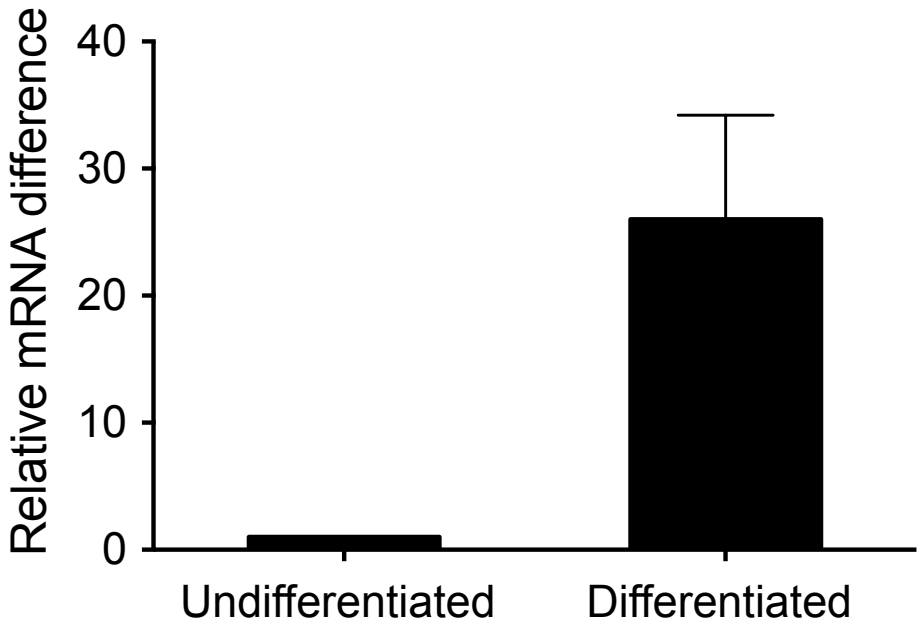

Figure 5: Transcriptional dynamics of *Chd5* during *in vitro* neural differentiation

Expression changes of *Chd5* during *in vitro* neural differentiation were analyzed by RT-qPCR. Average expression of *Chd5* in day 4 "differentiated" neural cells is compared to average expression of day 0 "undifferentiated" NSCs. Relative mRNA difference is shown in fold change (y-axis). Error bar indicates standard deviation of 3 biological samples (n=3).

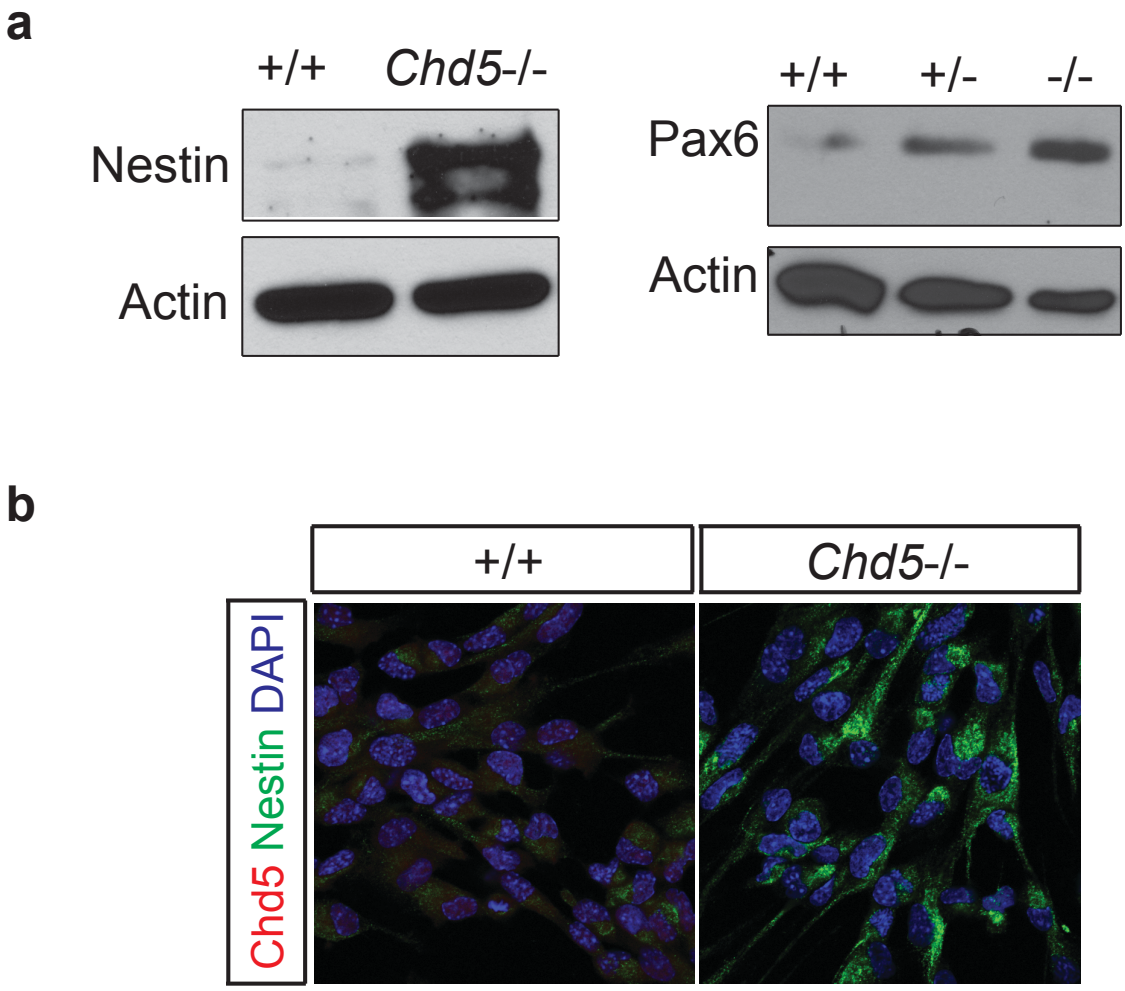

Figure 6: Increased expression of activated NSC markers in *Chd5*-/- NSCs

Expression of Nestin and Pax6 were examined by western blotting and immunofluorescent analyses of +/+, *Chd5*+/-, and *Chd5*-/- NSCs. (a) Shown are representative western blots of +/+, *Chd5*+/-, and *Chd5*-/- NSCs. Blots are probed for Nestin and Actin (left) and for Pax6 and Actin (right). (b) Shown are representative merged images of +/+ and *Chd5*-/- NSCs. Chd5 is in red; Nestin is in green; DAPI is in blue.

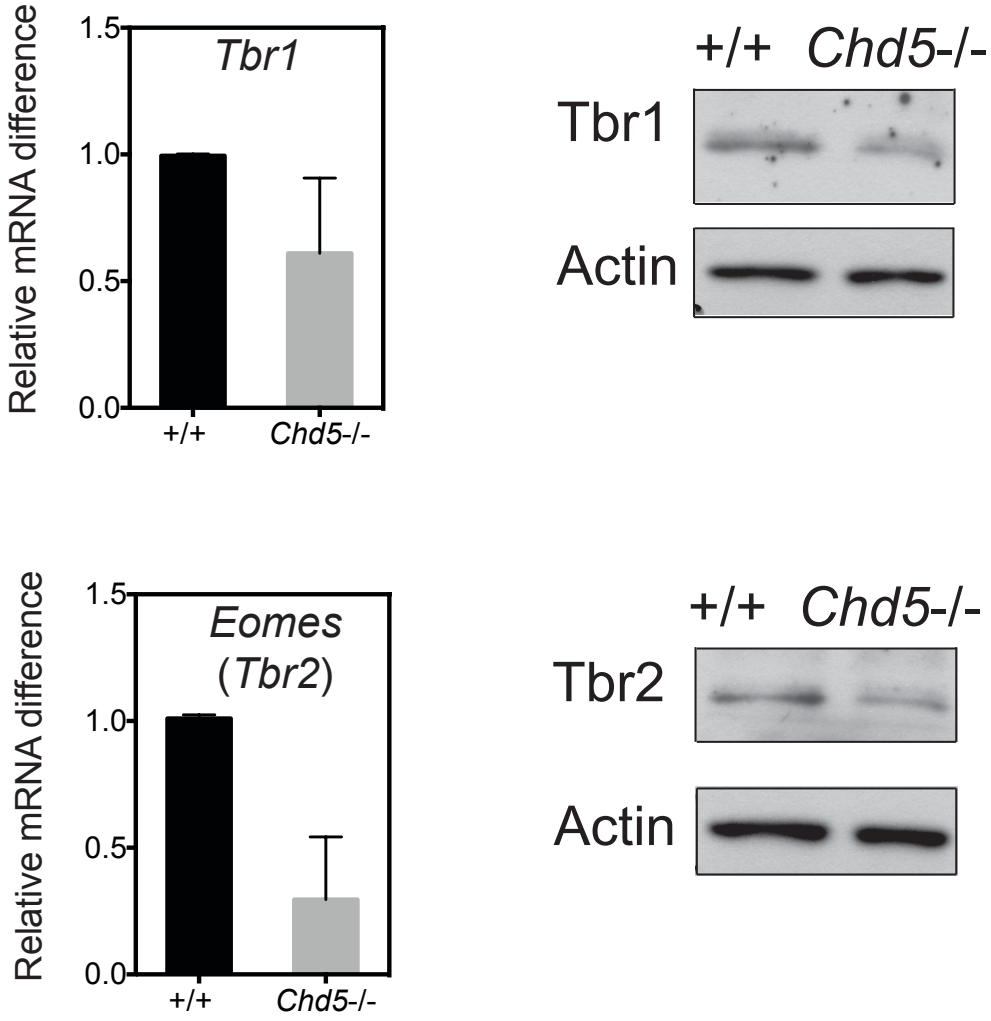

Figure 7: Decreased expression of early committed neuronal precursor markers in *Chd5*-/- NSCs

Expression of *Tbr1* and *Eomes* were analyzed by RT-qPCR and western blotting of +/+ and *Chd5*-/- NSCs. Average expression of *Tbr1* (above) and *Eomes* (Tbr2) (below) in *Chd5*-/- NSCs is compared to average expression of +/+ NSCs. Relative mRNA difference is shown in fold change (y-axis). Error bar indicates standard deviation of 3 biological samples (n=3).

Shown are representative western blots of +/+ and *Chd5*-/- NSCs. Blots are probed for Tbr1 (above), Tbr2 (below), and Actin in each blot.

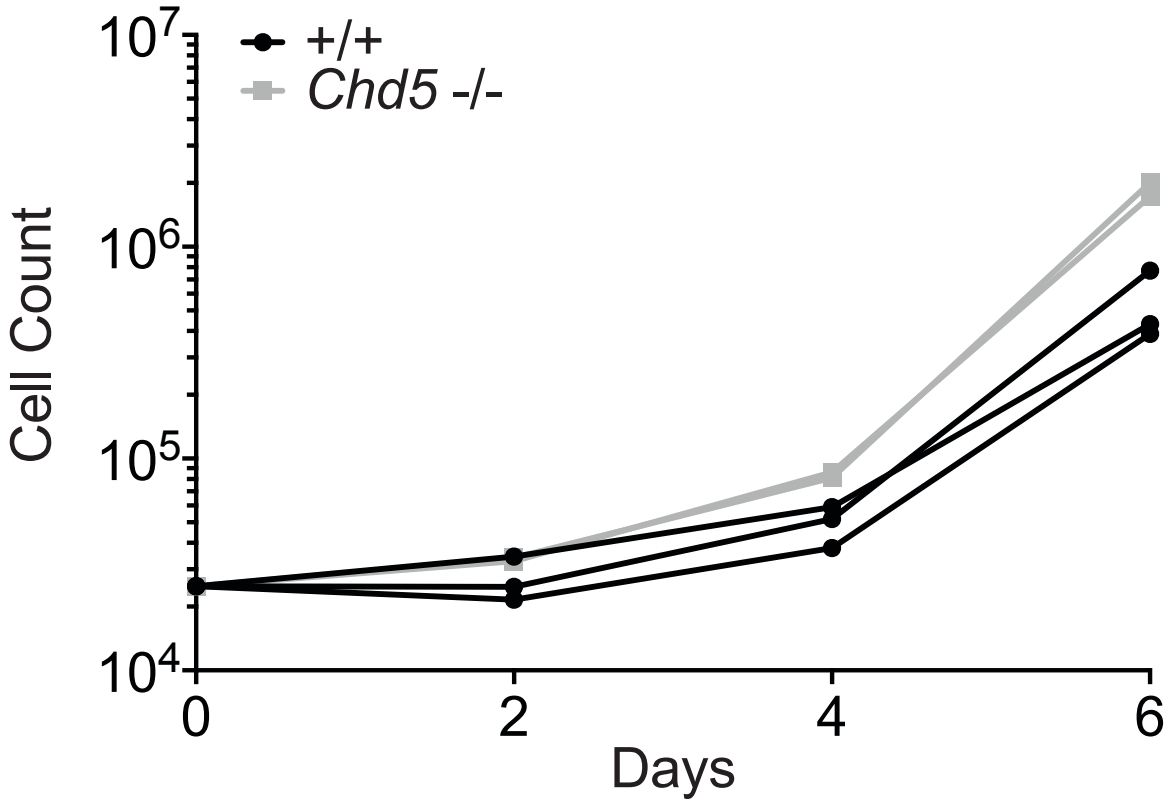

Figure 8: Increased proliferation of *Chd5*-/- NSCs

Proliferation of +/+ and *Chd5*-/- NSCs were analyzed by monitoring growth of cells over time. Shown are cell growth plots over 6 days. Cell counts at day 2,4, and 6 of +/+ NSCs (n=3) and *Chd5*-/- NSCs (n=2) are shown in black and gray, respectively.

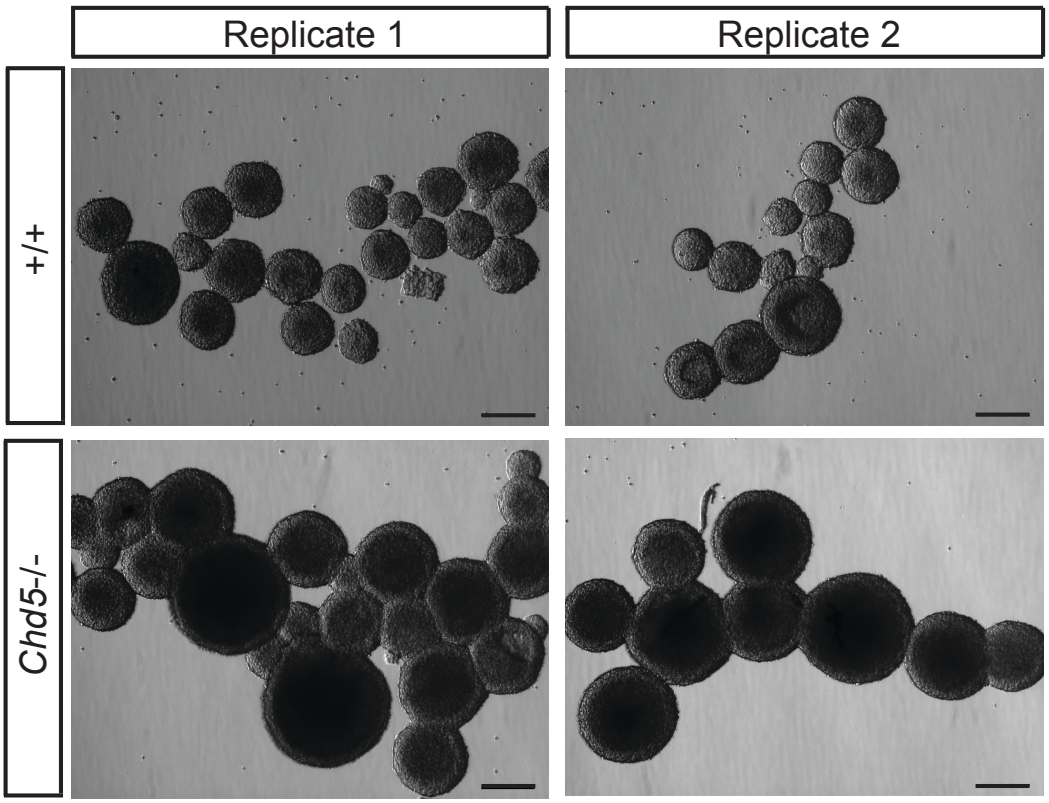

Figure 9: Enlarged neurospheres from *Chd5*-/- NSCs

Neurospheres of +/+ and *Chd5*-/- NSCs were analyzed by contrast microscopic image analysis. Shown are two representative constrast micrographs of +/+ neurospheres (above) and *Chd5*-/- neurospheres (below). Biological replicates of +/+ and *Chd5*-/- NSCs were cultured for 9 days and subject to image analysis. Scale bar: 200 µm.

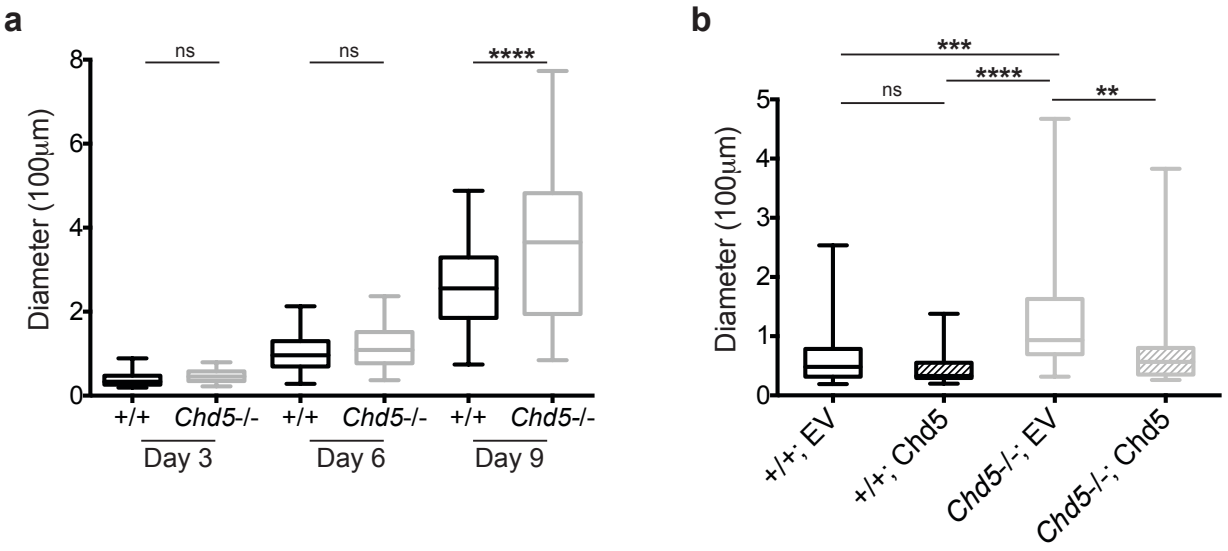

Figure 10: Enhanced neurosphere formation capacity of *Chd5*-/- NSCs

Neurosphere formation of +/+ and *Chd5*-/- NSCs were analyzed by contrast microscope image analysis. (a) Shown are quantification of diameters of +/+ (black) and *Chd5*-/- (gray) neurospheres. Size measurements (in diameter) of biological replicates of +/+ neurospheres (n=3) and *Chd5*-/- neurospheres (n=3) at day 3, 6, and 9 are plotted as box plots. **** indicates statistical signficance ($p<0.0001$). Tukey's multiple comparison test was used for statistical assessment.

(b) Shown are quantification of diameters of +/+; EV (black), +/+; Chd5 (patterned black), *Chd5*-/-; EV (gray), and *Chd5*-/-; Chd5 (patterned gray) neurospheres. Size measurements (in diameter) of biological replicates (n=3) of each group at day 9 are plotted as box plots. ** indicates statistical signficance ($p=0.0046$); *** indicates statistical significance ($p=0.0003$); **** indicates statistical significance ($p<0.0001$). ns indicates no statistical significance. Tukey's multiple comparison test, is used for statistical assessment.

+/+; EV: +/+ NSCs transduced with empty vector. +/+; Chd5: +/+ NSCs transduced with Chd5 cDNA. *Chd5*-/-; EV: Chd5-deficient NSCs trasduced with empty vector. *Chd5*-/-; Chd5: Chd5-deficient NSCs. transduced with Chd5 cDNA

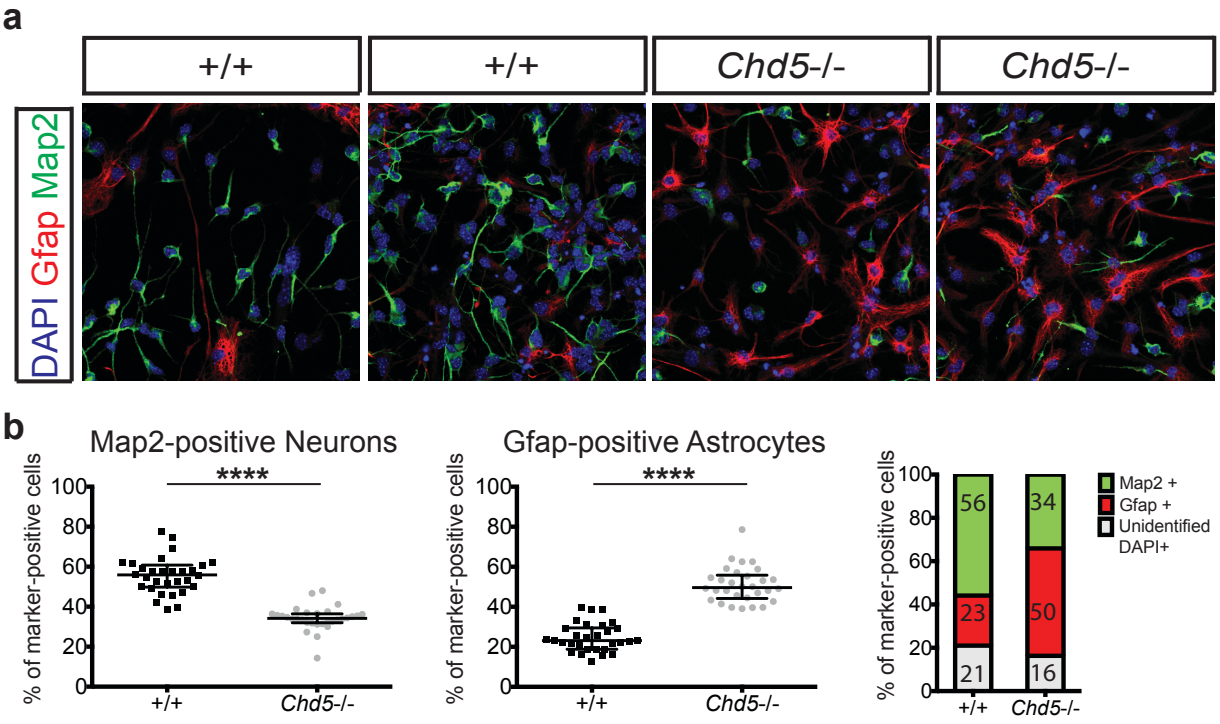

Figure 11: Altered neural cell fates of *Chd5*-/- NSCs at day 4 post *in vitro* neurogenesis

Cell fate decisions of +/+ and *Chd5*-/- NSCs were examined by immunofluorescent analyses of NSC-derived differentiated neural cells. (a) Shown are representative images of biological replicates of +/+ (n=3) and *Chd5*-/- (n=3) neural cells. Map2-positive (green) cells are neurons; Gfap-positive (red) cells are astrocytes.

(b) Shown is comparision of Map2-positive neuronal distribution (left), Gfap-positive astrocytic distribution (middle), and composite distribution of 3 biological samples (n=3). +/+ and *Chd5*-/- differentiated neural cells at day 4 post *in vitro* neurogenesis are plotted. **** indicates statistical signficance ($p<0.0001$). Mann-Whitney's test is used for statistical assessment. Numbers indicate median values of each category.

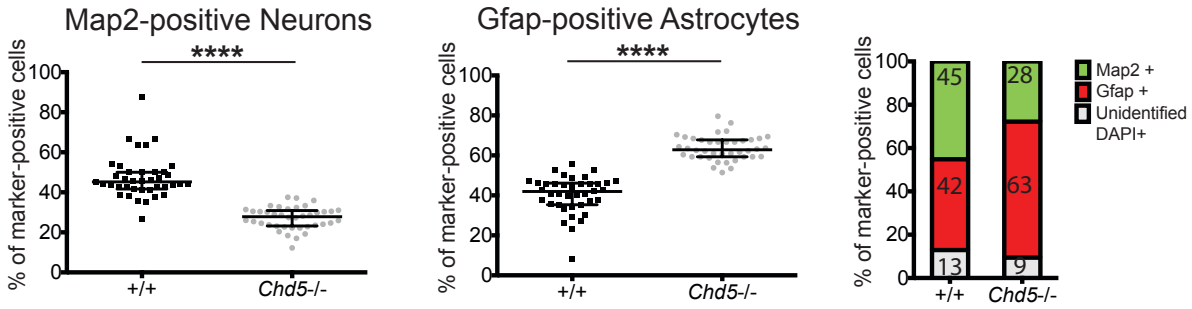

Figure 12: Altered neural cell fates of *Chd5*-/- NSCs at day 7 post *in vitro* neurogenesis

Cell fate decisions of +/+ and *Chd5*-/- NSCs were examined by immunofluorescent analyses of NSC-derived differentiated neural cells. Shown is the comparision of Map2-positive neuronal distribution (left), Gfap-positive astrocytic distribution (middle), and composite distribution of biological replicates (n=2). +/+ and *Chd5*-/- differentiated neural cells at day 7 post *in vitro* neurogenesis are plotted. **** indicates statistical signficance ($p<0.0001$). Mann-Whitney's test is used for statistical assessment. Numbers indicate median values of each category.

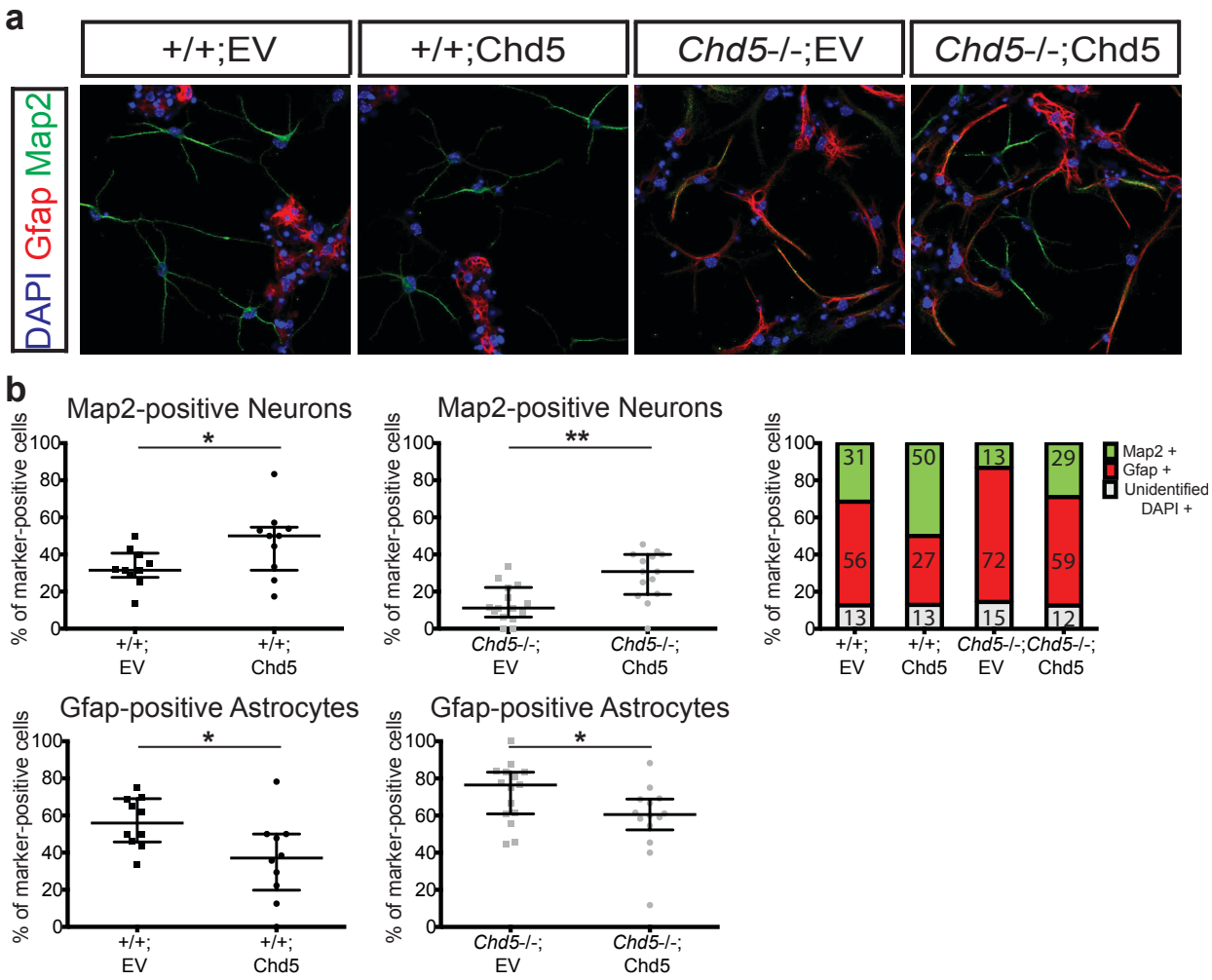

Figure 13: Rescued neural cell fates of *Chd5*-/- NSCs at day 7 post *in vitro* neurogenesis
Cell fate decisions of +/+; EV, +/+; Chd5, *Chd5*-/-; EV, and *Chd5*-/-; Chd5 NSCs were analyzed by immunofluorescent analyses of NSC-derived differentiated neural cells. (a) Shown are representative images of +/+ (n=1) and *Chd5*-/- (n=1) neural cells. Map2+ (green) cells are neurons; Gfap+ (red) cells are astrocytes.

(b) Shown is the comparision of the Map2+ neuronal distribution (above), Gfap+ astrocytic distribution (below), and composite distribution (right) between +/+; EV, +/+; Chd5, *Chd5*-/-; EV, and *Chd5*-/-; Chd5 differentiated neural cells. Distribution of Map2+ neurons (ten technical replicates from a signgle biological sample) at day 7 are plotted. Distribution of Gfap+ astrocytes (ten technical replicates from a signle sample) at day 7 are plotted. * (Map2-positive neurons +/+; EV vs +/+; Chd5) indicates statistical signficance (p=0.0409). ** (Map2-positive neurons *Chd5*-/-; EV vs *Chd5*-/-; Chd5) indicated statistical significance (p=0.0011). * (Gfap-positive astrocytes +/+; EV vs +/+; Chd5) indicates statistical significance (p= 0.0405). * (Gfap-positive astrocytes *Chd5*-/-; EV vs *Chd5*-/-; Chd5) indicates statistical significance (p= 0.0445). Mann-Whitney's test is used for statistical assessment. Numbers indicate median values of each category.

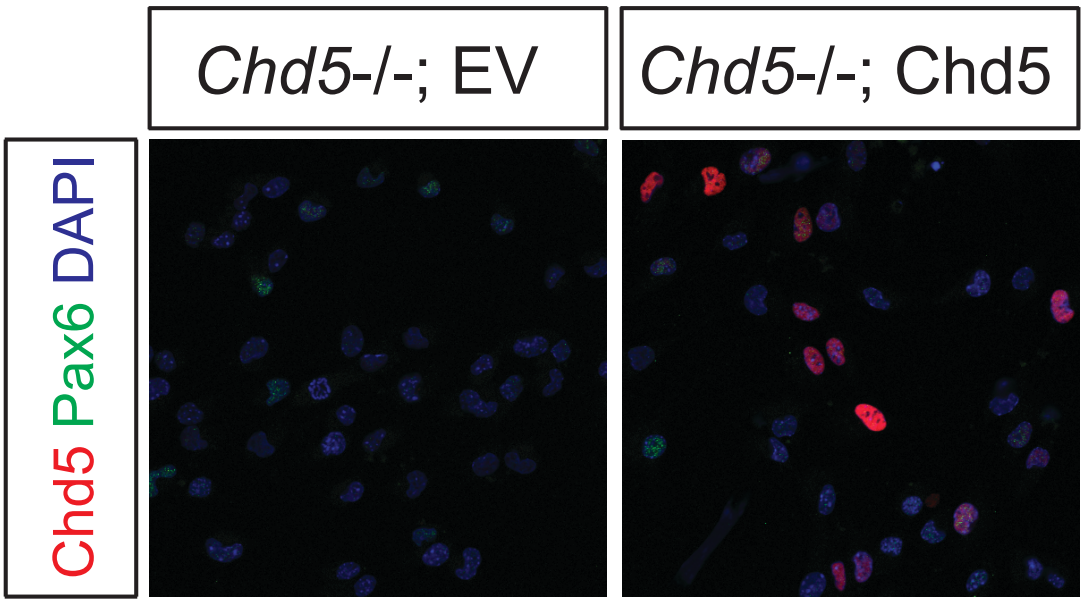

Figure 14: Ectopic expression of Chd5 in *Chd5*-/-; Chd5 NSCs at day 0 post *in vitro* neuro genesis

Extent of ectopic exression of Chd5 in *Chd5*-/- NSCs was examined by immunofluorescent analyses in neurosphere-derived adherent culture. Shown are representative images of *Chd5*-/-; EV and *Chd5*-/-; Chd5 adherent NSCs. Chd5 expression is shown in red; Pax6 expression is shown in green. Scale bar:

Chd5-/-; EV: Chd5-deficient NSCs trasduced with empty vector. *Chd5*-/-; Chd5: Chd5-deficient NSCs transduced with Chd5 cDNA.

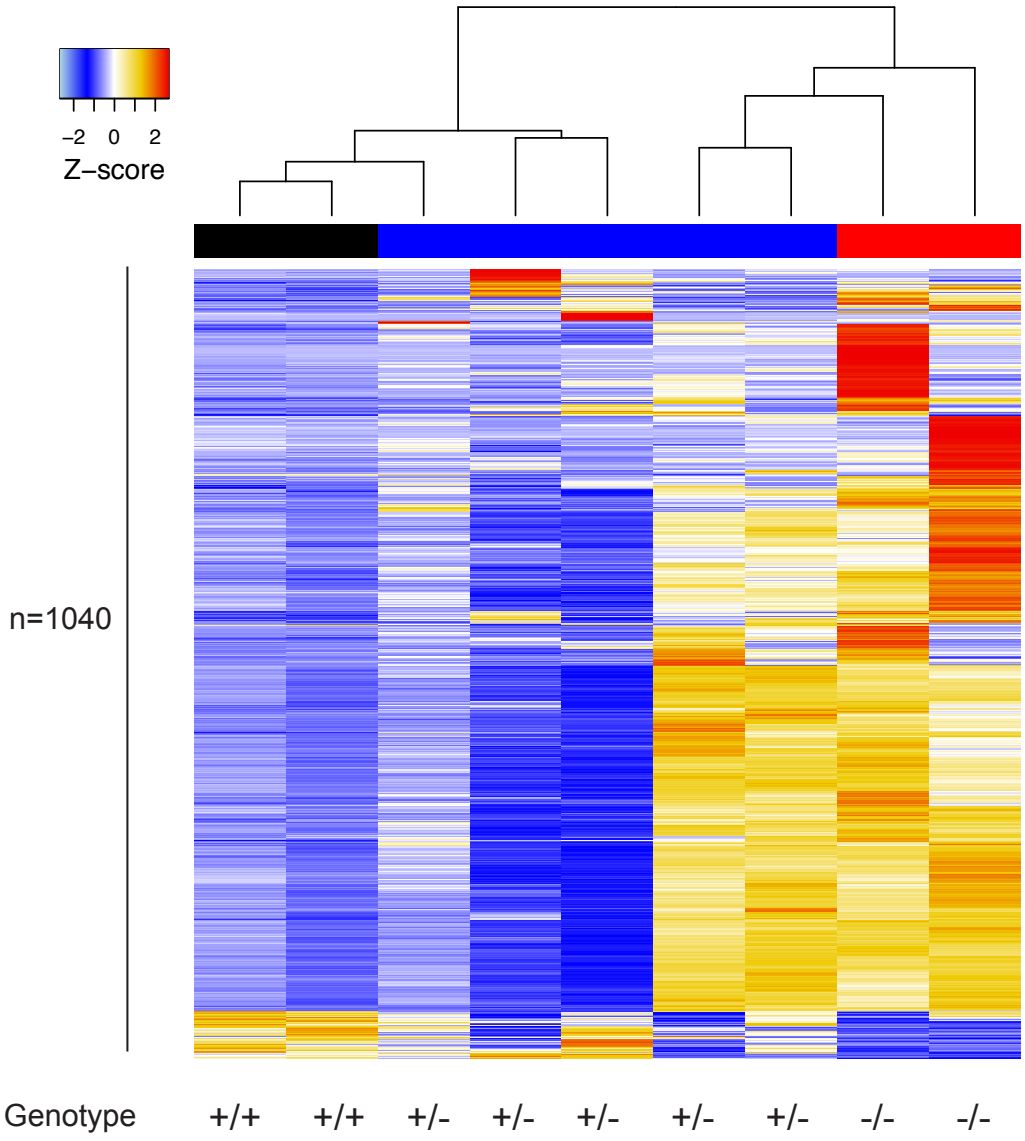

Figure 15: Hierarchical clustering of gene expression patterns of +/+, *Chd5*+/-, and *Chd5*-/- NSCs

Global gene expression profiles of +/+, *Chd5*+/-, and *Chd5*-/- NSCs were analyzed by RNA-sequencing analysis and hierarchical clustering analyses. Shown are heat map representations of gene expression patterns of female +/+ NSCs (n=2), *Chd5*+/- NSCs (n=5), and *Chd5*-/- NSCs (n=2). Z-score is standard score, indicating deviation from the mean. Here Z-score is to indicate the extent of upregulation (yellow and red) and downregulation (light blue and dark blue).

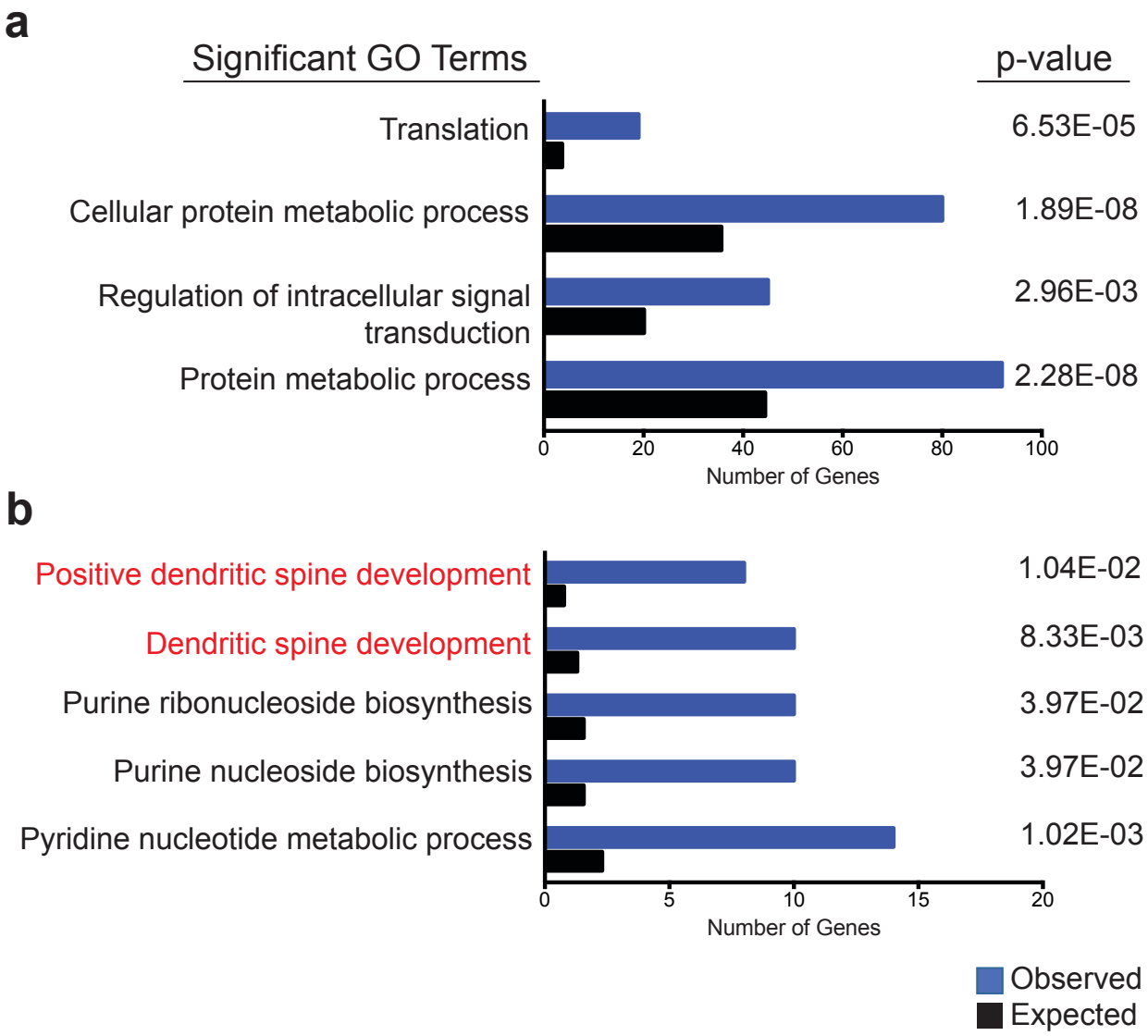

Figure 16: Gene ontology analysis of differentially expressed genes in *Chd5*+/- NSCs and *Chd5*-/- NSCs

Significantly enriched gene ontology terms in differentially expressed genes of *Chd5*+/- NSCs and *Chd5*-/- NSCs NSCs were analyzed by the PANTHER classification system. (a) Shown are sinificantly enriched biological process categories of consistently altered genes. (b) Shown are sinificantly enriched biological process categories of inconsistently altered genes. Observed number of genes (blue) enriched in each category is shown. Expected number of genes (black) for each corresponding category is shown. p-value indicates statistical significance of the enrichment.

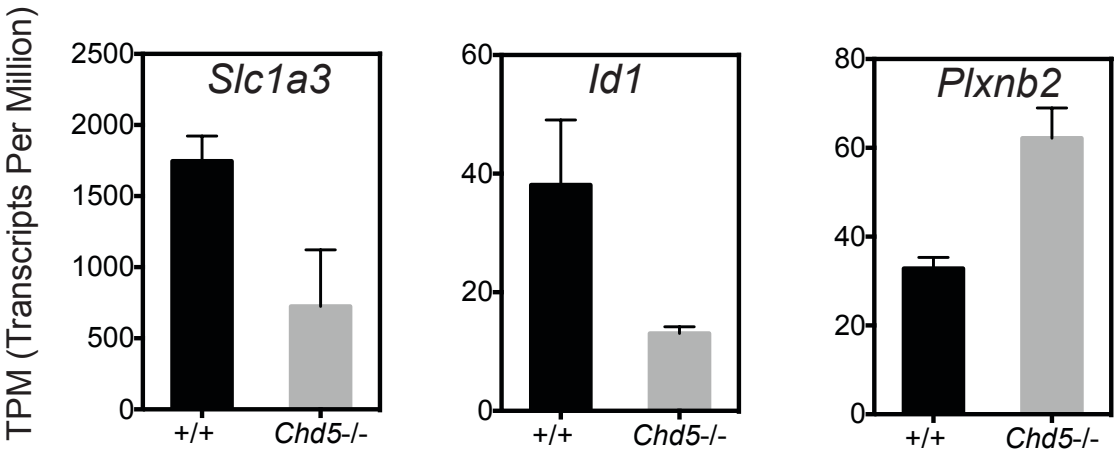

Figure 17: Decreased expression of neural stem cells markers and increased expression of neural progenitor markers in *Chd5*-/- NSCs

Expression of *Slc1a3*, *Id1,* and *Plxnb2* were analyzed by RNA-seq analysis. Average expression of *Slc1a3* (left), *Id1* (middle), and *Plxnb2* (right) in female +/+ NSCs (black column) and *Chd5*-/- NSCs (gray column) are plotted. Expression levels are shown in transcripts per million (TPM) on the y-axis. Error bars indicate standard deviation of two biological replicates (n=2).

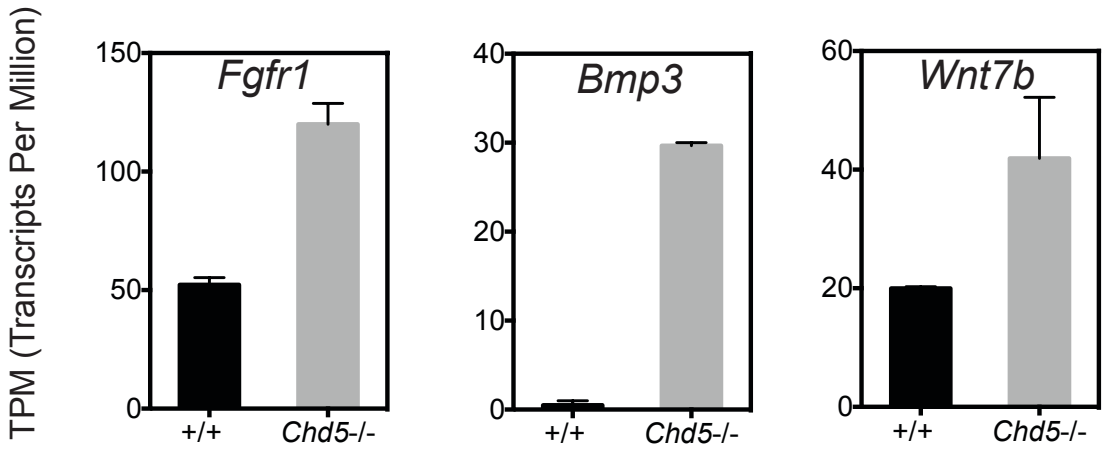

Figure 18: Deregulated expression of components of signaling pathways in *Chd5*-/- NSCs

Expression of *Fgfr1*, *Bmp3,* and *Wnt7b* were analyzed by RNA-seq analysis. Average expression of *Fgfr1* (left), *Bmp3* (middle), and *Wnt7b* (right) in female +/+ NSCs (black column) and female *Chd5*-/- NSCs (gray column) are plotted. Expression levels are shown in transcripts per million (TPM) on the y-axis. Error bars indicate standard deviation of two biological replicates (n=2).

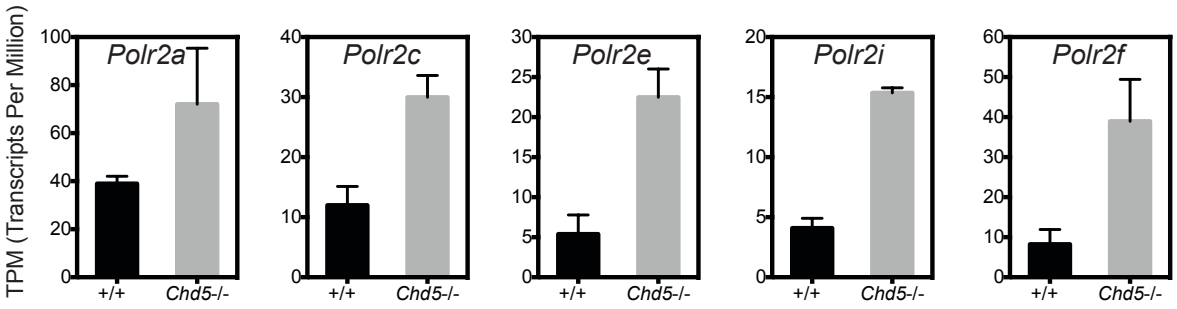

Figure 19: Increased expression of components of RNA polymerase II subunits in *Chd5*-/- NSCs

Expression of *Polr2a*, *Polr2c, Polr2e, Polr2i,* and *Polr2f* were analyzed by RNA-seq analysis. Average expression of these genes in female +/+ NSCs (black column) and female *Chd5*-/- NSCs (gray column) are plotted. Expression levels are shown in transcripts per million (TPM) on the y-axis. Error bars indicate standard deviation of two biological replicates (n=2).

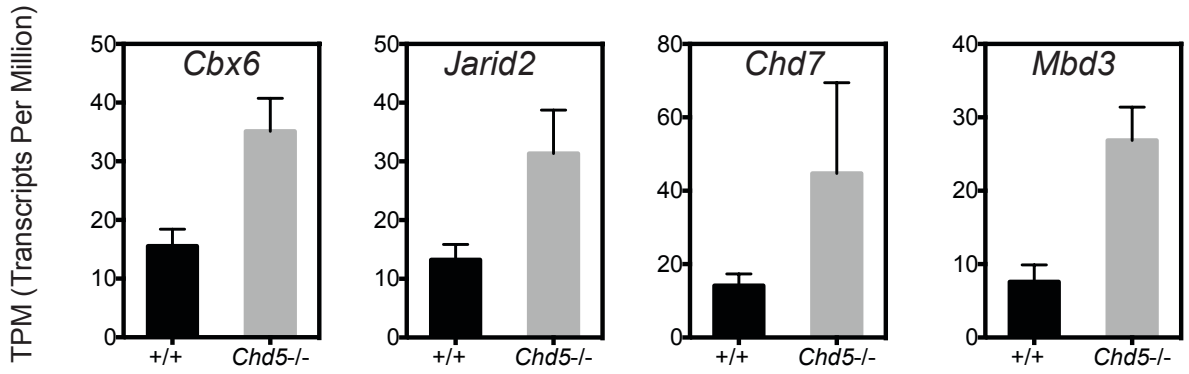

Figure 20: Increased expression of chromatin regulators in *Chd5*-/- NSCs

Expression of *Cbx6*, *Jarid2, Chd7,* and *Mbd3* are analyzed by RNA-seq analysis. Average expression of these genes in female +/+ NSCs (black column) and female *Chd5*-/- NSCs (gray column) are plotted. Expression levels are shown in transcripts per million (TPM) on the y-axis. Error bars indicate standard deviation of two biological replicates (n=2).

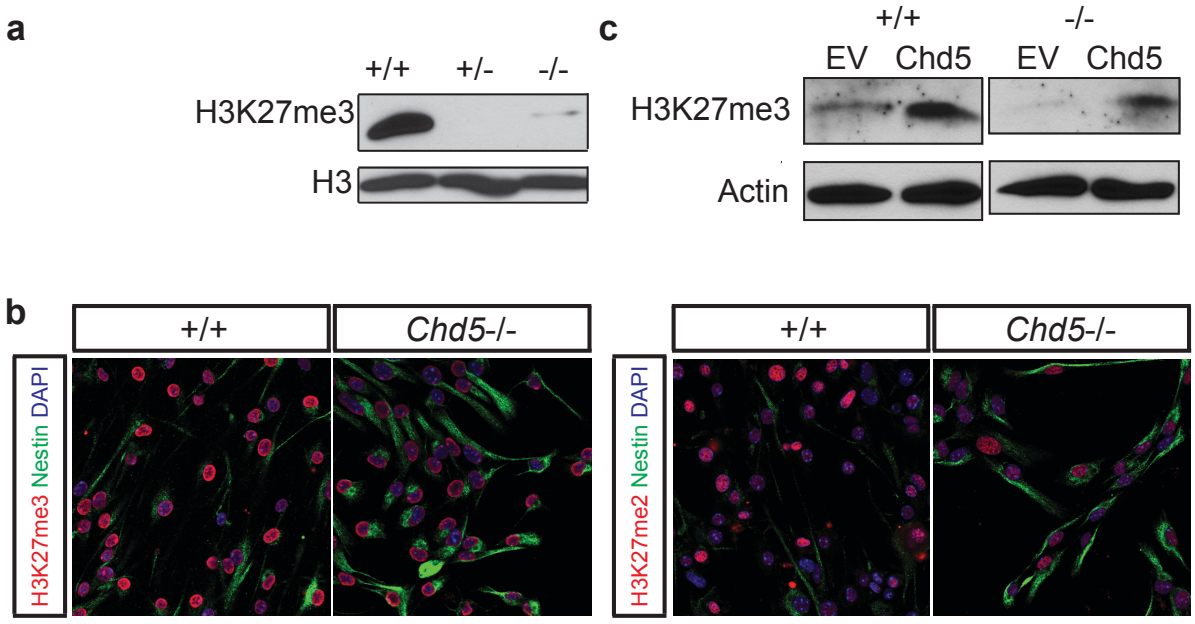

Figure 21: Reduction of H3K27me3 and H3K27me2 levels in *Chd5*+/- and *Chd5*-/- NSCs

Expression of H3K27me3 was examined by western blotting and immunofluorescent analyses of +/+, *Chd5*+/-, and *Chd5*-/- NSCs. (a) Shown are representative western blots of +/+, *Chd5*+/-, and *Chd5*-/- NSCs. Blots are probed for H3K27me3 and H3. (b) Shown are representative merged images of +/+ and *Chd5*-/- NSCs. H3K27me3 (left) and H3K27me2 (right) is in red; Nestin is in green; DAPI is in blue. (c) Shown are representative western blots of +/+; EV, +/+; Chd5, *Chd5*-/-; EV, and *Chd5*-/-; Chd5 NSCs. Blots were probed for H3K27me3 and Actin.

+/+; EV: +/+ NSCs transduced with empty vector. +/+; Chd5: +/+ NSCs transduced with Chd5 cDNA.*Chd5*-/-; EV: Chd5-deficient NSCs trasduced with empty vector. *Chd5*-/-; Chd5: Chd5-deficient NSCs transduced with Chd5 cDNA

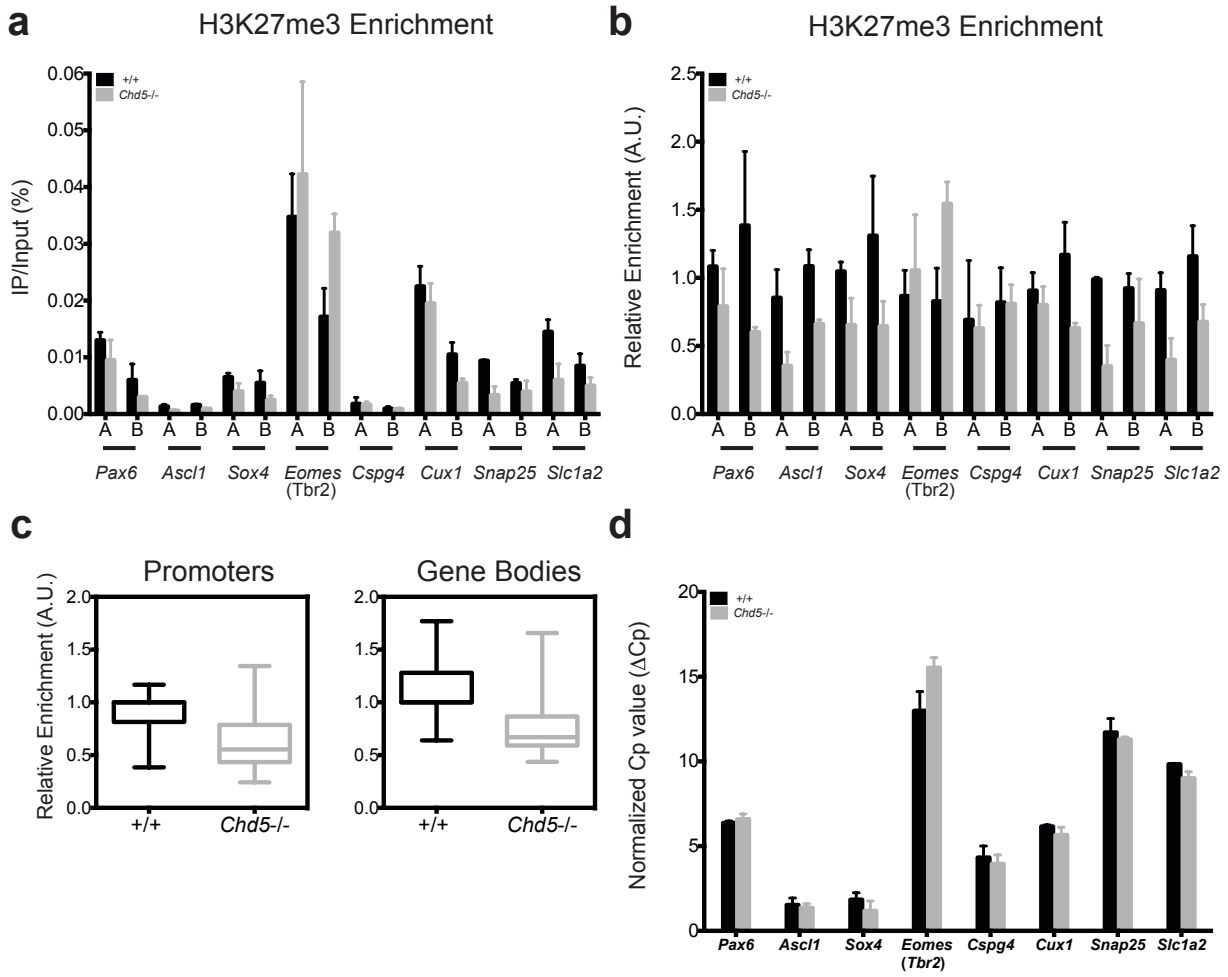

Figure 22: Reduced H3K27me3 enrichment on various genomic sites in *Chd5*-/- NSCs

Erichment of H3K27me3 at promoters and in gene bodies of 8 genomic loci encoding cell-type-specific markers were analyzed by ChIP-qPCR. Gene expression levels of corresponding genes in corresponding samples were analyzed by RT-qPCR. (a) Averge enrichment of H3K27me3 is estimated and plotted as percentage on the y-axis. Average enrichment of H3K27me3 in +/+ NSCs (n=2) is shown in black columns. Average enrichment of H3K27me3 in *Chd5*-/- NSCs (n=2) is shown in gray columns. "A" indicates promoters of corresponding genes. "B" indicates intragenic regions in gene bodies of corresponding genes. (b) Relative enrichment of H3K27me3 is a comparison between average H3K27me3 levels of *Chd5*-/- NSCs (n=2) and +/+ NSCs (n=2). (c) Composite relative enrichment of H3K27me3 are plotted as box plots. (d) Expression levels of these genes in +/+ and *Chd5*-/- NSCs are normalized Cp values of each genes by Cp values of endogenous control *Actb*. Average expression levels of the genes in +/+ NSCs (n=2) is shown in black columns. Average expression levels of the genes in *Chd5*-/- NSCs (n=2) is shown in gray columns.

.

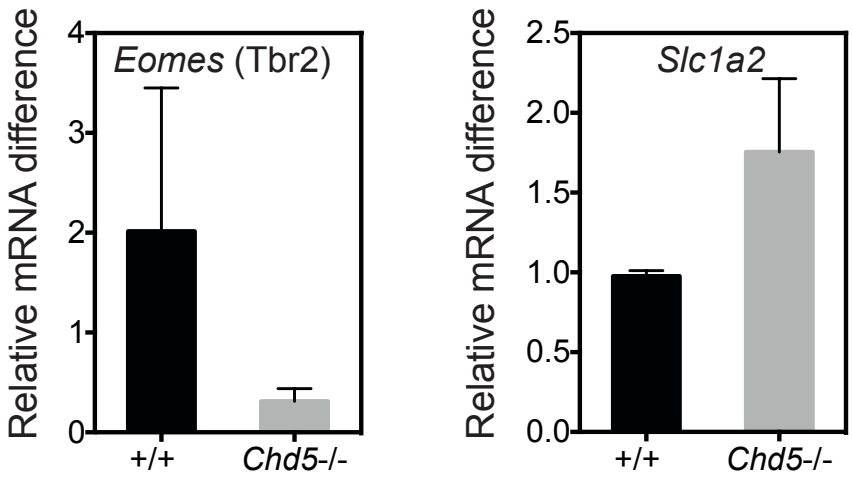

Figure 23: Decreased expression of *Eomes* and increased expression of *Slc1a2* in *Chd5*-/- NSCs

Expression of *Eomes* (Tbr2) and *Slc1a2* was analyzed by RT-qPCR. Average expression of *Eomes* (left) and *Slc1a2* (right) in +/+ NSCs is compared to average expression of *Chd5*-/- NSCs. Relative mRNA difference is shown in fold change (y-axis). Error bars indicate standard deviation of three biological replicates (n=3).

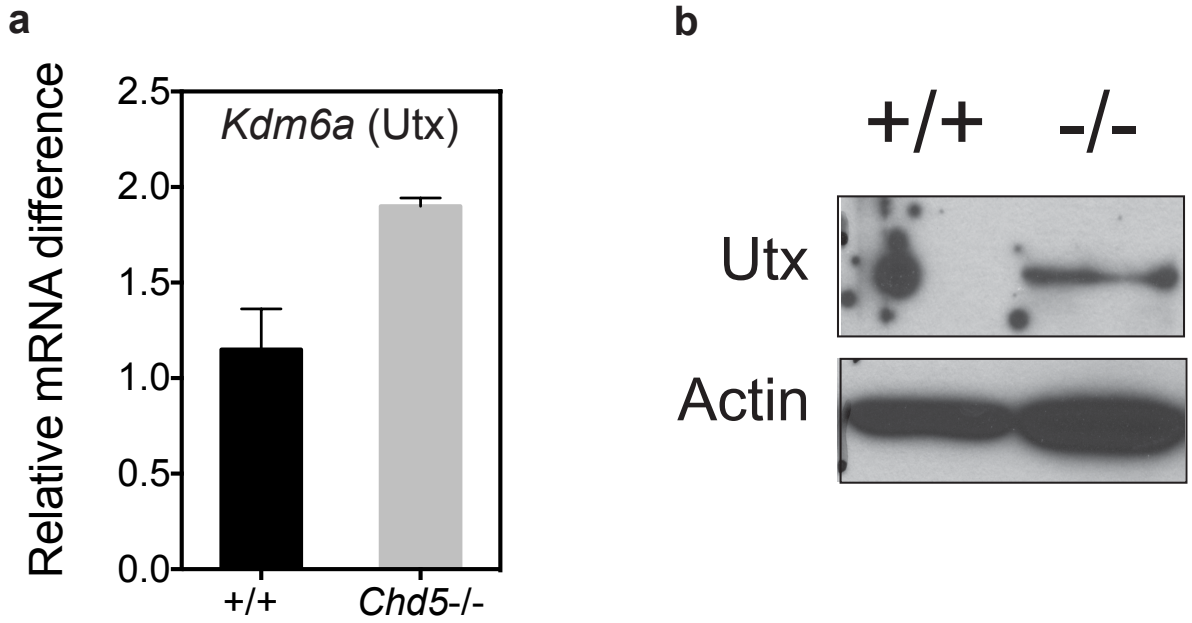

Figure 24: Increased expression of H3K27me3-specific demethylase Utx in *Chd5*-/- NSCs

Expression of *Kdm6a* (Utx) was analyzed by RT-qPCR and western blotting analyses of +/+ and *Chd5*-/- NSCs. (a) Average expression of *Kdm6a* (left) in *Chd5*-/- NSCs is compared to average expression of +/+ NSCs. Relative mRNA difference is shown in fold change (y-axis). Error bar indicates standard deviation of two biological replicates (n=2). (b) Shown are representative western blots of +/+ and *Chd5*-/- NSCs. Blots are probed for Utx (upper panel) and Actin (lower panel).

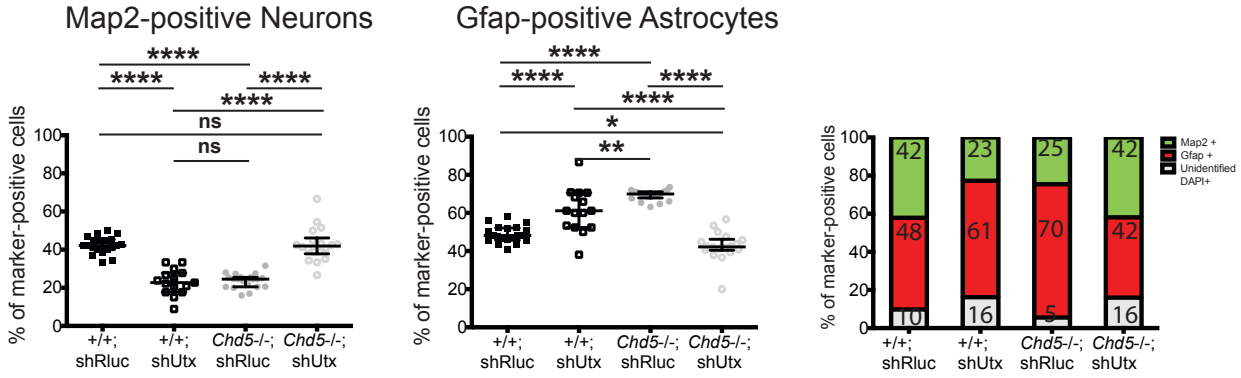

Figure 25: Rescued neural cell fate defects by Utx knockdown in *Chd5*-/- NSCs at day 7 post *in vitro* neurogenesis

Cell fate decisions of +/+; shRluc, +/+; shUtx, *Chd5*-/-; shRluc, and *Chd5*-/-;shUtx NSCs were examined by immunofluorescent analyses of NSC-derived differentiated neural cells. Shown is the comparision of the Map2-positive neuronal distribution (left), Gfap-positive astrocytic distribution (middle), and composite distribution (right) between +/+; shRluc, +/+; shUtx, *Chd5*-/-; shRluc, and *Chd5*-/-;shUtx differentiated neural cells. Distribution of technical replicates of Map2-positive neurons (n=15-20 from a single biological sample) at day 7 are plotted as scatter plots. Distribution of technical replicates of Gfap-positive astrocytes (n=15-20 from a signle sample) at day 7 are plotted as scatter plots. **** indicates statistical signficance ($p<0.0001$). ** indicates statistical significance ($p=0.0096$). * indicates statistical significance ($p=0.0378$). ns indicates no statistical significance. Tukey's multiple comparison test is used for statistical assessment. Composite distribution of Map2+, Gfap+, and DAPI+ (only DAPI-positive unidentified cells) are plotted together (right). Numbers indcate median values of each category.

Chapter 3. Conclusions, Perspectives, and Future Directions

3.1 Chd5 Regulates Neural Cell Fate Decision of Neural Stem/Progenitor Cells

Chd5 is expressed robustly in post-mitotic, differentiated neurons throughout the embryonic, neonatal, and adult brain (Egan et al., 2013; Vestin and Mills, 2013). Based on this predominant, but cell-type-specific expression patterns of Chd5 in post-mitotic neurons, it has been postulated that Chd5 plays a functional role within the neuronal lineage. My findings over the course of this thesis project is in agreement with a model in which Chd5 is expressed in type C neural transit amplifying progenitors—a NSC subtype that is the direct progeny of undifferentiated neural stem cells. These cells are multipotent progenitors, but in contrast to their parental populations, they are highly proliferative (Kriegstein and Alvarez-Buylla, 2009). Type C neural transit amplifying progenitors are characterized by cell-type-specific markers, such as Nestin in the cytoplasm and Sox3 within the nucleus. Consistent with my findings in E15.5 embryonic brain, Egan at al. demonstrated that at later stage of gestation (E18.5) Chd5 is also expressed in type A early committed neuronal precursor population (i.e. Dcx-positive early neuronal precursors)—which is also consistent with findings from our group (Egan et al., 2013; Vestin and Mills, 2013).

Based on these findings, it was postulated that Chd5 expression begins in uncommitted multipotent late-stage neural progenitors (i.e. type C transit amplifying progenitors). Its expression increases as neuronal differentiation proceeds, culminating as robust levels in fully differentiated post-mitotic neurons. This pattern implicates Chd5 as a crucial regulator of

neuronal differentiation (Egan et al., 2013; Vestin and Mills, 2013). Acute knockdown of Chd5 during a critical period of early brain development (E14.5-E18.5) disrupts the migration of neural progenitors and early committed neuronal precursors during neocortical development (Egan et al., 2013). A caveat of this study was that Chd5 levels were not completely abolished, and hence untransduced neural progenitor cells by shRNA targeting Chd5 make it difficult to interpret the results comprehensively, as cells with unperturbed Chd5 still can undergo normal neuronal differentiation. In agreement with this, immunofluorescent analyses seem to indicate that neocortex was intact, and this finding in agreement from findings in our laboratory that brain development proceeds in Chd5-deficient mice (Horev et al. unpublished). Therefore, it appears that cortical neuronal differentiation still take place in the absence of Chd5. These findings highlight the need for better model systems to scrutinize the role of Chd5 during neuronal differentiation, the main motivation of my thesis.

We previously generated several Chd5-deficient mouse models, one of which with an early critical exon (i.e. exon2) being deleted by Cre/Lox recombinase strategy (Li et al., 2014). We confirmed the absence of Chd5 expression in mouse brain (Figure 27). This mouse model has been instrumental for addressing many important questions with regards to the biological role of Chd5. I took advantage of this model to investigate the role of Chd5 in the context of neural differentiation, and subsequently was the first in our lab to develop a primary NSC culture system to identify underlying molecular mechanisms. I was able to address several critical questions regarding Chd5's role in neural cell fate determination and modulation of cell-type-specific gene expression programs that direct epigenetic control of NSC differentiation.

To identify the role of Chd5 in neurogenesis within the developing mammalian brain, I examined brains of *Chd5*-/- mice, looking for noticeable changes at the brain structural and cellular level. As expected, Chd5 was not detectable in *Chd5-/-* brain. Yet, the overall brains structure appeared grossly normal, and NSC and neuron-specific markers were still expressed at comparable levels (Figure 26). These findings verified our previous findings that neurogenesis still took place in Chd5-compromised brain. In addition, these findings were consistent with intact cortical structures of Chd5-perturbed brain in which Chd5 was knockdown by shRNA (Egan et al., 2013). Most importantly, parallels work in our laboratory indicates that *Chd5*+/- and *Chd5-/-* animals have showed neurological phenotypes such as hyperactivity, repetitive behaviors, and hyperarborization of dendritic spines at synapses (Horev et al., unpublished).

By focusing on a specific cellular system—i.e. neural stem/progenitor cells—I revealed that Chd5 was expressed in type C transit amplifying neural progenitor cells (i.e. Pax6-positive cells), located in the periventricular neurogenic niche (i.e. VZ-SVZ) of mouse brain. Furthermore, I verified expression of Chd5 in primary NSC cultures in which the majority of cells were Nestin-positive (Figure 25). These cells are *in vitro* counterparts of type C transit amplifying neural progenitor cells that are characterized by cellular properties such as high proliferation as well as corresponding marker expression profiles which mirror *in vivo* type C transit amplifying neural progenitors. Therefore, characterization of primary NSCs has been an integral part of my thesis research.

The first line of evidence that Chd5 plays an important role in neural differentiation came from my observation that expression of endogenous *Chd5* changes dramatically during *in vitro* neural differentiation. I observed >25-fold increase of *Chd5* transcript during this process (see Figure 5). Similar significant induction of *Chd5* transcript was also observed in the ES cell-derived neural progenitor cell (NPCs) system where neuronal differentiation of NPCs was induced by retinoic acid (RA) treatment (Egan et al., 2013). The extent and the timing of induction, however, was hard to compare because of the difference between two systems (i.e. primary NSCs vs ES cell-derived NPCs with complete knockout vs shRNA-mediated knockdown, respectively). Nonetheless, the results of my study are in agreement with those of an independent study that Chd5's mutual link to neuronal differentiation.

Strikingly, loss of Chd5 in primary NSCs causes significant changes in cellular states and fundamental properties. Cell-type-specific marker analysis revealed that *Chd5*-/- NSCs were enriched for highly proliferative aNSCs markers (see Figure 6-7). This enrichment coincided with increased proliferation and enhanced neurosphere formation capacity (see Figure 8-10). While it may be difficult to decouple proliferation from neurosphere formation, both aspects pointed toward the generally enhanced proliferation activity of *Chd5*-/- NSCs. Importantly, this increased proliferation is a hallmark of aNSCs, which may be accounted for by a skewed enrichment in *Chd5*-/- NSCs. As discussed, enrichment of aNSCs was further supported by increased expression of the aNSC markers Nestin, Pax6, and the gene encoding Plexin B2 (i.e. *Plxnb2*) (see Figure 6 and Figure 17). Conversely, decreased expression of the genes encoding the neural stem cell markers Sla1a3 and Id1 as well as the committed neuronal precursor markers

Tbr1 and Tbr2 support the notion that Chd5 loss causes enrichment of aNSCs (see Figure 7 and Figure 17).

Cell surface marker profile analysis revealed the heterogeneity of primary NSC cultures as it has been shown previously (Codega et al., 2014; Mich et al., 2014). +/+ NSCs were composed of three closely related populations: Cd133-positive less proliferative neural stem cells (~22% of cells), Egfr-positive highly proliferative neural progenitor cells (~86% of cells), and Cd24-positive early committed neuronal precursor cells (~54%) (see Figure 4). Subsequent comparison between genotypes revealed the striking phenotype of *Chd5*+/- NSCs relative to both +/+ and *Chd5*-/- NSCs in all three populations. In particular, Cd133-positive neural stem cells and Cd24-positive committed neuronal precursors were significantly enriched in *Chd5*+/- NSCs. This observation is especially compelling. From the differentiation-based perspective, it appears that cells are undergoing cellular transitions in the opposite directions: undifferentiated neural stem cells and differentiated early committed neuronal precursor. The nature of this opposing behavior needs to be investigated.

Furthermore, *Chd5*-/- NSCs also have an enrichment of the Cd24-positive population in comparison with +/+ NSCs (~65% of Cd24-positive population in *Chd5*-/- NSCs vs only ~53% Cd24-positive population in +/+ NSCs). This difference is mostly accounted for by an enrichment of $Cd24^{Low}$ population. Therefore, it will be important to determine the exact identity of $Cd24^{Low}$ population, as the nature of this population is currently not clear. However, it appears that Egfr/PlexinB2-positive activated NSCs display low levels of Cd24 expression (Codega et

al., 2014; Mich et al., 2014). These cells are presumably the population that is in transition between multipotent neural progenitors and committed early neuronal precursors. Codega et al. further demonstrate that expression of Egfr precedes expression of Nestin in aNSCs. This may explain why the comparison of cell surface marker profiles between +/+ and *Chd5*-/- NSCs did not show significant enrichment for Egfr-positive population (see Figure 4). Enriched $Cd24^{Low}$ population perhaps reflects a late stage neural progenitor that expresses Nestin and Pax6. Nonetheless, the hierarchical relationship among Egfr-positive, Nestin-positive, and Cd24-positive cells should be delineated more in detail using flow cytometry and immunofluorescent analyses.

To gain mechanistic insight into the phenotype at the cellular level, I further characterized primary NSCs from brains of Chd5-compromised mice and assessed neural differentiation capacity. As a result, I verified that neural differentiation did occur; I observed two major neural lineages of the CNS: neurons and astrocytes. While neuronal differentiation still takes place in the absence of Chd5, a significantly skewed trend toward the astrocytic lineage was observed in *Chd5*-/- NSCs. Day 4 samples of +/+ differentiated neural cells were mostly comprised of Map2-positive neurons (~56%) and a smaller fraction of Gfap-astrocytes (~23%), whereas *Chd5*-/- differentiated neural cells were made up of a significantly smaller fraction of Map2-positive neurons (~34%) and a significantly larger proportion of Gfap-positive astrocytes (~50%) (see Figure 11). I initially used two different time points (i.e. day 4 and day 7) to show that they produced the same general trend and subsequently focused on day 4 differentiation. This astrocytic propensity in cell fate decisions of *Chd5*-/- NSCs was consistent between day 4 and

day 7 differentiated neural cells, thereby clearly indicating that Chd5 is involved in modulation of precise cell fate determination process in NSCs (see Figure 11-12).

In differentiated neural cells, *Chd5*-/- NSCs consistently displayed a skewed propensity in cell fate decisions toward the astrocytic lineage (see Figures 11-12). Importantly, this astrocytic propensity was reversed by ectopic expression of Chd5 cDNA (*Chd5* variant 2, NCBI Reference Sequence ID: NM_029216.2). In *Chd5*-/- NSCs that had been in differentiation-inducing condition for 7 days, exogenous Chd5 clearly reversed the cell fate decisions; *Chd5*-/-; EV neural cells were made up of ~13% of Map-positive neurons and ~72% of Gfap-positive astrocytes, whereas *Chd5*-/-; Chd5 neural cells were comprised of ~29% of Map2-positive neurons and ~59% of Gfap-positive astrocytes (see Figure 13). This result provides evidence that ectopic expression of Chd5 effectively rescued cell fate defects, thereby suggesting that Chd5 in NSCs is required to precisely execute spatiotemporal cell fate decisions of neural lineages.

Although this system was useful for discovering the skewed cell fate decisions between neuronal and astrocytic lineages, the presence of astrocytes (Gfap-positive cells) and unidentified cells (Map2-negative/Gfap-negative/DAPI-positive cells) in these cultures was a potential confounding factor for faithfully examining the role of Chd5 in neurogenesis. In particular, it is plausible that the higher proliferation property of astrocytes confers a selective advantage for this lineage of cells. To reduce heterogeneity within differentiated neural cells, the protocol could be modified to induce neuronal differentiation using (RA) and forskolin treatment (Hsieh et al., 2004). In addition, a motor neuron differentiation protocol has recently been developed, in which

ES cells are treated with RA and smoothened agonist (SAG), to achieve highly homogeneous populations of motor neurons (Mazzoni et al., 2013; Narendra et al., 2015). Therefore, it is feasible that this motor neuron differentiation protocol can be modified to more fully characterize the role of Chd5 in primary NSC differentiation.

3.2 Chd5 Maintains Neural Cell-Type-Specific Gene Expression Programs

So far, I have discussed the functional consequences of Chd5 loss on undifferentiated NSCs, where I have discovered aberrant changes in cellular properties and differentiation states of primary NSCs are observed, and abnormal cell fate decisions upon neural differentiation, with where Chd5 loss creating a skewed cell fate toward the astrocytic lineage. It has been demonstrated that cell-type-specific gene expression programs are prominent regulatory mechanism that coordinate appropriate spatiotemporal cell fate decisions (Jaenisch and Young, 2008; Jojic et al., 2013). I had hypothesized that Chd5 loss led to disarray in neural cell fate determination, which underlies the skewed cell fate defects of *Chd5*-/- NSCs. In addition, altered gene expression programs may explain distinct cellular properties of *Chd5*+/- NSCs (see Figure 15).

I examined global gene expression patterns of a panel of NSC samples of all three genotypes (i.e. +/+ n=2; *Chd5*+/- n=6; *Chd5*-/- n=4). In my initial global gene expression analysis, a group of genes located on the Y chromosome was identified to be highly upregulated in Chd5 compromised NSCs. *Uty* was upregulated by 27-fold, *Kdm5d* was upregulated by 12.5-fold, *Eif2s3y* was upregulated by 65-fold, and *Ddx3y* was upregulated by 14-fold. Therefore, it

seemed as though these genes were under gender biases. Subsequent gender analysis identified gender biases on 56 genes—these genes displayed significantly biased expression in either males or females. To minimize gender bias in differential gene expression analysis, we decided to focus specifically on female samples of three genotypes for hierarchical clustering analysis (i.e. +/+ n=2, *Chd5*+/- n=5, and *Chd5*-/- NSCs n=2). Lastly, we also separately compared gene expression patterns of male *Chd5*-/- NSC samples (n=2) with corresponding female *Chd5*-/- samples (n=2) to probe gender biases (Data not shown). Notably, recent study has demonstrated the histone demethylase activity of Uty (Kdm6c), and hence it is highly plausible that a significant increase in *Uty* in male mouse brain is at least in part responsible for the marked reduction of H3K27me3 in *Chd5*-/- NSCs.

My findings revealed that total 1040 genes were differentially expressed (Figure 13). Most strikingly, among these differentially expressed genes, the majority of genes (n=981) were upregulated more than 1.75-fold (i.e. 0.80 in Log2 ratio) and a smaller fraction of genes (n=59) were downregulated more than 1.75-fold (i.e. -0.80 in Log2 ratio), thereby indicating that Chd5 mostly confers a transcriptional repressive function in NSCs. Given its close structural identity to Chd3 and Chd4, both of which are subunits of the transcriptional repressive complex NuRD, it is certainly plausible that Chd5 may work as a subunit of NuRD. To support this notion, biochemical approaches have discovered that CHD5 physically interacts with essential components of NuRD complex (i.e. HDAC1/2, RBBP7, and MTA2/4) (Kloet et al., 2015; Kolla et al., 2015; Potts et al., 2011). Interestingly, components of the transcription repressive complexes including PRC1, PRC2, and NuRD, were upregulated in *Chd5*-/- NSCs, thereby suggesting potential chromatin deregulation (see Figure 20).

Another noticeable feature in gene expression patterns of these female NSCs was that *Chd5*+/- samples displayed bimodal expression patterns: two heterozygous samples were clustered with +/+ NSC samples and the other three were clustered with *Chd5*-/- NSC samples, thereby providing potent mechanistic insights for previously observed bimodal behaviors and dendritic arborization defects of *Chd5*+/- mice (Horev et al., unpublished) (see Figure 15). Among differentially regulated genes, ~68% of genes showed variability across genotypes, mostly explained by bimodal expression of *Chd5*+/- samples. Subsequently, we divided the set of genes into two groups: consistently altered genes and inconsistently altered genes. Gene ontology analyses revealed that both gene sets were highly enriched for a variety of biological processes (Mi et al., 2013). Consistently altered genes were significantly enriched for translation (GO:0006412) and cellular protein metabolic process (GO:0044267) (see Figure 16A). In contrast, inconsistently altered genes were highly enriched for positive regulation of dendritic spine development (GO:0060999) and regulation of dendritic spine development (GO:0060998) (see Figure 16B). Therefore, it appears that two groups of genes were altered by loss of Chd5 in NSCs. One group of genes was involved in homeostatic maintenance of NSCs, such as translation. The other group of genes might be involved in more specific biological processes. Yet, individual genes enriched in each category of gene ontology term should be validated by RT-qPCR, and the reproducibility also needs to be verified with bigger sample sizes. Functionality of identified genes should be probed by the manipulation using currently available technologies such as shRNA libraries or the CRISPR/Cas9 system.

The gene set enrichment analysis (GSEA) is useful to identify a specific biological setting where two sets of genes behave in a similar manner. As a result, the GSEA identified a gene set

(MEISSNER_BRAIN_HCP_WITH_H3K4ME3_AND_H3K27ME3, normalized enrichment score: 2.588, FDR q-value: 0.000484) in which 68 altered genes in *Chd5*+/- and *Chd5*-/- NSCs displayed a statistically significant enrichment (Data not shown). Intriguingly, these genes are expressed in mouse brain and are characterized by high density CpG islands at their promoters. Nonetheless, DNA methylation is not prominent. The most notable feature of these genes is the simultaneous presence of the transcriptional activation mark H3K4me3 (and H3K4me2) and the transcriptional repression mark H3K27me3. These genes are critical genes for development (Meissner et al., 2008). This observation, therefore, reinforces a potent connection between Chd5 and the repressive mark H3K27me3, consistent with my discovery that H3K27me3 and the enzymes that regulate it are intimately linked to Chd5.

In summary, RNA-seq analysis illustrated that Chd5 is indeed involved in transcriptional modulation of a sizable fraction of genes, perhaps through regulation of chromatin structure and organization. This list of differentially expressed genes may or may not be direct targets of Chd5. ChIP with a specific antibody against Chd5 is necessary to probe a direct relationship and has been in progress.

3.3 Chd5 Modulates H3K27me3 Modification through Utx

In addition to aforementioned potential connection between Chd5 and general transcriptional repression, Chd5 interacts with unmodified tail of histone H3 through its dual plant homeodomains (PHDs) (Oliver et al., 2012; Paul et al., 2013), an interaction that is essential for Chd5 activity (Paul et al., 2013). Chd5 can also bind other covalently modified

histone tails; Chd5 physically interacts with histones, where lysine 27 residue of the N-terminal tail is covalently modified with a trimethyl group (Egan et al., 2013; Paul et al., 2013). Therefore, it raises an important question whether Chd5 mediates transcriptional repression through H3K27me3 or the interaction with histone H3K27-specific methyltransferase (i.e. Ezh2) or demethylases (i.e. Utx and Jmjd3).

To test this hypothesis, I assessed the overall level of H3K27me3 in *Chd5*-/- NSCs by western blot analyses and immunofluorescent analyses (see Figure 21A). As a result, I identified a marked reduction of H3K27me3 levels as well as H3K27me2 in *Chd5*-/- NSCs (see Figure 21B). Most importantly, ectopic expression of Chd5 cDNA (*Chd5* variant 2, NCBI Reference Sequence ID: NM_029216.2) restored the overall levels of H3K27me3 in *Chd5*-/- NSCs, thereby providing evidence that Chd5 directly modulates H3K27me levels in NSCs (see Figure 21C).

Subsequent ChIP-qPCR to assess H3K27me3 enrichment levels on 16 genomic sites (i.e. 8 promoters and 8 intragenic gene body regions of cell-type-specific marker genes) (see Figure 22A-D). This analysis revealed that H3K27me3 is reduced at specific genomic loci in *Chd5*-/- NSCs. In addition, the extent of H3K27me3 enrichment inversely correlates with gene expression for these targets in *Chd5*-/- NSCs (see Figure 22D). I measured gene expression levels of each gene in *Chd5*-/- NSCs by qPCR, and the ΔCp values indicated normalized gene expression levels with respect to endogenous control *Actb*. The higher enrichment H3K27me3 yielded the larger ΔCp value (i.e. lower gene expression). As I predicted, expression of genes encoding neural stem/progenitor markers (i.e. Ascl1, Cspg4, Sox4, and Pax6) were high in NSC

samples, whereas expression of genes encoding the neuronal marker (i.e. Snap25) and the astrocytic marker (i.e. Slc1a2) were reduced (see Figure 22D). Therefore, this analysis demonstrated that altered transcriptional regulation, observed in *Chd5*-/- NSCs, is likely mediated by H3K27me3.

Intriguingly, the promoter and intragenic region within the gene body of early neuronal progenitor marker *Eomes* (Tbr2) clearly displayed an opposite trend, where H3K27me3 enrichment at these genomic sites in *Chd5*-/- NSCs is comparable at promoter but enhanced within the gene body (see Figure 22A-B). Importantly, this pattern inversely correlates with the relatively low expression of *Eomes* in *Chd5*-/- NSCs (see Figure 23). On the other hand, H3K27me3 enrichment at the *Slc1a2* locus showed a clear reduction both at the promoter and within the gene body (see Figure 22A-B). This pattern inversely correlates with high relative expression of *Slc1a2* in *Chd5*-/- NSCs (see Figure 23). *Cspg4* also displayed similar pattern, where H3K27me3 enrichment was comparable both at the promoter and within the gene body (see Figure 22, A-B). Yet, this pattern was not inversely correlated with expression of *Cspg4* (Data not shown). One explanation for this is that overall enrichment of H3K27me3 on *Cspg4* genomic sites was low, which potentially impedes the reliable measurement of H3K27me3 enrichment (see Figure 22A-B). Taken together, these findings provided evidence that Chd5 exerts transcriptional regulatory control through modulation of H3K27me3 at specific genomic sites. Nonetheless, the small sample size is a potential caveat of this analysis. Therefore, it will be necessary to expand this analysis with a larger sample size. More importantly, unbiased genome-wide assessment of H3K27me3 histone mark along with additional marks such as the transcriptional activation mark H3K4me3 or open-chromatin associated mark H3K4me2 can

yield more comprehensive data and provide more insights into the nuances of Chd5-mediated chromatin regulatory mechanisms across the genome.

From a structural perspective, Chd5 does not contain either a histone methyltransferase or a histone demethylase module (Flaus et al., 2006) (see Figure 1). Therefore, in order for Chd5 deficiency to affect H3K27me3 levels, Chd5 must normally facilitate or inhibit the activity of H3K27me3-specific methyltransferase (i.e. Ezh2) or the activity of demethylases (i.e. Utx and Jmjd3, respectively). To test this hypothesis, I examined transcriptional levels of *Ezh2*, *Kdm6a* (Utx), and *Kdm6b* (Jmjd3) in *Chd5*-/- NSCs. While expression levels of *Ezh2* and *Kdm6b* were not significantly different, *Kdm6a* and Utx (encoded by *Kdm6a*) were aberrantly upregulated in Chd5-deficient NSCs (see Figure 24). However, unbiased RNA-seq gene expression analysis did not identify *Kdm6a* as being upregulated. Therefore, it appears that Utx is not directly regulated by Chd5 at the transcriptional level, but rather is indirectly regulated at the posttranscriptional level. Nonetheless, subsequent western blot analysis confirms the increased expression of Utx *Chd5*-/- NSCs (see Figure 24). It seems plausible that increased expression of Utx, due to Chd5 loss, is responsible for a marked reduction of H3K27me3 in *Chd5*-/- NSCs. To probe a genetic and functional relationship between Chd5 and Utx, I performed *in vitro* neurogenesis experiments with +/+ and *Chd5*-/- NSCs that had been transduced with shRNA against Utx. As a result, Utx knockdown remarkably rescued cell fate defects of *Chd5*-/- NSCs, thereby supporting my hypothesis that Chd5 mediates the regulation of H3K27me3 in NSCs through the functional interaction with H3K27me3-specific demethylase Utx (see Figure 25).

This Chd5-Utx axis is the first to be described. A novel functional relationship between the chromatin remodeler and the histone demethylase has important mechanistic implications for regulation of chromatin structure and organization. While Chd5 is shown to physically interact with several components of NuRD complex, it has not been reported to directly interact with any other chromatin regulator or chromatin regulator complexes (Kloet et al., 2015; Kolla et al., 2015). Likewise, while UTX has been shown to interact with trithorax group complex MLL2/3, it has not been reported to interact with other chromatin remodelers (Lee et al., 2007). Therefore, it is extremely important to investigate the nature of this functional interaction and find whether there is a physical interaction between Chd5 and Utx.

In summary, these findings comprehensively illustrate that Chd5 is deeply rooted in homeostatic maintenance of NSCs. Loss of Chd5 causes these important neural stem/progenitor cells to acquire aberrant cellular properties and to change their differentiation states. These changes manifest in altered cell fate decisions of NSCs, and Chd5 directly regulates this process. From a mechanistic perspective, Chd5 mediates H3K27me3 regulation through the H3K27me3-specific histone demethylase Utx. Loss of Chd5 causes deregulation of H3K27me3 that in turn leads to a global misregulation of genes, including NSC-specific genes. Therefore, Chd5 plays a critical chromatin regulator in NSCs.

This findings have critical implications for the pediatric glioma, diffuse intrinsic pontine gliomas (DIPGs), where a gene encoding histone H3.3 (*H3F3A*) is frequently mutated to harbor a methionine mutation on lysine 27 (i.e. K27M). Most intriguingly, this switch from lysine to

methionine causes the global reduction of H3K27me3—precisely the alteration that I discovered in Chd5-compromised NSCs (Lewis et al., 2013). Accordingly, it was proposed that this reduced H3K27me3 impedes the proper interaction between amino terminal domains of histone H3 and their cognate regulators EZH2 of PRC2 complex, thereby causing disregulation of PRC2-mediated gene expression programs. Importantly, follow-up studies using ES cell-derived NPC system demonstrated compelling evidence that the marked reduction caused by H3.3K27M mutation, leads to an altered cell state and differentiation capacity of NPCs, which are characterized by a more primitive stem-like state. Lastly, the alteration in cellular states coincides with misregulation of global gene expression programs in NPCs (Funato et al., 2014). My findings and these findings converge upon the regulation of H3K27me3 and modulation of gene expression programs in neural progenitor cells. Thus, my findings in this thesis shed light on novel regulatory mechanisms of chromatin structure, which is mediated by the functional interaction between the chromatin remodeler Chd5 and the histone demethylase Utx.

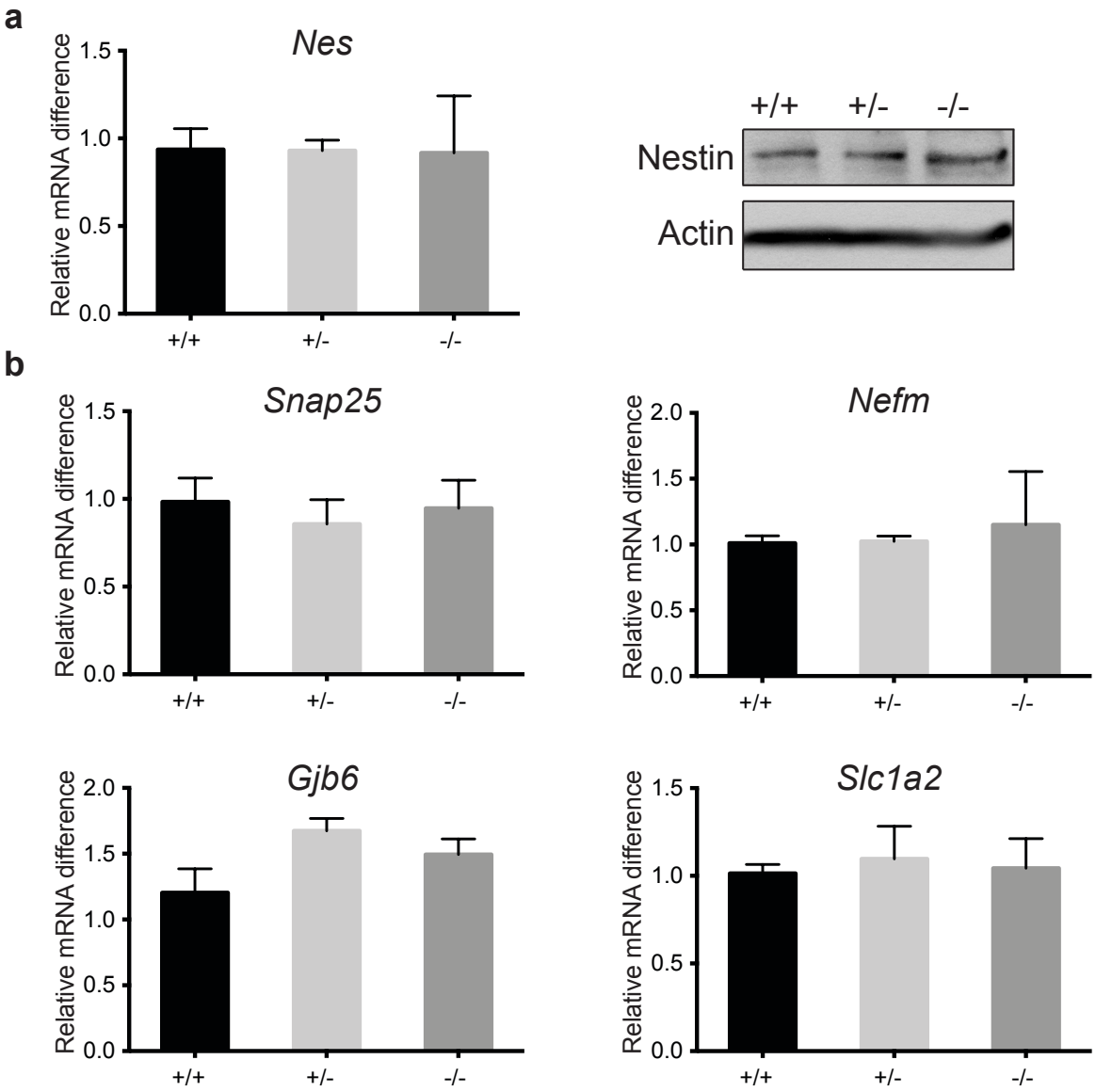

Figure 26: Comparable expression of cell-type-specific markers in *Chd5*+/- and *Chd5*-/- brain

Expression of *Nes* (Nestin) and Nesin was analyzed by RT-qPCR and western blotting analyses of +/+, *Chd5*+/- and *Chd5*-/- P1 brains. (a) Average expression of *Nes* (Nestin) in +/+ NSCs is compared to average expression in *Chd5*+/- and *Chd5*-/- brain samples, which were isolated from the same litter. Relative mRNA difference is shown in fold change (y-axis). Error bars indicate standard deviation of three biological replicates (n=3). Shown are representative western blots of +/+, *Chd5*+/-, and *Chd5*-/- total brain lysates. Blots are probed for Nestin (right) and Actin. (b) Average expression of *Snap25* (left,above), *Nefm* (right, above), *Gjb6* (left, below), and *Slc1a2* (right, below) in +/+ brain (P1) is compared to average expression in *Chd5*+/- and *Chd5*-/- littermate brain samples. Relative mRNA difference is shown in fold change (y-axis). Error bar indicates standard deviation of three biological replicates (n=3).

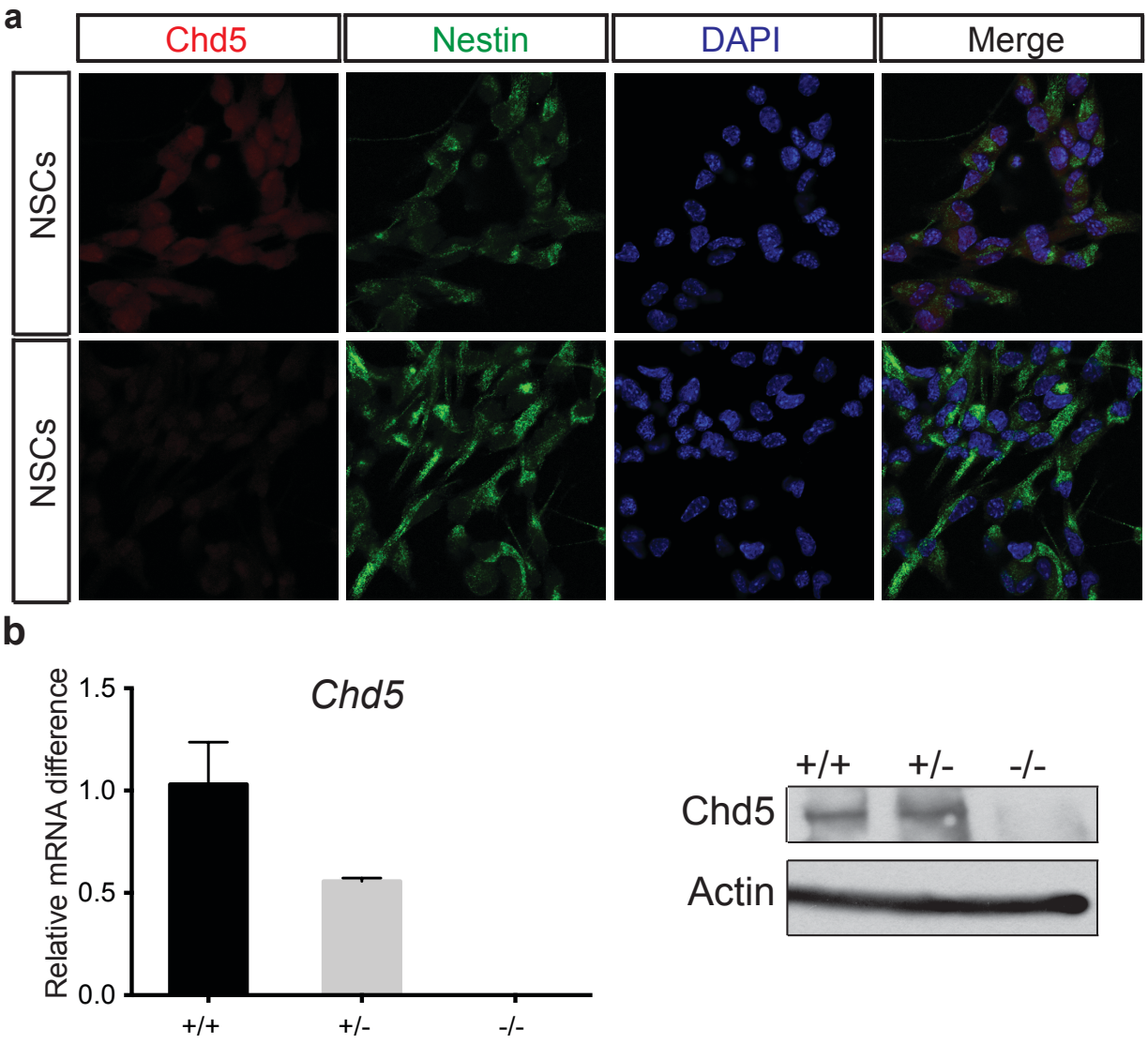

Figure 27: Expression of Chd5 in primary NSCs and neonatal mouse brain

Expression of Chd5 in neurosphere-derived adherent NSCs and its transcript in neonatal brain were analyzed by immunofluorescent analyses, RT-qPCR, and western blot analyses. (a) Shown are representative images of wild type (above) and *Chd5*-/- NSCs (below). Individual images of each channel, Chd5 (red), Nestin (green), DAPI (blue), and merged (merge), are shown. (b) Average expression of *Chd5* in +/+ P1 brain is compared to average expression in *Chd5*+/- and *Chd5*-/- littermate brain samples (n=3) (left). Relative mRNA difference is shown in fold change (y-axis). Error bars indicate standard deviation of three biological replicates (n=3). (b) Shown are representative western blots of +/+, *Chd5*+/-, and *Chd5*-/- total brain lysates (P1 brain). Blots were probed for Chd5 (upper panel) and Actin (lower panel).

Chapter 4. Materials and Methods

4.1 Primary Neural Stem/Progenitor Cell Culture

To isolate primary neural stem/progenitor cells (primary NSCs), the mouse brain explant culture method was utilized as previously described (Deleyrolle and Reynolds, 2009; Marshall et al., 2008; Reynolds and Weiss, 1992). Briefly, the periventricular region, including ventricular zone (VZ) and subventricular zone (SVZ), of neonatal (postnatal day 0-1) mouse brain was dissected. The VZ-SVZ explant was immediately subject to enzymatic and mechanical dissociation procedures. The explant was initially treated with 0.25% trypsin-EDTA, composed of 0.25% Trypsin (Gibco) and 0.04% EDTA (Fisher Chemical) for 5 minutes in a 37°C tissue culture incubator in which the level of CO_2 was maintained at 5%. A trypsin reaction was quenched with 0.5% fetal bovine serum (FBS) containing NSC basal medium, comprised of DMEM/F-12 1:1 mix (HyClone), 1x N-2 media supplement (Gibco), 0.1% bovine serum albumin (BSA) fraction V (Sigma), and 0.5% penicillin-streptomycin (In-house). Subsequently, a series of trituration was implemented utilizing pipets with descending diameters to obtain single-cell suspensions. Dissociated cells were pelleted by centrifugation for 5 minutes at 1000 rpm. Cell pellets were carefully resuspended in freash NSC proliferation medium—NSC basal medium supplemented with 20 ng/ml of epidermal growth factor (EGF: Pepro Tech) and 20 ng/ml of fibroblast growth factor 2 (FGF-2: Pepro Tech). Resuspended cells were plated in 6-well plates (Corning) and incubated for 6-8 days in a 37°C tissue culture incubator (5% CO_2) until the first passage.

During this initial incubation period (before the first passage), the vast majority of cells died, yet EGF- and FGF-2-responsive cells survived to give rise to spherical clusters of cells (see Figure 9). These spheroids (i.e neurospheres) were heterogenous mixture of three populations: less proliferative neural stem cells (i.e. the Cd133-positive population), proliferative transit amplifying progenitors (i.e. Egfr-positive population) and early neuronal precursor cells (i.e. the $Cd24^{Low/High}$ population) (see Figure 4A). Primary NSC neurospheres were allowed to grow to reach 100-200 μm in diameter during the initial incubation (Siebzehnrubl et al., 2011). Spheroids of varying sizes were observed (see Figure 9). To compensate for loss of EGF and FGF-2 by extended incubation to 6-8 days, the culture medium in tissue culture plates was partially replenished with an equal volume of fresh medium containing increased amount of EGF (40 ng/ml) and FGF-2 (40 ng/ml) every three days.

After the first passage, primary NSCs were subject to routine passages between 5 and 15 times. It took approximately 6 days for the majority of neurospheres to grow over 100μm in diameter. Therefore, I passaged cells every 6 days. This passage procedure was carried out by enzymatic dissociation of neurosheres using 0.25% trypsinization-EDTA and subsequent reseeding in fresh NSC proliferation medium. At either passage 5 or 6, a portion of the neurosphere culturea were dissociated and frozen in a freezing medium composed of 90% NSC proliferation medium and 10% DMSO (Mallinckrodt Chemicals). Cells were allowed to freeze slowly in a cryogenic container at -80 degree for a day, and transferred to liquid nitrogen tank for long-term storage.

4.2 *In Vitro* Neural Differentiation of Neural Stem/Progenitor Cells

The capacity of NSCs to give rise to major neural lineages is a defining feature of primary NSCs (Louis et al., 2013). To examine the differentiation capacity of primary NSCs, I performed *in vitro* differentiation assays utilizing the neurosphere-derived adherent culture system. Primary NSC neurospheres at mid passage (i.e. passage number 5-10) were enzymatically dissociated using 0.25% trypsin-EDTA. An enzymatic reaction of trypsin was quenched by addition of NSC basal medium containing 0.5% FBS. After a brief centrifugation for 5 minutes at 1000 rpm, cell pellets were resuspended in fresh NSC proliferation medium. Using 0.4% trypan blue (Gibco) and Countess® cell counter (Invitrogen), cell density (cells/ml) of the viable fraction of cells in suspensions was quantified. Based on the estimated cellular density, a low cell density (i.e. $5.0 \times 10^4 - 1.0 \times 10^5$ cells/ml) suspension was prepared for seeding. To obtain the uniform cellular density (2.25×10^4 cells/cm^2), an appropriate amount of cell suspension was added to previously prepared coated 8-well-chamber slides (Thermo Scientific) and 100 mm tissue culture plates (Corning). Plates were prepared prior to seeding (1-2 days prior) by coating with poly-D-lysine (Sigma) and laminin (Sigma). Coated chamber slides and plates were prepared as previously described (Louis et al., 2013).

Neuropshere-derived adherent cultures were incubated for 1-2 days in a 37°C tissue culture incubator (5% CO_2). I found that within 24-48 hours post seeding, the majority of seeded cells settled and attached onto the coated-surface of chamber slides and plates. During this incubation period, dissociated cells were cultured in NSC proliferation medium supplemented with growth factors (i.e. EGF and FGF-2) to ensure differentiation in check. One to two days

after seeding, the culture medium for adherent NSCs was replaced with "Neuronal differentiation" medium—Neurobasal medium (Gibco) supplemented with B-27 (Gibco). This medium was formulated to promote neuronal differentiation and growth of neuronal lineage of cells. This time point was designated as the initial time point (i.e. day 0 post differentiation), and the sample was named, "Undifferentiated" NSCs. I observed that cells underwent rapid growth period between day 0 and day 2 as they exited from the multipotent stem/progenitor states. By day 4 post differentiation, cells acquired premature neuronal morphologies (i.e. neurites projecting from the opposite ends of the compact cell body) and astrocytic morphologies (i.e. start-shaped protoplasmic cell body) (see Figure 11 and Figure 13). By day 7, a sizable fraction of cells underwent apparent cell death as the cell number drastically decreased. This process seemed to operate rather stochastically as the extent of apoptosis between different biological samples varied. Therefore, I performed most image analyses on the day 4 samples. Notably, in this "Neuronal differentiation" condition, the oligodendrocytic lineage did not differentiate and proliferate as efficiently as did the neuronal and astrocytic lineages. Oligodendrocytes were rarely observed in the day 4 and day 7 samples. The vast majority of cells acquired either neuronal or astrocytic morphologies. These samples are named "Differentiated" NSC-derived neural cells. Subsequently, both the initial and final time point samples were directly subject to either image analysis with an inverted phase contrast microscope (Zeiss Avio Vert. A1) or immunofluorescent staining followed by image analysis with a confocal laser scanning microscopes (Zeiss LSM 710 and LSM 780).

4.3 Phase Contrast Image Analysis

To examine morphological features of "Undifferentiated" NSCs and "Differentiated" NSC-derived neural cells, phase contrast images of NSC neurospheres and neurosphere-derived adherent cultures were analyzed (Data not shown). Neurospheres and neuropshere-derived adherent cells were prepared as described above. Subsequently, images were obtained using an inverted phase contrast microscope (Zeiss). ImageJ software was utilized to perform image analysis, including the quantification of diameters of neurospheres.

4.4 Immunofluorescent Analysis of Brain Sections and NSCs

To examine expression of Chd5 in embryonic mouse brain (E15.5) and neonatal mouse brain (P1), immunofluorescent analyses method were employed. Whole mouse brain at E15.5 and P1 developmental stages were dissected from a litter of previously generated Chd5-deficient mouse model, where the mating scheme was designed to generate three genotypes: wild type (+/+), heterozygotes (+/-), and homozygotes (*Chd5*-/-). PCR genotyping was carried out to select a pair of wild type and homozygote littermate samples. Corresponding brain samples were fixed in 4% paraformaldehyde (PFA) over night at 4°C. Frontal regions of fixed brain tissues, where the periventricular regions (i.e. VZ-SVZ) were located, were coronally cut and embedded in paraffin blocks. Subsequently, sequential coronal sections at 5μm thickness were prepared through the histology core facility (Histology Shared Resource, Cold Spring Harbor Laboratory).

In order to verify the identities of "Undifferentiated" and "Differentiated" NSC-derived neural cells, immunofluorescent staining method was employed to examine the presence of cell-type-specific markers on neurosphere-derived adherent cultures. "Undifferentiated" NSCs were immunolabeled with specific antibodies that recognized neural stem/progenitor cell markers (Nestin and Pax6) and neuronal precursor marker (Tbr1). "Differentiated" NSC-derived neural cells (i.e. day 4 and day 7 samples) were immunolabeled with antibodies against neuronal marker (Map2) and astrocytic marker (Gfap). Briefly, immunofluorescent staining was performed as follows. Neurosphere-derived adherent cells were fixed in 4% paraformaldehyde (PFA) at room temperature for 20 minutes. Subsequently, permeabilization was carried out in 0.5% Triton X-100 (Sigma) in phosphate buffered saline (PBS) on ice for 5 minutes. To reduce background noise, fixed and permeabilized cells were incubated in 3% BSA blocking solution (3% BSA in PBS) at room temperature for 1 hour. Subsequently, cells were incubated with corresponding primary antibodies in 1% BSA solution (1% BSA in PBS) at 4°C for 14-16 hours. After 3 washes with 1x PBS, cells were incubated with secondary antibodies, conjugated with fluorophores (Alexa Fluor 488 and Alex Fluor 568: Life Technologies). Lastly, cells were incubated with PBS, supplemented with 4',6-diamidino-2-phenylindole **(**DAPI) at the concentration of 1µg/ml, to label the nuclei. All images were obtained using Zeiss LSM 710 and 780 confocal microscopes. ImageJ software was utilized to conduct image analysis. Information about the antibodies and staining conditions can be found in Table 1.

To quantify of Map2-positive (i.e. neurons) and Gfap-positive (i.e. astrocytes) cells in "Differentiated" samples, cell counter plugin function of ImageJ software was used to track and faithfully score DAPI-positive/Map2-positive "Map2-positive neurons", DAPI-positive/Gfap-

positive “Gfap-positive astrocytes,” and DAPI-positive/Map2-negative/Gfap-negative “DAPI-positive unidentified” cells. Images were taken in randomly selected fields (10-15 fields, 40x magnification) from each biological sample (n=3) were collected (total 30-45 images for each experimental group). Within each image, fractions (%) of 3 cellular classes (i.e. neurons, astrocytes and DAPI+ unidentified cells) were computed by dividing the number with an individual class by the total number for the three classes. These percentages of each image were recorded in Excel spreadsheet (Microsoft). Using Prism software (GraphPad software), combined percentages of all three biological samples were plotted as a box plot. Unpaired t test and Tukey’s multiple comparison test were performed to compute a statistical significance between different biological groups (e.g. +/+ vs *Chd5* -/-).

4.5 Cell Surface Marker Assessment of Neural Stem/Progenitor Cells by Flow Cytometry

To validate the identities of subpopulations within culture and to quantify the extent of heterogeneity at the subpopulation level, neurospheres were analyzed for cell surface marker expressions by flow cytometry. Three well-characterized cell surface markers were used to identify each subpoplution as described (Codega et al., 2014; Mich et al., 2014). Cd133 is a transmembrane glycoprotein, also known as prominin 1, and is exclusively expressed in neural stem cells. Egfr is a receptor of epidermal growth factor (Egf) and is expressed in activated neural stem cells, which was used to identify neural progenitor cells in this study. Cd24 is a Glycosylphosphatidylinositol (GPI)-anchored transmembrane glycoprotein and highly expressed in neuronal precursor cells (i.e. neuroblasts). All antibodies were fluorochrome-conjugated: Cd133-PE (eBioscience), Egfr-Alexa Fluor 647 (Life Technologies) and Cd24-APC and Cd-PE

(eBioscience). Flow cytometry assessment was performed on LSRII (BD Bioscience). Subsequently, data analysis and graphing was performed with FlowJo software.

4.6 Proliferation Assessment of Neural Stem/Progenitor Cells by Flow Cytometry

Aforementioned subpopulations are characterized differing proliferation rates. Therefore, I examined the proliferation of neurospheres by utilizing a commercially available EdU (5-ethynyl-2´-deoxyuridine) incorporation strategy (Click-iT® Plus Edu, Molecular Probes), which is based on the incorporation of thymidine analog EdU into newly synthesized DNA during S phase. Cells were allowed to grow in EdU-containing NSC proliferation medium (at the final concentration of 10μM) for 2 hours in a 37°C tissue culture incubator (5% CO_2). Cells were fixed and permeabilized according to the kit's instruction. Incorporated EdU was chemically conjugated with a specific fluorochrome (Pacific Blue). The rate of proliferation, which is directly correlated with the degree of EdU incorporation, was measured by flow cytometry. Data analysis was performed with FlowJo software.

4.7 RNA-sequencing Analysis of Global Gene Expression

To assess the impact of Chd5 loss on gene expression programs of NSCs, I compared global gene expression patterns of NSCs isolated from mice of three different genotypes: wild type (+/+), *Chd5* heterozygote (*Chd5*+/-) and *Chd5* null (*Chd5*-/-). Each group was composed of 2-6 biological samples. Using a column-based RNA isolation kit (Qiagen, RNase Mini Kit), total RNA was directly isolated from NSC neurospheres. DNase I-treated total RNA samples were

subject to a quality control procedure to ensure that the extent of degradation was minimal. A high sensitive electrophoresis-based assay (Bioanalyzer 2100, Agilent) was used. With samples that passed quality control, I proceeded to prepare cDNA sequencing libraries using a commercially available library preparation kit (TruSeq® Stranded mRNA Sample Preparation Kit, Illumina). Briefly, mRNA molecules, containing poly-A tails were selected and fragmented to generate corresponding cDNA fragments, cDNA molecules were ligated with specific adapters to uniquely mark each sample, and adapter-ligated DNA fragments were amplified by PCR reaction (12 cycles). PCR-amplified DNA fragments were size-selected, repurified and subject to a quality control procedure using Bioanalyzer 2100 and quantitative PCR. The sequencing core facility (Next Generation Sequencing Shared Resource, Cold Spring Harbor Laboratory) performed the sequencing run on the NextSeq 500 (Illumina) in the high output mode. All data analysis, including the gene ontology (GO) term enrichment analysis and gene set enrichment analysis (GSEA) was conducted through the bioinformatics core facility (Bioinformatics Shared Resource, Cold Spring Harbor Laboratory) (Mi et al., 2013; Subramanian et al., 2005).

4.8 Quantitative Real-Time PCR of Gene Expression

To examine expression of individual genes, quantitative RT-PCR (RT-qPCR) was utilized. Total RNA was isolated from wild type (+/+), *Chd5* heterozygote (*Chd5*+/-), *Chd5* null (*Chd5*-/-) , wild type with exogenous Chd5 (+/+; Chd5), corresponding empty vector control (+/+; EV), *Chd5* null with exogenous Chd5 (*Chd5*-/-; Chd5), and corresponding empty vector control (*Chd5*-/-; EV). DNase I-treated total RNA was converted to cDNA by a reverse transcriptase

enzymatic reaction (SuperScript® III First-Strand Synthesis System, Invitrogen). PCR reaction (total volume of 10µl) was prepared by mixing diluted cDNA (4 µl) with 1µl of primer pair (i.e. sense and anti-sense) and 5µl of 2 x SYBR Green PCR mix (Roche). PCR runs were performed on the Light Cycler 480 thermocycler (Roche). Each reaction for individual primer pairs was composed of 3 technical replicates. To estimate the normalized expression level in each sample, the average Ct value (i.e. cycle number where the exponential amplification of molecules occurs) of endogenous control (i.e. *Actb*) was subtracted from the average Ct value of each gene (i.e. ΔCt). Subsequently, ΔCt values of wild type control (e.g. one of the biological replicates of wild type group) were subtracted from ΔCt values of corresponding other samples (i.e. ΔΔCt). These numerical differential values among each group (e.g. +/+ and Chd5-/-) were then converted to a fold-difference. All graphs were plotted, using Prism software (GraphPad software). The sequence information about the primers utilized in RT-qPCR can be found in Table 2.

4.9 Chromatin Immunoprecipitation Analysis

To assess the enrichment of H3K27me3 at multiple genomic sites, I implemented chromatin immunoprecipitation and analyzed the signals by qPCR (ChIP-qPCR). ChIP was performed as described (Steger et al., 2008). Briefly, +/+ and *Chd5*-/- NSCs were enzymatically dissociated and were counted to obtain ~5.0 x 10^6 cells per a single ChIP assay. Dissociated cells were crosslinked with 1% formaldehyde (at the final concentration) (J.T.Baker), which was not older than 6 months. Crosslinking was quenched with 125mM of Glycine (at the final concentration). Crosslinked cells were washed once with 1X PBS buffer and pelleted by a brief centrifuge at 2000 RPM for 5 minutes. Pellets were immediately resuspended in cell lysis buffer

(10mM Tris-Cl, pH 8.0, 10mM NaCl, and 0.2% NP-40) that contained protease inhibitor cocktail (Roche). Cell lysis was done on ice for 15 minutes. Immediately after the lysis procedure, cells were pelleted and resuspended in nuclear lysis buffer (50mM Tris-Cl, pH 8.0, 10mM EDTA, and 1% SDS) that contains protease inhibitor cocktail (Roche). Resuspended cells were sonicated by 2 rounds of 15 sonication cycles (30 second on/30 second off), using Bioruptor® Standard (Diagenode). Chromatin containing supernatant were diluted in IP dilution buffer (20mM Tris-Cl, pH 8.0, 2mM EDTA, 150mM NaCl, 1% Triton X-100, and 0.01% SDS) and were subject to a preclearing procedure with 35µl of protein A beads (Roche) and 50 µg of IgG at 4°C for 2 hours. Precleared materials were immunoprecipitated 35 µl of either protein A beads with 2 µg of the specific antibody recognizing H3K27me3 (Millipore EMD) and the same amount of normal rabbit IgG (Santa Cruz Biotechnology). Immunoprecipitation was performed at 4°C for 14-18 hours. Next, protein A beads were subject to a series of washing regimen with four buffers (IP wash buffer 1: 20mM Tris-Cl, pH 8.0, 2mM EDTA, 50 mM NaCl, 1% Triton X-100, 0.1% SDS; High salt buffer: 20mM Tris-Cl, PH 8.0, 2mM EDTA, 500mM NaCl, 1% Triton X-100, 0.01% SDS; IP wash buffer 2: 10mM Tris-Cl, pH 8.0, 1mM EDTA, 0.25M LiCl, 1% NP-40, 1% Sodium Deoxycholate; TE, pH 8.0). Chromatin was eluted from the beads and reverse-crosslinked at 65°C for 14-18 hours with RNase A (Roche) treatment. Reverse-crosslinked chromatin was digested with Proteinase K (New England Biolab) at 42°C for 2 hours. Proteinase K-treated chromatin then was extracted by phenol:chloroform:isoamyl alcohol and extracted by chloroform. Extracted chromatin DNA was subject to qPCR as described earlier. 5% input material was serially diluted to prepare 4-5 standards. These standards run along with ChIP sample and IgG controls. Based on ΔCt values of each sample, the absolute enrichment of

H3K27me3 was estimated. The sequence information about the primers utilized in ChIP-qPCR can be found in Table 3.

4.10 Western Blot Analysis of Protein Expression

To assess the expression of proteins at the population level, western blot analysis was implemented. Briefly, total protein lysates of NSCs were prepared using protease-inhibitor (Roche) supplemented RIPA lysis buffer composed of 50 mM Tris-HCl (pH 8.0), 150 mM sodium chloride, 1.0% NP-40 substitute, 0.5% sodium deoxycholate and 0.1% sodium dodecyl sulfate. Cells were incubated in RIPA buffer for 10 minutes on ice, immediately followed by 2-5 sonication cycles (30 second on/30 second off) using the Bioruptor® Standard (Diagenode). The lysates were centrifuged at the full speed for 10 minutes at 4°C, supernatants, in which soluble proteins are present, were transferred into a set of new microcentrifuge tubes, and protein concentration was quantified by the Bradford-method-based protein quantification assay kit (Bio-Rad). SDS-PAGE and immunoblotting were performed as previously described (Gallagher, 2001). A set of specific antibodies that recognize cell-type-specific markers and histone modifications were utilized for immunoblotting. As for immunoblot detection, an enhanced chemiluminescence (ECL) kit (SuperSignal™ West Dura Extended Duration Substrate, Thermo Scientific) was applied to the membrane. Subsequently, the membrane was exposed onto blue autography films (Crystalgen) for varying durations typically ranging from 5 seconds to 12 minutes in a dark room. Developed autographs were scanned on a scanner (V500, Epson), and the scanned images were visualized on Photo Shop software (Adobe). Information about the antibodies and immunoblotting conditions can be found in Table 4.

Table 1: Sources and conditions of antibodies utilized in immunofluorescent analyses

Protein ID	Sources	Catalog Number	Working Dilution
Chd5	Santa Cruz Biotechnology	sc-68389	1:200
Pax6	Abcam	ab78545	1:400
Nestin	Abcam	ab6142	1:400
Tbr1	Abcam	ab31940	1:500
Map2	Abcam	ab11267	1:500
Gfap	Dako	Z0334	1:500

Table 2: Sequences of primers utilized in gene expression analyses by qRT-PCR

Primer ID	Sequence (sense)	Sequence (anti-sense)
Chd5	CGGAGGAGATGGAGAACGAG	GCTCTGCAGGGAAGAAGTCC
Nes (Nestin)	GTGCAGCGCGACAACCTTGC	TCCTCGATGGTCCGCTCCCG
Pax6	TCGGAGGGAGTAAGCCAAGA	GGTACAGACCCCCTCGGATA
Ascl1	TCTCGTCCTACTCCTCCGAC	ATCTGCTGCCATCCTGCTTC
Sox4	GACAGCGACAAGATTCCGTT	GTTGCCCGACTTCACCTTCTTT
Tbr1	TAAACAGGGAAGGCGCATGT	TGGGATCCGCCAAAATCACA
Eomes (Tbr2)	TGTGACGGCCTACCAAAACA	TCTAGGGGAATCCGTGGGAG
Cspg4 (Ng2)	CGCCTTGAGGGTGGCACCAG	GTGCGCCGTCAGAGAGGTCG
Cux1	TCAACCTGAAGACCAGCACC	GAGCTGAAGGTGAGTCGCTG
Snap25	GGATGAGCAAGGCGAACAAC	TCCTGATTATTGCCCCAGGC
Nefm	ACCAGCTGCTCCGCTATAAA	AGTCCAGCGTGTAGCTCATC
Slc1a2	GGTGATGTCAGCTCTGGACAAA	TTGCAAGGTTTAGCCCAGCC
Gjb6	GCTTACCTGTGTTGGCGAGT	TAATAACCGCGCCTTTCACG
Ezh2	TGCTTCCTACATCGTAAGTGC	AAGGCTTGTTGTCCAAAGCTG
Kdm6a (Utx) #1	ATGTGACCCTACAGCCGAGC	TCCTAACGCGGTAGAGGTGA
Kdm6a (Utx*)* #2	GTGACCCTACAGCCGAGC	AAGACCGGCACACCAACTTT
Kdm6b (Jmjd3)	GGAGAGCAAACGAGATGCCT	GGCCTAAGTTGAGCCGAAGT
Actb (β-actin)	AGTACGATGAGTCCGGCCCCT	AACGCAGCTCAGTAACAGTCCGCC

Table 3: Sequences of primers utilized in H3K27me3 enrichment analyses by ChIP-qPCR

Primer ID	Sequence (sense)	Sequence (anti-sense)	Genomic Locations
Pax6 A	TCAGTTCCAAGCGAGGGAAG	CCCAAACCCGGCCAAATCTA	chr2:105668252-105668340
Pax6 B	GGCTTGGAGACATGAGGCTG	CTGTTTGCGACAGAAAACTTCC	chr2:105678134-105678204
Ascl1 A	TCCTTCCCACCCTTAGCGAG	GTTGCCACTGCTGTTCCATT	chr10:87494370-87494440
Ascl1 B	GCTGTCTTAGCCCCCTGAAA	TCCGAGAACTGACGTTGCTT	chr10:87491504-87491606
Sox4 A	CTGTATTCACCATGATCGCCC	GCTAAGGCAGTGGCCCATAA	chr13:28954565-28954641
Sox4 B	AACGAACCGATCACCAGCTC	AGCACAGATTTGAGTTGCGTT	chr13:28950374-28950445
Eomes (Tbr2) A	CTGCCTTCTGTATTGTGCCG	CTTTGGTGGGGACTGACACT	chr9:118477286-118477379
Eomes (Tbr2) B	CGGCAAAGCGGACAATAACAT	CCAACACTGAGGCTCCGAC	chr9:118480596-118480672
Cspg4 A	CCAGCTCCTGGTTGGGACTA	TGGCCCTGGATTTAGCTCCT	chr9:56864304-56864403
Cspg4 B	CCGAGCCCTGGTTTGTTTTG	ACACGAGCCGTTTCAATCCT	chr9:56867205-56867291
Cux1 A	AGCATGGTTGGGACAGAGTT	TTGCAATCCCCAACTTGCAC	chr5:136568096-136568221
Cux1 B	TAATGAACACCGCCGGATGG	TTCCACAACGGGTTTTACAGT	chr5:136564722-136564836
Snap25 A	AACCCGAATACCGCTCTAGG	GGGCTTTGAGTTGCGAGTTG	chr2:136712594-136712685
Snap25 B	TGCGTCAAATGCAAAGCCTAA	GGCACCTTAGCCAGCTTTAC	chr2:136715722-136715850
Slc1a2 A	AAGCCTCTGGGCTAGAATCC	ACTTGGGACCTGCTAGGCT	chr2:102657530-102657630
Slc1a2 B	ATCGTGTGATAACAAGTCAGTAGAA	CCACACACAAGACACTGGGTT	chr2:102664795-102664876

Table 4: Sources and conditions of antibodies utilized in western blotting analyses

Protein ID	Sources	Catalog Number	Working Dilution
Chd5	Santa Cruz Biotechnology	sc-68389	1:200
Pax6	Abcam	ab78545	1:400
Nestin	Abcam	ab6142	1:400
Tbr1	Abcam	ab31940	1:500
Tbr2 (Eomes)	Abcam	ab23345	1:500
Map2	Abcam	ab11267	1:500
Gfap	Dako	Z0334	1:500
Utx	EMD Millipore	ABE409	1:400
Actin (β-actin)	Sigma-Aldrich	A2228	1:1000
H3K4me3	EMD Millipore	07-473	1:1000
H3K9me3	Active Motif	39286	1:1000
H3K27me2	Active Motif	39920	1:1000
H3K27me3	EMD Millipore	07-449	1:1000
H3K27Ac	Abcam	ab4729	1:1000
H3	Active Motif	61475	1:5000

References

Aguirre, A., Dupree, J.L., Mangin, J.M., and Gallo, V. (2007). A functional role for EGFR signaling in myelination and remyelination. Nature neuroscience *10*, 990-1002.

Aoto, T., Saitoh, N., Ichimura, T., Niwa, H., and Nakao, M. (2006). Nuclear and chromatin reorganization in the MHC-Oct3/4 locus at developmental phases of embryonic stem cell differentiation. Developmental biology *298*, 354-367.

Aubry, F., Mattei, M.G., and Galibert, F. (1998). Identification of a human 17p-located cDNA encoding a protein of the Snf2-like helicase family. European journal of biochemistry / FEBS *254*, 558-564.

Azuara, V., Perry, P., Sauer, S., Spivakov, M., Jorgensen, H.F., John, R.M., Gouti, M., Casanova, M., Warnes, G., Merkenschlager, M.*, et al.* (2006). Chromatin signatures of pluripotent cell lines. Nature cell biology *8*, 532-538.

Bagchi, A., and Mills, A.A. (2008). The quest for the 1p36 tumor suppressor. Cancer research *68*, 2551-2556.

Bagchi, A., Papazoglu, C., Wu, Y., Capurso, D., Brodt, M., Francis, D., Bredel, M., Vogel, H., and Mills, A.A. (2007). CHD5 is a tumor suppressor at human 1p36. Cell *128*, 459-475.

Bell, O., Tiwari, V.K., Thoma, N.H., and Schubeler, D. (2011). Determinants and dynamics of genome accessibility. Nature reviews Genetics *12*, 554-564.

Bernstein, B.E., Mikkelsen, T.S., Xie, X., Kamal, M., Huebert, D.J., Cuff, J., Fry, B., Meissner, A., Wernig, M., Plath, K.*, et al.* (2006). A bivalent chromatin structure marks key developmental genes in embryonic stem cells. Cell *125*, 315-326.

Bertrand, N., Castro, D.S., and Guillemot, F. (2002). Proneural genes and the specification of neural cell types. Nature reviews Neuroscience *3*, 517-530.

Bickmore, W.A. (2013). The spatial organization of the human genome. Annual review of genomics and human genetics *14*, 67-84.

Bouazoune, K., Mitterweger, A., Langst, G., Imhof, A., Akhtar, A., Becker, P.B., and Brehm, A. (2002). The dMi-2 chromodomains are DNA binding modules important for ATP-dependent nucleosome mobilization. The EMBO journal *21*, 2430-2440.

Boyer, L.A., Plath, K., Zeitlinger, J., Brambrink, T., Medeiros, L.A., Lee, T.I., Levine, S.S., Wernig, M., Tajonar, A., Ray, M.K.*, et al.* (2006). Polycomb complexes repress developmental regulators in murine embryonic stem cells. Nature *441*, 349-353.

Buganim, Y., Faddah, D.A., and Jaenisch, R. (2013). Mechanisms and models of somatic cell reprogramming. Nature reviews Genetics *14*, 427-439.

Cairns, B.R. (2009). The logic of chromatin architecture and remodelling at promoters. Nature *461*, 193-198.

Casarosa, S., Fode, C., and Guillemot, F. (1999). Mash1 regulates neurogenesis in the ventral telencephalon. Development *126*, 525-534.

Castro, D.S., Skowronska-Krawczyk, D., Armant, O., Donaldson, I.J., Parras, C., Hunt, C., Critchley, J.A., Nguyen, L., Gossler, A., Gottgens, B.*, et al.* (2006). Proneural bHLH and Brn proteins coregulate a neurogenic program through cooperative binding to a conserved DNA motif. Developmental cell *11*, 831-844.

Codega, P., Silva-Vargas, V., Paul, A., Maldonado-Soto, A.R., Deleo, A.M., Pastrana, E., and Doetsch, F. (2014). Prospective identification and purification of quiescent adult neural stem cells from their in vivo niche. Neuron *82*, 545-559.

Dekker, J., Marti-Renom, M.A., and Mirny, L.A. (2013). Exploring the three-dimensional organization of genomes: interpreting chromatin interaction data. Nature reviews Genetics *14*, 390-403.

Deleyrolle, L.P., and Reynolds, B.A. (2009). Isolation, expansion, and differentiation of adult Mammalian neural stem and progenitor cells using the neurosphere assay. Methods in molecular biology *549*, 91-101.

Dion, M.F., Altschuler, S.J., Wu, L.F., and Rando, O.J. (2005). Genomic characterization reveals a simple histone H4 acetylation code. Proceedings of the National Academy of Sciences of the United States of America *102*, 5501-5506.

Dixon, J.R., Jung, I., Selvaraj, S., Shen, Y., Antosiewicz-Bourget, J.E., Lee, A.Y., Ye, Z., Kim, A., Rajagopal, N., Xie, W.*, et al.* (2015). Chromatin architecture reorganization during stem cell differentiation. Nature *518*, 331-336.

Efroni, S., Duttagupta, R., Cheng, J., Dehghani, H., Hoeppner, D.J., Dash, C., Bazett-Jones, D.P., Le Grice, S., McKay, R.D., Buetow, K.H.*, et al.* (2008). Global transcription in pluripotent embryonic stem cells. Cell stem cell *2*, 437-447.

Egan, C.M., Nyman, U., Skotte, J., Streubel, G., Turner, S., O'Connell, D.J., Rraklli, V., Dolan, M.J., Chadderton, N., Hansen, K.*, et al.* (2013). CHD5 is required for neurogenesis and has a dual role in facilitating gene expression and polycomb gene repression. Developmental cell *26*, 223-236.

Faigle, R., and Song, H. (2013). Signaling mechanisms regulating adult neural stem cells and neurogenesis. Biochimica et biophysica acta *1830*, 2435-2448.

Faust, C., Schumacher, A., Holdener, B., and Magnuson, T. (1995). The eed mutation disrupts anterior mesoderm production in mice. Development *121*, 273-285.

Feldman, B., Poueymirou, W., Papaioannou, V.E., DeChiara, T.M., and Goldfarb, M. (1995). Requirement of FGF-4 for postimplantation mouse development. Science *267*, 246-249.

Feng, W., Khan, M.A., Bellvis, P., Zhu, Z., Bernhardt, O., Herold-Mende, C., and Liu, H.K. (2013). The chromatin remodeler CHD7 regulates adult neurogenesis via activation of SoxC transcription factors. Cell stem cell *13*, 62-72.

Flanagan, J.F., Mi, L.Z., Chruszcz, M., Cymborowski, M., Clines, K.L., Kim, Y., Minor, W., Rastinejad, F., and Khorasanizadeh, S. (2005). Double chromodomains cooperate to recognize the methylated histone H3 tail. Nature *438*, 1181-1185.

Flaus, A., Martin, D.M., Barton, G.J., and Owen-Hughes, T. (2006). Identification of multiple distinct Snf2 subfamilies with conserved structural motifs. Nucleic acids research *34*, 2887-2905.
Franco, S.J., and Muller, U. (2013). Shaping our minds: stem and progenitor cell diversity in the mammalian neocortex. Neuron *77*, 19-34.

Friedmann-Morvinski, D., and Verma, I.M. (2014). Dedifferentiation and reprogramming: origins of cancer stem cells. EMBO reports *15*, 244-253.

Funato, K., Major, T., Lewis, P.W., Allis, C.D., and Tabar, V. (2014). Use of human embryonic stem cells to model pediatric gliomas with H3.3K27M histone mutation. Science *346*, 1529-1533.

Gallagher, S. (2001). Immunoblot detection. Current protocols in protein science / editorial board, John E Coligan [et al] *Chapter 10*, Unit 10 10.

Gao, D., Vela, I., Sboner, A., Iaquinta, P.J., Karthaus, W.R., Gopalan, A., Dowling, C., Wanjala, J.N., Undvall, E.A., Arora, V.K.*, et al.* (2014). Organoid cultures derived from patients with advanced prostate cancer. Cell *159*, 176-187.

Garraway, L.A., and Lander, E.S. (2013). Lessons from the cancer genome. Cell *153*, 17-37.
Gaspar-Maia, A., Alajem, A., Polesso, F., Sridharan, R., Mason, M.J., Heidersbach, A., Ramalho-Santos, J., McManus, M.T., Plath, K., Meshorer, E.*, et al.* (2009). Chd1 regulates open chromatin and pluripotency of embryonic stem cells. Nature *460*, 863-868.

Gkikopoulos, T., Schofield, P., Singh, V., Pinskaya, M., Mellor, J., Smolle, M., Workman, J.L., Barton, G.J., and Owen-Hughes, T. (2011). A role for Snf2-related nucleosome-spacing enzymes in genome-wide nucleosome organization. Science *333*, 1758-1760.

Gorkin, D.U., Leung, D., and Ren, B. (2014). The 3D genome in transcriptional regulation and pluripotency. Cell stem cell *14*, 762-775.

Grasso, C.S., Wu, Y.M., Robinson, D.R., Cao, X., Dhanasekaran, S.M., Khan, A.P., Quist, M.J., Jing, X., Lonigro, R.J., Brenner, J.C.*, et al.* (2012). The mutational landscape of lethal castration-resistant prostate cancer. Nature *487*, 239-243.

Guillemot, F., Lo, L.C., Johnson, J.E., Auerbach, A., Anderson, D.J., and Joyner, A.L. (1993). Mammalian achaete-scute homolog 1 is required for the early development of olfactory and autonomic neurons. Cell *75*, 463-476.

Guzman-Ayala, M., Sachs, M., Koh, F.M., Onodera, C., Bulut-Karslioglu, A., Lin, C.J., Wong, P., Nitta, R., Song, J.S., and Ramalho-Santos, M. (2015). Chd1 is essential for the high transcriptional output and rapid growth of the mouse epiblast. Development *142*, 118-127.

Hebert, J.M., and Fishell, G. (2008). The genetics of early telencephalon patterning: some assembly required. Nature reviews Neuroscience *9*, 678-685.

Hsieh, J., Aimone, J.B., Kaspar, B.K., Kuwabara, T., Nakashima, K., and Gage, F.H. (2004). IGF-I instructs multipotent adult neural progenitor cells to become oligodendrocytes. The Journal of cell biology *164*, 111-122.

Ihrie, R.A., and Alvarez-Buylla, A. (2011). Lake-front property: a unique germinal niche by the lateral ventricles of the adult brain. Neuron *70*, 674-686.

Iossifov, I., O'Roak, B.J., Sanders, S.J., Ronemus, M., Krumm, N., Levy, D., Stessman, H.A., Witherspoon, K.T., Vives, L., Patterson, K.E.*, et al.* (2014). The contribution of de novo coding mutations to autism spectrum disorder. Nature *515*, 216-221.

Jaenisch, R., and Young, R. (2008). Stem cells, the molecular circuitry of pluripotency and nuclear reprogramming. Cell *132*, 567-582.

Jojic, V., Shay, T., Sylvia, K., Zuk, O., Sun, X., Kang, J., Regev, A., Koller, D., Immunological Genome Project, C., Best, A.J.*, et al.* (2013). Identification of transcriptional regulators in the mouse immune system. Nature immunology *14*, 633-643.

Kandoth, C., McLellan, M.D., Vandin, F., Ye, K., Niu, B., Lu, C., Xie, M., Zhang, Q., McMichael, J.F., Wyczalkowski, M.A.*, et al.* (2013). Mutational landscape and significance across 12 major cancer types. Nature *502*, 333-339.

Kehle, J., Beuchle, D., Treuheit, S., Christen, B., Kennison, J.A., Bienz, M., and Muller, J. (1998). dMi-2, a hunchback-interacting protein that functions in polycomb repression. Science *282*, 1897-1900.

Keller, G. (2005). Embryonic stem cell differentiation: emergence of a new era in biology and medicine. Genes & development *19*, 1129-1155.

Kim, K.H., and Roberts, C.W. (2013). CHD7 in charge of neurogenesis. Cell stem cell *13*, 1-2.
Kim, W.Y., Wang, X., Wu, Y., Doble, B.W., Patel, S., Woodgett, J.R., and Snider, W.D. (2009). GSK-3 is a master regulator of neural progenitor homeostasis. Nature neuroscience *12*, 1390-1397.

Kloet, S.L., Baymaz, H.I., Makowski, M., Groenewold, V., Jansen, P.W., Berendsen, M., Niazi, H., Kops, G.J., and Vermeulen, M. (2015). Towards elucidating the stability, dynamics and architecture of the nucleosome remodeling and deacetylase complex by using quantitative interaction proteomics. The FEBS journal *282*, 1774-1785.

Koh, F.M., Lizama, C.O., Wong, P., Hawkins, J.S., Zovein, A.C., and Ramalho-Santos, M. (2015). Emergence of hematopoietic stem and progenitor cells involves a Chd1-dependent increase in total nascent transcription. Proceedings of the National Academy of Sciences of the United States of America *112*, E1734-1743.

Kolla, V., Naraparaju, K., Zhuang, T., Higashi, M., Kolla, S., Blobel, G.A., and Brodeur, G.M. (2015). The tumour suppressor CHD5 forms a NuRD-type chromatin remodelling complex. The Biochemical journal *468*, 345-352.

Kolla, V., Zhuang, T., Higashi, M., Naraparaju, K., and Brodeur, G.M. (2014). Role of CHD5 in human cancers: 10 years later. Cancer research *74*, 652-658.

Kornberg, R.D., and Lorch, Y. (1999). Twenty-five years of the nucleosome, fundamental particle of the eukaryote chromosome. Cell *98*, 285-294.

Kouzarides, T. (2007). Chromatin modifications and their function. Cell *128*, 693-705.

Koyama, H., Zhuang, T., Light, J.E., Kolla, V., Higashi, M., McGrady, P.W., London, W.B., and Brodeur, G.M. (2012). Mechanisms of CHD5 Inactivation in neuroblastomas. Clinical cancer research : an official journal of the American Association for Cancer Research *18*, 1588-1597.

Kreso, A., and Dick, J.E. (2014). Evolution of the cancer stem cell model. Cell stem cell *14*, 275-291.

Kriegstein, A., and Alvarez-Buylla, A. (2009). The glial nature of embryonic and adult neural stem cells. Annual review of neuroscience *32*, 149-184.

Kumamoto, T., and Hanashima, C. (2014). Neuronal subtype specification in establishing mammalian neocortical circuits. Neuroscience research *86*, 37-49.

Ladewig, J., Koch, P., and Brustle, O. (2013). Leveling Waddington: the emergence of direct programming and the loss of cell fate hierarchies. Nature reviews Molecular cell biology *14*, 225-236.

Laugesen, A., and Helin, K. (2014). Chromatin repressive complexes in stem cells, development, and cancer. Cell stem cell *14*, 735-751.

Lawrence, M.S., Stojanov, P., Mermel, C.H., Robinson, J.T., Garraway, L.A., Golub, T.R., Meyerson, M., Gabriel, S.B., Lander, E.S., and Getz, G. (2014). Discovery and saturation analysis of cancer genes across 21 tumour types. Nature *505*, 495-501.

Lee, K.K., and Workman, J.L. (2007). Histone acetyltransferase complexes: one size doesn't fit all. Nature reviews Molecular cell biology *8*, 284-295.

Lee, M.G., Villa, R., Trojer, P., Norman, J., Yan, K.P., Reinberg, D., Di Croce, L., and Shiekhattar, R. (2007). Demethylation of H3K27 regulates polycomb recruitment and H2A ubiquitination. Science *318*, 447-450.

Lewis, P.W., Muller, M.M., Koletsky, M.S., Cordero, F., Lin, S., Banaszynski, L.A., Garcia, B.A., Muir, T.W., Becher, O.J., and Allis, C.D. (2013). Inhibition of PRC2 activity by a gain-of-function H3 mutation found in pediatric glioblastoma. Science *340*, 857-861.

Li, W., Wu, J., Kim, S.Y., Zhao, M., Hearn, S.A., Zhang, M.Q., Meistrich, M.L., and Mills, A.A. (2014). Chd5 orchestrates chromatin remodelling during sperm development. Nature communications *5*, 3812.

Lie, D.C., Colamarino, S.A., Song, H.J., Desire, L., Mira, H., Consiglio, A., Lein, E.S., Jessberger, S., Lansford, H., Dearie, A.R.*, et al.* (2005). Wnt signalling regulates adult hippocampal neurogenesis. Nature *437*, 1370-1375.

Lim, D.A., and Alvarez-Buylla, A. (2014). Adult neural stem cells stake their ground. Trends in neurosciences *37*, 563-571.

Louis, S.A., Mak, C.K., and Reynolds, B.A. (2013). Methods to culture, differentiate, and characterize neural stem cells from the adult and embryonic mouse central nervous system. Methods in molecular biology *946*, 479-506.

Luger, K., Mader, A.W., Richmond, R.K., Sargent, D.F., and Richmond, T.J. (1997). Crystal structure of the nucleosome core particle at 2.8 A resolution. Nature *389*, 251-260.

Luk, E., Ranjan, A., Fitzgerald, P.C., Mizuguchi, G., Huang, Y., Wei, D., and Wu, C. (2010). Stepwise histone replacement by SWR1 requires dual activation with histone H2A.Z and canonical nucleosome. Cell *143*, 725-736.

Marshall, G.P., 2nd, Ross, H.H., Suslov, O., Zheng, T., Steindler, D.A., and Laywell, E.D. (2008). Production of neurospheres from CNS tissue. Methods in molecular biology *438*, 135-150.

Martello, G., and Smith, A. (2014). The nature of embryonic stem cells. Annual review of cell and developmental biology *30*, 647-675.

Mazzoni, E.O., Mahony, S., Peljto, M., Patel, T., Thornton, S.R., McCuine, S., Reeder, C., Boyer, L.A., Young, R.A., Gifford, D.K.*, et al.* (2013). Saltatory remodeling of Hox chromatin in response to rostrocaudal patterning signals. Nature neuroscience *16*, 1191-1198.

Meissner, A., Mikkelsen, T.S., Gu, H., Wernig, M., Hanna, J., Sivachenko, A., Zhang, X., Bernstein, B.E., Nusbaum, C., Jaffe, D.B.*, et al.* (2008). Genome-scale DNA methylation maps of pluripotent and differentiated cells. Nature *454*, 766-770.

Meshorer, E., Yellajoshula, D., George, E., Scambler, P.J., Brown, D.T., and Misteli, T. (2006). Hyperdynamic plasticity of chromatin proteins in pluripotent embryonic stem cells. Developmental cell *10*, 105-116.

Mi, H., Muruganujan, A., and Thomas, P.D. (2013). PANTHER in 2013: modeling the evolution of gene function, and other gene attributes, in the context of phylogenetic trees. Nucleic acids research *41*, D377-386.

Mich, J.K., Signer, R.A., Nakada, D., Pineda, A., Burgess, R.J., Vue, T.Y., Johnson, J.E., and Morrison, S.J. (2014). Prospective identification of functionally distinct stem cells and neurosphere-initiating cells in adult mouse forebrain. eLife *3*, e02669.

Mitsui, K., Tokuzawa, Y., Itoh, H., Segawa, K., Murakami, M., Takahashi, K., Maruyama, M., Maeda, M., and Yamanaka, S. (2003). The homeoprotein Nanog is required for maintenance of pluripotency in mouse epiblast and ES cells. Cell *113*, 631-642.

Mulero-Navarro, S., and Esteller, M. (2008). Chromatin remodeling factor CHD5 is silenced by promoter CpG island hypermethylation in human cancer. Epigenetics : official journal of the DNA Methylation Society *3*, 210-215.

Nam, H.S., and Benezra, R. (2009). High levels of Id1 expression define B1 type adult neural stem cells. Cell stem cell *5*, 515-526.

Narendra, V., Rocha, P.P., An, D., Raviram, R., Skok, J.A., Mazzoni, E.O., and Reinberg, D. (2015). Transcription. CTCF establishes discrete functional chromatin domains at the Hox clusters during differentiation. Science *347*, 1017-1021.

Narlikar, G.J., Sundaramoorthy, R., and Owen-Hughes, T. (2013). Mechanisms and functions of ATP-dependent chromatin-remodeling enzymes. Cell *154*, 490-503.

Niwa, H., Burdon, T., Chambers, I., and Smith, A. (1998). Self-renewal of pluripotent embryonic stem cells is mediated via activation of STAT3. Genes & development *12*, 2048-2060.

O'Carroll, D., Erhardt, S., Pagani, M., Barton, S.C., Surani, M.A., and Jenuwein, T. (2001). The polycomb-group gene Ezh2 is required for early mouse development. Molecular and cellular biology *21*, 4330-4336.

O'Roak, B.J., Vives, L., Girirajan, S., Karakoc, E., Krumm, N., Coe, B.P., Levy, R., Ko, A., Lee, C., Smith, J.D.*, et al.* (2012). Sporadic autism exomes reveal a highly interconnected protein network of de novo mutations. Nature *485*, 246-250.

Obri, A., Ouararhni, K., Papin, C., Diebold, M.L., Padmanabhan, K., Marek, M., Stoll, I., Roy, L., Reilly, P.T., Mak, T.W.*, et al.* (2014). ANP32E is a histone chaperone that removes H2A.Z from chromatin. Nature *505*, 648-653.

Oguro, H., Yuan, J., Ichikawa, H., Ikawa, T., Yamazaki, S., Kawamoto, H., Nakauchi, H., and Iwama, A. (2010). Poised lineage specification in multipotential hematopoietic stem and progenitor cells by the polycomb protein Bmi1. Cell stem cell *6*, 279-286.

Oliver, S.S., Musselman, C.A., Srinivasan, R., Svaren, J.P., Kutateladze, T.G., and Denu, J.M. (2012). Multivalent recognition of histone tails by the PHD fingers of CHD5. Biochemistry *51*, 6534-6544.

Ong, C.T., and Corces, V.G. (2014). CTCF: an architectural protein bridging genome topology and function. Nature reviews Genetics *15*, 234-246.

Owen-Hughes, T., and Gkikopoulos, T. (2012). Making sense of transcribing chromatin. Current opinion in cell biology *24*, 296-304.

Papamichos-Chronakis, M., Watanabe, S., Rando, O.J., and Peterson, C.L. (2011). Global regulation of H2A.Z localization by the INO80 chromatin-remodeling enzyme is essential for genome integrity. Cell *144*, 200-213.

Paridaen, J.T., and Huttner, W.B. (2014). Neurogenesis during development of the vertebrate central nervous system. EMBO reports *15*, 351-364.

Pasini, D., Bracken, A.P., Hansen, J.B., Capillo, M., and Helin, K. (2007). The polycomb group protein Suz12 is required for embryonic stem cell differentiation. Molecular and cellular biology *27*, 3769-3779.

Pasini, D., Bracken, A.P., Jensen, M.R., Lazzerini Denchi, E., and Helin, K. (2004). Suz12 is essential for mouse development and for EZH2 histone methyltransferase activity. The EMBO journal *23*, 4061-4071.

Paul, S., Kuo, A., Schalch, T., Vogel, H., Joshua-Tor, L., McCombie, W.R., Gozani, O., Hammell, M., and Mills, A.A. (2013). Chd5 requires PHD-mediated histone 3 binding for tumor suppression. Cell reports *3*, 92-102.

Pope, B.D., Ryba, T., Dileep, V., Yue, F., Wu, W., Denas, O., Vera, D.L., Wang, Y., Hansen, R.S., Canfield, T.K.*, et al.* (2014). Topologically associating domains are stable units of replication-timing regulation. Nature *515*, 402-405.

Potts, R.C., Zhang, P., Wurster, A.L., Precht, P., Mughal, M.R., Wood, W.H., 3rd, Zhang, Y., Becker, K.G., Mattson, M.P., and Pazin, M.J. (2011). CHD5, a brain-specific paralog of Mi2 chromatin remodeling enzymes, regulates expression of neuronal genes. PloS one *6*, e24515.

Quan, J., and Yusufzai, T. (2014). The tumor suppressor chromodomain helicase DNA-binding protein 5 (CHD5) remodels nucleosomes by unwrapping. The Journal of biological chemistry *289*, 20717-20726.

Rando, O.J., and Ahmad, K. (2007). Rules and regulation in the primary structure of chromatin. Current opinion in cell biology *19*, 250-256.

Ranjan, A., Mizuguchi, G., FitzGerald, P.C., Wei, D., Wang, F., Huang, Y., Luk, E., Woodcock, C.L., and Wu, C. (2013). Nucleosome-free region dominates histone acetylation in targeting SWR1 to promoters for H2A.Z replacement. Cell *154*, 1232-1245.

Rappolee, D.A., Basilico, C., Patel, Y., and Werb, Z. (1994). Expression and function of FGF-4 in peri-implantation development in mouse embryos. Development *120*, 2259-2269.

Reynolds, B.A., and Weiss, S. (1992). Generation of neurons and astrocytes from isolated cells of the adult mammalian central nervous system. Science *255*, 1707-1710.

Ronemus, M., Iossifov, I., Levy, D., and Wigler, M. (2014). The role of de novo mutations in the genetics of autism spectrum disorders. Nature reviews Genetics *15*, 133-141.

Siebzehnrubl, F.A., Vedam-Mai, V., Azari, H., Reynolds, B.A., and Deleyrolle, L.P. (2011). Isolation and characterization of adult neural stem cells. Methods in molecular biology *750*, 61-77.

Simon, J.A., and Kingston, R.E. (2013). Occupying chromatin: Polycomb mechanisms for getting to genomic targets, stopping transcriptional traffic, and staying put. Molecular cell *49*, 808-824.

Sims, R.J., 3rd, Chen, C.F., Santos-Rosa, H., Kouzarides, T., Patel, S.S., and Reinberg, D. (2005). Human but not yeast CHD1 binds directly and selectively to histone H3 methylated at lysine 4 via its tandem chromodomains. The Journal of biological chemistry *280*, 41789-41792.

Sims, R.J., 3rd, Millhouse, S., Chen, C.F., Lewis, B.A., Erdjument-Bromage, H., Tempst, P., Manley, J.L., and Reinberg, D. (2007). Recognition of trimethylated histone H3 lysine 4 facilitates the recruitment of transcription postinitiation factors and pre-mRNA splicing. Molecular cell *28*, 665-676.

Skene, P.J., Hernandez, A.E., Groudine, M., and Henikoff, S. (2014). The nucleosomal barrier to promoter escape by RNA polymerase II is overcome by the chromatin remodeler Chd1. eLife *3*, e02042.

Song, L., Zhang, Z., Grasfeder, L.L., Boyle, A.P., Giresi, P.G., Lee, B.K., Sheffield, N.C., Graf, S., Huss, M., Keefe, D.*, et al.* (2011). Open chromatin defined by DNaseI and FAIRE identifies regulatory elements that shape cell-type identity. Genome research *21*, 1757-1767.

Steger, D.J., Lefterova, M.I., Ying, L., Stonestrom, A.J., Schupp, M., Zhuo, D., Vakoc, A.L., Kim, J.E., Chen, J., Lazar, M.A.*, et al.* (2008). DOT1L/KMT4 recruitment and H3K79 methylation are ubiquitously coupled with gene transcription in mammalian cells. Molecular and cellular biology *28*, 2825-2839.

Stratton, M.R., Campbell, P.J., and Futreal, P.A. (2009). The cancer genome. Nature *458*, 719-724.

Subramanian, A., Tamayo, P., Mootha, V.K., Mukherjee, S., Ebert, B.L., Gillette, M.A., Paulovich, A., Pomeroy, S.L., Golub, T.R., Lander, E.S.*, et al.* (2005). Gene set enrichment analysis: a knowledge-based approach for interpreting genome-wide expression profiles. Proceedings of the National Academy of Sciences of the United States of America *102*, 15545-15550.

Suganuma, T., and Workman, J.L. (2011). Signals and combinatorial functions of histone modifications. Annual review of biochemistry *80*, 473-499.

Suto, R.K., Clarkson, M.J., Tremethick, D.J., and Luger, K. (2000). Crystal structure of a nucleosome core particle containing the variant histone H2A.Z. Nature structural biology *7*, 1121-1124.

Suva, M.L., Riggi, N., and Bernstein, B.E. (2013). Epigenetic reprogramming in cancer. Science *339*, 1567-1570.

Tessarz, P., and Kouzarides, T. (2014). Histone core modifications regulating nucleosome structure and dynamics. Nature reviews Molecular cell biology *15*, 703-708.

Thurman, R.E., Rynes, E., Humbert, R., Vierstra, J., Maurano, M.T., Haugen, E., Sheffield, N.C., Stergachis, A.B., Wang, H., Vernot, B.*, et al.* (2012). The accessible chromatin landscape of the human genome. Nature *489*, 75-82.

Venkatesh, S., and Workman, J.L. (2015). Histone exchange, chromatin structure and the regulation of transcription. Nature reviews Molecular cell biology *16*, 178-189.

Vestin, A., and Mills, A.A. (2013). The tumor suppressor Chd5 is induced during neuronal differentiation in the developing mouse brain. Gene expression patterns : GEP *13*, 482-489.
Vissers, L.E., van Ravenswaaij, C.M., Admiraal, R., Hurst, J.A., de Vries, B.B., Janssen, I.M., van der Vliet, W.A., Huys, E.H., de Jong, P.J., Hamel, B.C.*, et al.* (2004). Mutations in a new member of the chromodomain gene family cause CHARGE syndrome. Nature genetics *36*, 955-957.

Voncken, J.W., Roelen, B.A., Roefs, M., de Vries, S., Verhoeven, E., Marino, S., Deschamps, J., and van Lohuizen, M. (2003). Rnf2 (Ring1b) deficiency causes gastrulation arrest and cell cycle inhibition. Proceedings of the National Academy of Sciences of the United States of America *100*, 2468-2473.

Weber, C.M., and Henikoff, S. (2014). Histone variants: dynamic punctuation in transcription. Genes & development *28*, 672-682.

Wong, M.T., Scholvinck, E.H., Lambeck, A.J., and van Ravenswaaij-Arts, C.M. (2015). CHARGE syndrome: a review of the immunological aspects. European journal of human genetics : EJHG.

Xue, Y., Wong, J., Moreno, G.T., Young, M.K., Cote, J., and Wang, W. (1998). NURD, a novel complex with both ATP-dependent chromatin-remodeling and histone deacetylase activities. Molecular cell *2*, 851-861.

Yang, N., Ng, Y.H., Pang, Z.P., Sudhof, T.C., and Wernig, M. (2011). Induced neuronal cells: how to make and define a neuron. Cell stem cell *9*, 517-525.

Yap, K.L., and Zhou, M.M. (2011). Structure and mechanisms of lysine methylation recognition by the chromodomain in gene transcription. Biochemistry *50*, 1966-1980.

Yates, L.R., and Campbell, P.J. (2012). Evolution of the cancer genome. Nature reviews Genetics *13*, 795-806.

Yen, K., Vinayachandran, V., Batta, K., Koerber, R.T., and Pugh, B.F. (2012). Genome-wide nucleosome specificity and directionality of chromatin remodelers. Cell *149*, 1461-1473.

Ying, Q.L., Nichols, J., Chambers, I., and Smith, A. (2003). BMP induction of Id proteins suppresses differentiation and sustains embryonic stem cell self-renewal in collaboration with STAT3. Cell *115*, 281-292.

Zentner, G.E., and Henikoff, S. (2013). Regulation of nucleosome dynamics by histone modifications. Nature structural & molecular biology *20*, 259-266.

Zhang, Y., LeRoy, G., Seelig, H.P., Lane, W.S., and Reinberg, D. (1998). The dermatomyositis-specific autoantigen Mi2 is a component of a complex containing histone deacetylase and nucleosome remodeling activities. Cell *95*, 279-289.

Zhu, J., Adli, M., Zou, J.Y., Verstappen, G., Coyne, M., Zhang, X., Durham, T., Miri, M., Deshpande, V., De Jager, P.L.*, et al.* (2013). Genome-wide chromatin state transitions associated with developmental and environmental cues. Cell *152*, 642-654.

Zhuang, T., Hess, R.A., Kolla, V., Higashi, M., Raabe, T.D., and Brodeur, G.M. (2014). CHD5 is required for spermiogenesis and chromatin condensation. Mechanisms of development *131*, 35-46.

Ziv, O., Glaser, B., and Dor, Y. (2013). The plastic pancreas. Developmental cell *26*, 3-7.